NPS-OC-97-004

NAVAL POSTGRADUATE SCHOOL
MONTEREY, CALIFORNIA

THESIS

WIND-FORCED MODELING STUDIES OF CURRENTS, MEANDERS, EDDIES, AND FILAMENTS OF THE CANARY CURRENT SYSTEM

by

Eric J. Buch

June 1997

Thesis Advisor: Mary L. Batteen

Approved for public release; distribution is unlimited.

Prepared for:
National Science Foundation
1101 Wilson Boulevard
Arlington, VA 22230

NAVAL POSTGRADUATE SCHOOL
MONTEREY, CALIFORNIA

Rear Admiral Marsha J. Evans
Superintendent

This thesis was prepared in conjunction with research sponsored in part by the National Science Foundation, 4201 Wilson Boulevard, Arlington, VA 22230.

Released by:

REPORT DOCUMENTATION PAGE

Form Approved OMB No. 0704-0188

1. AGENCY USE ONLY *(Leave blank)*	2. REPORT DATE June 1997	3. REPORT TYPE AND DATES COVERED Master's Thesis

4. TITLE AND SUBTITLE WIND-FORCED MODELING STUDIES OF CURRENTS, MEANDERS, EDDIES, AND FILAMENTS OF THE CANARY CURRENT SYSTEM

5. FUNDING NUMBERS

6. AUTHOR(S) Eric J. Buch

7. PERFORMING ORGANIZATION NAME(S) AND ADDRESS(ES)
Naval Postgraduate School
Monterey, CA 93943-5000

8. PERFORMING ORGANIZATION REPORT NUMBER NPS-OC-96-004

9. SPONSORING/MONITORING AGENCY NAME(S) AND ADDRESS(ES)
National Science Foundation
4201 Wilson Boulevard Arlington, VA. 22230

10. SPONSORING/MONITORING AGENCY REPORT NUMBER

11. SUPPLEMENTARY NOTES The views expressed in this thesis are those of the author and do not reflect the official policy or position of the Department of Defense or the U.S. Government.

12a. DISTRIBUTION/AVAILABILITY STATEMENT
Approved for public release; distribution is unlimited.

12b. DISTRIBUTION CODE

13. ABSTRACT *(maximum 200 words)*

A high-resolution, multi-level, primitive equation ocean model is used to examine the response of an eastern boundary oceanic regime to both wind forcing and irregular coastline geometry. The focus of this study is the coastal region from 30° N to 42.5° N, a portion of the Canary Current System (CCS). To study the generation, evolution, and sustainment of the currents, meanders, eddies and filaments of the CCS, the model is forced from rest using seasonal climatological winds. To investigate the role of irregular coastline geometry, the first experiment uses climatological wind forcing along an idealized "straightened" coastline, while the second experiment uses the same wind forcing along an irregular coastline. In both cases a surface current, undercurrent, meanders, eddies, and filaments are generated. The results obtained while using the irregular, rather than the idealized coastline, however, show preferred eddy generation locations as well as enhanced growth of meanders, eddies, and filaments. The features produced by the model are consistent with available observations of the CCS. The model results support the hypothesis that both wind forcing and irregular coastline geometry are important mechanisms in the generation of many of the observed features of the CCS.

SUBJECT TERMS Primitive equation model, Canary Current System, currents, meanders, eddies, filaments			15. NUMBER OF PAGES 123 16. PRICE CODE
17. SECURITY CLASSIFICATION OF REPORT Unclassified	18. SECURITY CLASSIFICATION OF THIS PAGE Unclassified	19. SECURITY CLASSIFICATION OF ABSTRACT Unclassified	20. LIMITATION OF ABSTRACT UL

NSN 7540-01-280-5500

Standard Form 298 (Rev. 2-89)
Prescribed by ANSI Std. 239-18 298-102

Approved for public release; distribution is unlimited.

WIND-FORCED MODELING STUDIES OF CURRENTS, MEANDERS, EDDIES, AND FILAMENTS OF THE CANARY CURRENT SYSTEM

Eric J. Buch
Lieutenant, United States Navy
B.S., United States Naval Academy – 1988

Submitted in partial fulfillment
of the requirements for the degree of

MASTER OF SCIENCE IN METEOROLOGY AND PHYSICAL OCEANOGRAPHY

from the

NAVAL POSTGRADUATE SCHOOL
June 1997

ABSTRACT

A high-resolution, multi-level, primitive equation ocean model is used to examine the response of an eastern boundary oceanic regime to both wind forcing and irregular coastline geometry. The focus of this study is the coastal region from 30° N to 42.5° N, a portion of the Canary Current System (CCS). To study the generation, evolution, and sustainment of the currents, meanders, eddies and filaments of the CCS, the model is forced from rest using seasonal climatological winds. To investigate the role of irregular coastline geometry, the first experiment uses climatological wind forcing along an idealized "straightened" coastline, while the second experiment uses the same wind forcing along an irregular coastline. In both cases a surface current, undercurrent, meanders, eddies, and filaments are generated. The results obtained while using the irregular, rather than the idealized coastline, however, show preferred eddy generation locations as well as enhanced growth of meanders, eddies, and filaments. The features produced by the model are consistent with available observations of the CCS. The model results support the hypothesis that both wind forcing and irregular coastline geometry are important mechanisms in the generation of many of the observed features of the CCS.

TABLE OF CONTENTS

LIST OF FIGURES

LIST OF TABLES

ACKNOWLEDGEMENT

The professional guidance and support provided by my advisor, Dr. Mary Batteen, was an essential and invaluable part of this thesis without whose expertise, this could not have been accomplished. There is also the technical expertise and computer service requirements provided by Peter Braccio and Michael Cook, whose professionalism and on the spot availability helped me to overcome stumbling blocks while using FORTRAN, MATLAB, and FERRET. In addition, several of the excellent quality AVHRR SST images used in this study were provided by the NERC Remote Sensing Data Analysis Service, Plymouth Marine Laboratory, UK, through their outstanding web site (http:/www.npm.ac.uk/rsdas/).

Finally, the time needed to be dedicated on this project was fully supported by my wife and newborn daughter, Elyssa. Without their support, patience and flexibility I would not have been able to finish this thesis.

Thank you to all!

I. INTRODUCTION

The eastern boundary current (EBC) system off the west coast of the Iberian Peninsula and Northwest Africa is part of the Canary coastal upwelling system, which extends from ~10° N to 45° N. There is general agreement (e.g., Wooster *et al.*, 1976) that the Canary Current is generated as the closing eastern boundary for the North Atlantic Gyre, enhanced with northerly winds during and after the Spring Transition and reduced as the northerly winds relax or become westerly in the winter season or milder Fall Transition. The climatological mean Canary Current system (CCS) is a classical EBC, which consists of several large-scale currents. The predominant flow is the Canary Current (CC), which like other EBCs is a broad (~1000 km), relatively slow (~10-30 cm/s), equatorward, yearlong surface flow extending to depths of ~ 500 m (Wooster *et al.*, 1976). The extension of the CC which lies off the western coast of the Iberian Peninsula (IP) is also occasionally referred to as the Portugal Current (e.g., Tomczak and Godfrey, 1994). Embedded in the CC are narrower, somewhat swifter flows (occasionally reaching speeds of 100 cm/s (DMAH/TC, 1988)). Below the CC, lies the poleward undercurrent, which is narrower (~10-40 km) and weaker (~2-10 cm/s) than the surface current, and found near the coast. The depth and strength of the undercurrent varies both seasonally and latitudinally but is usually strongest near 300 m. In the winter the undercurrent shoals to the north, occasionally reaching the surface to form a third flow component. This current, which has recently been referred to as the Iberian Current (IC) (Haynes and Barton, 1990) is a seasonal surface poleward current, found normally north

of Cabo da Roca (see Figure 1 for geographical reference) but occasionally extending south nearly to Cabo de Sao Vincent during the winter months. The IC is also narrow (25-40 km) and relatively weak (~20-30 cm/s) and is found trapped near the coast against the shelf break (Fiuza, 1980; Frouin *et al.*, 1990; Haynes and Barton, 1990). A second deeper undercurrent also flows poleward off the western coast of the Iberian Peninsula. This flow is attributed to the Mediterranean Outflow (MO) which has at least two main cores, a shallow core at depths of 600-900 m and a deeper core at 1100-1200 m (Ambar, 1980). A third shallower poleward core of Mediterranean water has also been shown to exist around 400 m (Fiuza, 1979; Ambar, 1980).

The CCS is influenced predominantly by equatorward, upwelling favorable winds produced by the Azores High. The Azores High is a semi-permanent subtropical high pressure system that is similar in nature and behavior to its counterpart off the west coast of North America, the North Pacific Subtropical High, as described in Nelson (1977). The center of the Azores High migrates meridionally with the seasons, reaching its southernmost extent, ~27° N in March and ridging north to ~33° N by August. Because of this migration, maximum values of wind stress vary temporally at given locations. During the summer the mean east-west pressure contrast between Portugal and the center of the Azores High is ~8 mb, while in the winter it weakens to ~1 mb. This results in considerably stronger northerly to northwesterly winds in the summer followed by weaker northwesterly winds to winds with even a slight southerly component off of northern Portugal and northwest Spain in the winter. The shift of maximum wind stress also causes

the upwelling favorable winds to shift from about 27° N near the Canary Islands in January, to about 43° N off the IP by July (Fiuza, 1982).

Recent observations have shown that superimposed on the broad, climatological mean flow in this and other EBCs are highly energetic, mesoscale features such as jet-like surface currents, meanders, eddies, and filaments. Satellite images of sea surface temperatures have shown several filaments extending off the coast of Portugal and northwest Spain (Fiuza *et al.*, 1989) as well as off Cape Ghir in northwest Africa (Van Camp *et al.*, 1991; Hagen *et al.*, 1996). Observations have also shown pairs of anticyclonic and cyclonic mesoscale eddies on the order of 100 km (Fiuza, 1984) off the coast of Iberia. These features have been observed during periods of predominantly equatorward winds, which are upwelling favorable and many seem to be located near prominent coastal features such as capes. These observations provide evidence that wind forcing and coastal irregularities are possibly important mechanisms for the formation and sustainment of many of the mesoscale features found in EBC regions.

There have been numerous wind forcing models over the past few decades of EBCs, particularly for the California Current System. Early work included that of Pedlosky (1974) and Philander and Yoon (1982), who used steady wind stress and transient wind forcing, respectively. Carton (1984) and Carton and Philander (1984) investigated the response of reduced gravity models to realistic coastal winds. Another series of experiments were conducted by McCreary *et al.* (1987) utilizing a linear model with both transient and steady wind forcing in the California Current System. In all these

previous models, relatively weak currents (5-10 cm/s) were generated and no eddies or filaments developed.

Recent modeling studies have focused on the driving mechanisms for the complex features such as filaments observed in the EBC regions. While Ikeda *et al.* (1984) and Haidvogel *et al.* (1991) studied baroclinic and barotropic instability, coastal irregularities, and bottom topography as possible mechanisms, Batteen *et al.* (1989), McCreary *et al.* (1991), Pares-Sierra *et al.* (1993), and Batteen (1997) studied wind forcing as a possible generative mechanism. Recently, Batteen (1997) used a multilevel primitive equation (PE) model run with seasonal winds and coastal irregularities to realistically generate many of the observed features of the California Current System.

In contrast, modeling studies of the CCS have been scarce. McClain *et al.* (1986) performed the first limited modeling study in the region, using ship-derived winds to produce a large negative wind stress curl off the northwest coast of the IP. This resulted in opposing equatorward and poleward surface currents. Mittlestaedt (1991) looked at the near-surface circulation of the PE models of Bryan (1969) and Semtner (1974). Because these coarse resolution models could only resolve structures larger than 200 km, they missed the mesoscale features. Recently Batteen *et al.* (1992) used an eddy resolving PE model with both uniform and variable wind stress, the latter computed from synoptic surface pressure analyses, to produce realistic currents as well as mesoscale eddies. This study, however, covered only a limited region of the CCS off the northwest coast of the Iberian Peninsula and also used a straight coast for its model domain.

The objective of this study is to investigate the dependence of the generation of currents, eddies, jets and filaments on seasonal climatological wind forcing and on irregular coastal geometry for an extended region of the CCS. The high-resolution, multi-level, PE model of Batteen (1997) with seasonal wind forcing will be used. As in the California Current systems study, to allow larger scale eddies and elongated filaments to be generated and so that the model can reach equilibrium, the model will be allowed to run for ~3 years, significantly longer than in previous studies which ran for less than a year.

The study is organized as follows: The numerical model, types of forcing, initial and specific experimental conditions, and the energy analysis technique are described in section II. The results of the different model simulations and comparisons with observations are discussed in section III, while a summary and discussion are presented in section IV.

II. MODEL DESCRIPTION

A. MODEL EQUATIONS

The PE numerical model in this study was originally a coarse resolution model used in closed basin studies by Haney (1974). It has recently been adapted for eddy-resolving, limited EBC regions with open borders on the northern, western, and southern boundaries by Batteen (1997). The limited area EBC model is multi-level, non-adiabatic, and uses the beta-plane approximation. It has both baroclinic and barotropic velocity components and uses the hydrostatic, Boussinesq, and rigid lid approximations. The governing equations are as follows:

$$\frac{du}{dt} = \frac{-1}{\rho_0}\frac{\partial p}{\partial x} + fv - A_M \nabla^4 u + K_M \frac{\partial^2 u}{\partial z^2} \tag{1}$$

$$\frac{dv}{dt} = \frac{-1}{\rho_0}\frac{\partial p}{\partial y} - fu - A_M \nabla^4 v + K_M \frac{\partial^2 v}{\partial z^2} \tag{2}$$

$$\frac{\partial u}{\partial x} + \frac{\partial v}{\partial y} + \frac{\partial w}{\partial z} = 0 \tag{3}$$

$$\frac{\partial p}{\partial z} = -\rho g \tag{4}$$

$$\rho = \rho_0[1 - \alpha(T - T_0) + \beta(S - S_0)] \tag{5}$$

$$\frac{dT}{dt} = -A_H \nabla^4 T + K_H \frac{\partial^2 T}{\partial z^2} \tag{6}$$

$$\frac{dS}{dt} = -A_H \nabla^4 S + K_H \frac{\partial^2 S}{\partial z^2} \tag{7}$$

In the above equations, t is time, (x,y,z) is a right-handed Cartesian coordinate system with x pointing toward shore, y alongshore, and z upward. The corresponding velocity components are (u,v,w), T is temperature, S is salinity, ρ is density, and p is pressure. Table 1 provides a list of other symbols found in the model equations, as well as values of constants used throughout the study.

A space-staggered B-scheme (Arakawa and Lamb, 1977) is used for the horizontal finite differencing. This scheme has been shown by Batteen and Han (1981) to be appropriate when the grid spacing is approximately on the same order as, or less than, the Rossby radius of deformation. The horizontal grid spacing is 9 km in the east-west direction and 11 km in the north-south direction, while the internal Rossby radius of deformation is ~30 km. The model uses ten layers in the vertical, with constant z-levels, at depths of 13, 46, 98, 182, 316, 529, 870, 1416, 2283, and 3656 m. This spacing scheme concentrates more layers above the thermocline in the dynamically active portion of the ocean, consistent with Haney (1974).

The model domain (Figure 1) is rectangular, encompassing the west coast of the Iberian Peninsula and northwest Africa, from 30° N to 42.5° N (1408 km alongshore), and from 5° W to 17.5° W (1152 km cross-shore). The coastal boundaries of the model domain are closed, and have both the tangential and normal components of velocity set to zero. To focus on the roles played by climatological wind forcing, bottom topography has been omitted and the eastern boundary is modeled as a vertical wall. The constant depth used in the model is 4500 m. A modified version of the radiation boundary conditions of

Camerlengo and O'Brien (1980) is used for the open ocean domain boundaries to the north, south, and west with slight spatial smoothing applied in the vicinity of the open boundaries (Batteen, 1997).

Biharmonic lateral heat and momentum diffusion is used in the model with the same choice of coefficients (i.e., 2.0 $x10^{17}$ cm^4/s) as in Batteen (1997). Holland (1978) showed that the highly selective biharmonic diffusion acts predominantly on submesoscales, while Holland and Batteen (1986) found that baroclinic mesoscale processes can be damped by Laplacian lateral heat diffusion. As a result, the use of biharmonic lateral diffusion should allow mesoscale eddy generation via barotropic (horizontal shear) and/or baroclinic (vertical shear) instability mechanisms. As in Batteen (1997), weak (0.5 cm^2/s) vertical eddy viscosities and conductivities are used. Bottom stress is parameterized by a simplified quadratic drag law (Weatherly, 1972), as in Batteen (1997).

An annual climatological temperature profile based on Levitus (1982) centered at ~37.5° N (corresponding to the center of the model domain) was used to represent the initial temperature conditions for the model domain. An exponential profile was used to approximate the initial mean stratification in both experiments. The exact form was:

$$T(z) = T_B + \Delta T e^{z/h}.$$

The approximation uses a length scale of 450 m, and assumes T_B = 2° C to be the temperature at depth, and ΔT = 15.5 °C to be the change of temperature between the bottom and top of the profile.

To isolate the effects of wind forcing in this experiment, the net heat flux at the sea surface is zero. Therefore, any heat flux that is discernible during the model runs will have been generated by an increase or decrease of sea surface temperature resulting from wind-forcing effects (Batteen *et al.*, 1989). To accomplish this, an initial air temperature is chosen that forces the net flux of longwave radiation, sensible heat, and latent heat to balance the heating due to solar radiation. This air temperature is then used in the model for all wind forcing experiments. Any subsequent surface heat flux forcing is therefore a secondary effect of the changes to the sea surface temperature due to the wind forcing

B. METHOD OF SOLUTION

Equations (1) through (7) comprise a closed system of seven scalar equations and seven unknowns, u, v, w, p, ρ, T, and S. The variables, u, v, T, and S are prognostic variables whose time rates of change are predicted from (1), (3), (6) and (7), respectively. Although the diagnostic variables w, p, and ρ can be determined from (3), (4), and (5), respectively, additional constraints are imposed on p and w by the choice of the rigid lid boundary conditions. The vertically integrated pressure can no longer be obtained by

integrating the hydrostatic equation (4) for the free surface, and the vertically-integrated horizontal velocity is subsequently constrained to be non-divergent, i.e.,

$$\int_{-H}^{0}\left(\frac{\partial u}{\partial x}+\frac{\partial v}{\partial y}\right)d\varepsilon = 0 \ , \tag{8}$$

which is obtained by integrating (3) and applying the vertical boundary conditions where ε is a dummy variable representing the vertical coordinate.

For any quantity q, let its vertical average be denoted by $\overline{q}$ and its departure (vertical shear) by q'. From (8) the vertical mean flow can then be described by a streamfunction ψ, such that:

$$\overline{u} = -\frac{1}{H}\frac{\partial \psi}{\partial y} \ , \tag{9}$$

$$\overline{v} = \frac{1}{H}\frac{\partial \psi}{\partial x} \ . \tag{10}$$

The streamfunction ψ is predicted from the vorticity equation, which is derived by applying the curl operator to the vertical average of (1) and (2), and then using (9) and (10), the vorticity equation becomes

$$\begin{aligned}\frac{\partial \zeta}{\partial t} &= \frac{\partial}{\partial t}\left[\frac{1}{H}\left(\frac{\partial^2 \psi}{\partial x^2}\right)+\frac{1}{H}\left(\frac{\partial^2 \psi}{\partial y^2}\right)+\frac{\partial \psi}{\partial x}\frac{\partial H^{-1}}{\partial x}+\frac{\partial \psi}{\partial y}\frac{\partial H^{-1}}{\partial y}\right] \\ &= -\left[\frac{\partial}{\partial x}\left(\frac{f}{H}\frac{\partial \psi}{\partial y}\right)-\frac{\partial}{\partial y}\left(\frac{f}{H}\frac{\partial \psi}{\partial x}\right)\right] \\ &\quad -\left[\frac{\partial}{\partial x}\left(\frac{g}{H\rho_0}\int_{-H}^{0}\int_{z}^{0}\frac{\partial \rho}{\partial y}d\varepsilon dz\right)-\frac{\partial}{\partial y}\left(\frac{g}{H\rho_0}\int_{-H}^{0}\int_{z}^{0}\frac{\partial \rho}{\partial x}d\varepsilon dz\right)\right] \\ &\quad +\frac{\partial}{\partial x}\left(\frac{1}{H}\int_{-H}^{0}G dz\right)-\frac{\partial}{\partial y}\left(\frac{1}{H}\int_{-H}^{0}F dz\right),\end{aligned} \tag{11}$$

where G and F represent the collected contributions of the nonlinear and viscous terms from equations (1) and (2).

The vorticity equation (11) is solved by obtaining an updated value of ζ by application of the leapfrog (or every 11 time steps, the Euler-backward) time-differencing scheme. The associated value of ψ can then be obtained from:

$$\zeta = \frac{1}{H}\left(\frac{\partial^2 \psi}{\partial x^2}\right) + \frac{1}{H}\left(\frac{\partial^2 \psi}{\partial y^2}\right) + \frac{\partial \psi}{\partial x}\frac{\partial H^{-1}}{\partial x} + \frac{\partial \psi}{\partial y}\frac{\partial H^{-1}}{\partial y}, \qquad \textbf{(12)}$$

which is an elliptic equation. A solution to (12) is fully prescribed by specifying the values of ψ on the open and closed boundaries of the model domain. Currently, to solve (12), the model uses an elliptic solver when there are no variations in coastline geometry and/or topography, and successive over-relaxation techniques when there are variations in coastline geometry and/or topography.

The vertical shear current (u', v') is predicted from (1) and (2) after subtracting the vertical mean flow. The results are:

$$\frac{\partial u'}{\partial t} = \frac{-1}{\rho_0}\frac{\partial p'}{\partial x} + fv' - A_M \nabla^4 u' + K_M \frac{\partial^2 u'}{\partial z^2} + F - \overline{F} - \frac{\tau^y}{\rho_0 H}, \qquad \textbf{(13)}$$

$$\frac{\partial v'}{\partial t} = \frac{-1}{\rho_0}\frac{\partial p'}{\partial y} - fu' - A_M \nabla^4 v' + K_M \frac{\partial^2 v'}{\partial z^2} + G - \overline{G} - \frac{\tau^x}{\rho_0 H}. \qquad \textbf{(14)}$$

In (13) and (14), p', which represents the departure of the pressure from the vertical average, is, using (4), expressed in terms of ρ as:

$$p' = \int_z^0 \rho g \, d\varepsilon - \frac{1}{H}\int_{-H}^{0}\left(\int_z^0 \rho g \, d\varepsilon\right) dz. \qquad \textbf{(15)}$$

The method of solution consists of predicting $\nabla^2\psi, \psi, u', v', T,$ and S from (11), (12), (13), (14), (6) and (7), respectively. The total current is then obtained by adding the vertical shear part to the vertical average part, after the latter is obtained from ψ using (9) and (10). The diagnostics ρ, w, and p' are then obtained explicitly from the equation of state (5), continuity equation (8), and hydrostatic relation (15), respectively.

C. FORCING CONDITIONS AND EXPERIMENTAL DESIGN

Previous experiments by Batteen *et al.* (1992) investigated the role of steady equatorward winds with anticyclonic wind stress curl in the generation of features off the IP. In a more recent study by Batteen (1997) the role of seasonal wind forcing and irregular coastline geometry has been investigated in the generation of features such as eddies and filaments in the California Current system. Following Batteen (1997), in this study, seasonal wind forcing and irregular coastline geometry will be used to investigate the generation of similar features in the CCS.

To explore the effects of seasonal wind forcing, the model is forced from rest with climatological wind fields that originate from a 2.5° by 2.5° grid of the European Centre for Medium-Range Weather Forecasts (ECMWF) near-surface wind analyses (Trenberth *et al.*, 1990). The monthly mean stresses based on twice daily wind analyses from 1980-1989 have then been interpolated spatially to the 9 by 11 km model resolution and temporally to daily wind values.

An example of the wind fields used can be seen in Figure 2, which shows the annual migration of the Azores Subtropical High from the south in the winter (Figure 2d), to its most northern extent in the summer (Figure 2b). The atmospheric pressure pattern for November (Figure 2d) depicts a low to the north and the Azores High to the south, which results in a wind divergence at ~40° N. This pattern of weakly poleward winds north of 40° N and equatorward winds to the south continues through December. During January and February (Figure 2a) the divergence in the wind field migrates poleward. By March an equatorward component in the wind field is observed along the entire domain. The strongest equatorward winds are discernible from July (Figure 2b) through August. By September (Figure 2c) the winds start to weaken throughout the domain, and divergence in the wind field is observed in the north in October. In November the wind divergence returns to ~40° N.

The design of the model experiments is as follows. To focus on the role of seasonal winds and irregular coastline geometry, experiment 1 looks at the model response to seasonal wind forcing along an idealized "straightened" coastline (Figure 3a), while experiment 2 investigates the model response to the same wind forcing as in experiment 1, but with an irregular, more realistic coastline (Figure 3b). In both experiments the model integrations start from a state of rest and, once a day, the model is updated with interpolated ECMWF winds. To allow the model to reach quasi-equilibrium, each model integration is allowed to run for 3 years.

III. RESULTS FROM MODEL SIMULATIONS

A. EXPERIMENT 1 - EFFECTS OF WIND FORCING AND IDEALIZED COASTLINE GEOMETRY

1. Spin-up Phase

In response to the predominantly equatorward winds over the model domain, a coastal equatorward surface current develops along the entire coast by day 45. The current develops initially in the southern end of the domain in response to the stronger equatorward winds associated with the southerly position of the Azores High. By day 180 (Figure 4a) there is generally equatorward flow throughout the domain. In addition, a poleward undercurrent has also developed, initially, in the southern end of the domain and then extending along the entire coast. A cross-section of meridional velocity (Figure 5a) shows the typical vertical structure of the equatorward coastal jet and the poleward undercurrent. The coastal jet core remains within ~50 km of the coast, extending offshore to ~200 km. The core velocity ranges from ~30-35 cm/s, and extends from ~100 m depth near the coast to ~500-600 m depth offshore. The weaker undercurrent is also seen with a core velocity of ~5 cm/s lying beneath the coastal jet within ~40 km of the coast.

As the wind becomes equatorward over the entire domain and increases in intensity, increased stress is exerted on the ocean surface creating Ekman transport offshore. This results in upwelling of cooler water along the coast. In the spring, upwelling is confined to the south where the stronger winds exist, while by summer

upwelling is evident along the entire coast with fairly vigorous upwelling occurring just south of Cabo de Sao Vincent and south of Cape Beddouzza/Cape Ghir (e.g., Figure 4a).

As the coastal jet and undercurrent become fully established (for example. see Figure 5b, which shows the structure of the currents just prior to meander formation), the currents become unstable and form meanders. This occurs off northwest Africa first where there has been more time for the strong equatorward winds to act on the ocean surface. By day 255 (Figure 4b) a meander develops just upstream of Cape Beddouzza and by day 270 (Figure 4c) forms an eddy inshore of the coastal jet in the cold upwelled water. No meanders form in the northern portion of the model until approximately day 330 (Figure 4d). Since this meander develops in the late fall when the equatorward winds are diminishing (thus weakening the equatorward coastal current), this meander is not as extensive as that to the south off northwest Africa.

In the fall, the currents begin to weaken with the slacking winds. The upwelling also ends, first in the poleward end of the domain and then progressively equatorward until by around day 345 all upwelling has ceased. By approximately day 336 (Figure 4e) a surface poleward current appears in the extreme northern portion of the model domain in response to the weak poleward winds present off the northwestern coast of the IP in November and December.

In the spring of the second year, as the Azores High ridges back to the north, upwelling of cool water redevelops along the coast as the equatorward flow reestablishes itself and intensifies into the summer. In the second year, the coastal currents become unstable sooner, developing meanders earlier. To the south, the meanders are larger,

while to the north along the IP, the meanders become large enough to create eddies inshore of the coastal jet. Filaments also form as the coastal jet meanders through the anticyclonic eddies. The filaments then flow offshore and advect the cold upwelled water near the coast offshore. By April a large-scale anticyclonic circulation sets up in the Gulf of Cadiz and a fairly vigorous filament develops west of Cape Beddouzza. In May (Figure 4f) a cold core cyclonic eddy forms on the offshore extension of this filament. Through the remainder of the year the equatorward jet, embedded with eddies, continues to meander downstream.

After allowing the model to run long enough, it can be seen that the system reaches a quasi-equilibrium state and that many of the features continue to be generated and sustained. By the beginning of the third year, the mean kinetic energy has leveled off reaching a quasi-equilibrium state. This is quasi-equilibrium state is expected due to the seasonal variation of the wind forcing which is the source of the mean kinetic energy.

2. Quasi-equilibrium Phase

By year three, the model has reached a quasi-equilibrium state. To see the seasonal structures of the features of the CCS, the model output fields are time-averaged every month and also for the upwelling season.

In the spring (Figure 6a), a relatively strong equatorward current of ~30-35 cm/s exists ~200-250 km off the coast of Iberia lying near the 17.5° C isotherm, with a stronger coastal jet appearing closer to shore in regions where the current bends anticyclonically near the coast (e.g. between 37° N and 38° N in Figure 6a). A large anticyclonic eddy

that set up in the previous year in the Gulf of Cadiz remains. Off the northwest coast of Africa a series of large amplitude meanders exist with several cyclonic and anticyclonic eddies on the order of 150 km. Upwelling begins in the spring off Cape Beddouzza, spreading north through late spring and into summer. As the upwelling intensifies, the coastal jet advects the cold water offshore, forming a distinctive filament stretching westward to ~250 km.

By summer (Figure 6b), upwelling has spread north along the entire coast and in August reaches a maximum along the IP. A strong coastal equatorward flow also reappears along the entire IP in conjunction with the continued equatorward wind stress. By early summer the coastal jet becomes unstable, forming a meander at ~38.5° N. By July, two distinct meanders exist, one still near ~38.5° N and a second off Cabo de Sao Vincent, with cyclonic cold core eddies inshore of the currents at both locations. Along northwest Africa maximum upwelling occurs a month earlier than off the IP. Large meanders exist in response to the stronger currents. As the strengthened currents flow offshore in the regions of the developed meanders, the current advects cold upwelled water offshore with the result that several extensive filaments extend offshore for hundreds of kilometers.

Persistent patterns for the entire year 3 upwelling season were investigated by averaging the temperature and current fields over that season. The average maps (Figure 7a and 7b) reveal that an offshore equatorward meandering current, an equatorward coastal jet, a poleward undercurrent, eddies, and filaments, appear as regular features of the CCS during the upwelling season. Both the offshore current and coastal jet meander

cyclonically and anticyclonically. The offshore current has alongshore wavelengths of several hundred kilometers, cross-shore excursions of ~100-200 km (with a large anticyclonic meander occurring to the west of the Gulf of Cadiz), speeds of 15-25 cm/s; and a vertical excursion to ~400-600 m depth. The coastal jet flows alongshore of the Iberian coast until at ~39° N it develops a meander with a wavelength of ~150 km. Off Cabo de Sao Vincent, the coastal jet veers offshore again to form a second meander. The coastal jet then continues in a nearshore anticyclonic flow through the Gulf of Cadiz. At ~34° N a third meander exists along the coast of northwest Africa. The coastal jet has speeds of ~20-35 cm/s and extends to ~400 m depth. The filaments extend ~300 km offshore with widths of ~30-100 km. The eddies are on the order of 100-150 km in diameter and tend to extend fairly deep, below 600 m depth (e. g., see Figure 7b). Below the coastal jet lies the poleward undercurrent with speeds of ~5 cm/s (Figure 7b).

Figures 8a and 8b are horizontal maps of the upper layer mean kinetic energy (MKE) and eddy kinetic energy (EKE) averaged over the upwelling season. Holland *et al.* (1983) showed that maps of MKE and EKE can be used to locate sources of the mean and eddy energy. Comparisons of Figures 7a and 8a show that high values of MKE follow the coastal jet, with lower values further offshore (at ~13° W) near the core of the offshore equatorward flow. The highest values of MKE appear near areas of tightened temperature gradients (i.e. near areas of greatest upwelling) and high current velocities, with the maximum occurring off the Cape Beddouzza region. In contrast, a comparison of Figure 7a and 8b, shows that the highest values of EKE are found south of ~37° N where the

largest cyclonic meanders occur. Other areas of EKE are found near areas of weak cyclonic meanders off the IP and in the large-scale cyclonic flow west of the IP. The maximum EKE appears west of the Cape Beddouzza area in conjunction with the strong coastal jet turning equatorward as it merges with the equatorward flow further offshore. A comparison of Figures 8a and 8b shows that on average the MKE is larger than the EKE during the upwelling season; however, the EKE covers a larger portion of the domain. This is consistent with other observations of the model data, which show that eddies are generated from baroclinic instability due to vertical shear between the surface equatorward current and the poleward undercurrent, as well as from barotropic instability due to horizontal shear between the currents.

By fall (Figure 6c), upwelling has weakened along the entire coast. The strong equatorward coastal jet weakens first, moving offshore along with the temperature front. By November (Figure 6c), weak poleward and equatorward flows exist out to ~350 km where the stronger equatorward core is located. Relatively strong equatorward flow still exists near the IP to the south, where a large anticyclonic meander forces the current near the coast. A meander off Cabo de Sao Vincent with a cold core cyclonic eddy inshore of the current also remains through the fall as does the large scale anticyclonic eddy in the Gulf of Cadiz. Off northwest Africa major meanders are maintained, as are several large filaments.

By winter (not shown), only a weak equatorward flow exists over the entire domain. Embedded in this flow are numerous jets, eddies, and filaments.

On the basis of these results it is seen that a seasonal cycle occurs for the coastal currents, upwelling, and filaments. The eddies can be seasonal as well as quasi-permanent, while the meanders can be quasi-permanent. These quasi-permanent features appear to play a significant role in the modification of the seasonal features which leads to large temporal and spatial variability in the CCS.

B. EXPERIMENT 2 - EFFECTS OF WIND FORCING AND IRREGULAR COASTLINE GEOMETRY

1. Spin-up Phase

In experiment one, an idealized, "straightened" coastline was used. In experiment 2, a more realistic coastline with extensive coastline irregularities is used to investigate the effects of capes and bays on the formation and sustainment of the features found in the CCS. The same temporally and spatially varying winds as those used in experiment 1 are used to force the model in experiment 2. All other parameters are the same as in experiment 1.

The current and temperature (e.g., Figures 9 and 10) patterns in experiment 2 show that many of the same features that exist in experiment 1 are also present in experiment 2. Both an equatorward surface current and poleward undercurrent develop. The equatorward flow begins in the south and then progresses north as the equatorward wind forcing migrates north with the Azores High. In addition, as the core of the

undercurrent intensifies in conjunction with the progression of the upwelling season, it shallows and displaces the core of the equatorward surface current further offshore (Figures 10a and 10b) as in experiment 1 (e.g., Figures 5a and 5b). Strong vertical and horizontal shears in the upper layers develop between the opposing currents, causing the flow to become both barotropically and baroclinically unstable, which leads to the formation of meanders, eddies, and filaments.

As in the spin-up phase in experiment 1, an equatorward surface current develops rather uniformly along the entire coast. While the upwelling in experiment 1 was more uniform, only having increases near the two prominent capes (e.g., Cabo de Sao Vincent and Cape Beddouzza) depicted in the idealized coastline, in experiment 2 the corresponding upwelling is quite patchy, appearing most intense near even the less prominent capes (e.g., off Cabo de Roca in Figure 9a and 9b). Since these capes are areas where the alongshore component of the wind stress is at a local maximum, the coastal current velocity is also at a maximum, which leads to enhanced upwelling (Batteen, 1997).

In experiment 1 the majority of features had no geographical preference other than the features that appeared tied to the major geographical features depicted in the idealized coastline (e.g., the cyclonic eddy off Cabo de Sao Vincent, the anticyclonic flow through the Gulf of Cadiz, and the large filament off Cape Beddouzza). In contrast, experiment 2 frequently features additional eddies and filaments "anchored" off of less prominent coastal features (e.g., off Cabo da Roca, Cabo de Sines, Cabo de Santa Maria, and the Cape Beddouzza/Cape Ghir area shown in Figure 9d) that occur along the realistic

coastline. In addition, in experiment 2 upwelling occurs significantly sooner (~ two weeks) and with greater intensity off the IP, where the largest differences occur between the idealized and realistic coasts (e.g., compare Figures 4 and 9). Experiment 2 also develops more meanders in the vicinity of the additional capes of the realistic coastline which also form earlier then those in experiment 1. These meanders intensify and develop into predominantly cyclonic cold core eddies, which in time coalesce with other eddies to form larger cyclonic eddies on the order of ~100-300 km. Similar to that in experiment 1, by the end of the upwelling season (Figure 9c), the equatorward surface flow has taken the form of a meandering jet embedded with several eddies.

2. Quasi-equilibrium Phase

Similar to experiment 1, by year 3 the model reaches quasi-equilibrium and shows that most features continue to be generated and maintained. As in experiment 1, to see the seasonal structure of the CCS, the model output is time averaged every month as well as during the upwelling season.

The model results show that in the spring (Figure 11a) there is a mean equatorward flow embedded with numerous eddies. The core of the jet appears to follow the temperature gradient of 16.5-17.5° C. This jet flows close to the coast off northern Iberia, but leaves the coast as it impinges on Cabo de Roca. It then continues to meander equatorward following the temperature front south. By April (Figure 11a), a coastal jet

appears off the coast of Northwest Africa and, as in experiment 1, upwelling is also reestablished by this time. By early summer (Figure 11b) upwelling begins to appear in pockets along the Iberian coast and a cold core cyclonic eddy develops southeast of Cabo da Sao Vincent. A relatively robust coastal jet (of ~20-40 cm/s) extending to depths of ~ 600 m (Figure 11f) is also now found along the entire coastline. It appears to flow along the newly established tightened temperature gradient of 14.5-15.5° C as additional cold water is upwelled near the coast. The maximum velocity variations are normally found near the capes, with increases poleward and decreases equatorward of the capes. Note the cooler water inshore and warmer water offshore of the coastal jet and the numerous eddies extending beyond 800 m depth (Figure 11f).

Maximum upwelling occurs by late summer (Figure 11c). The strong equatorward coastal jets which have developed get deflected offshore by the large capes (e.g., Cabo da Roca) and advect the cold upwelled water offshore producing filaments. In addition to occurring off Cabo da Roca, filament generation is also observed off Cabo de Sao Vincent, Cabo de Santa Maria, and Cape Beddouzza/Cape Ghir.

To better observe the features of the upwelling season the temperature and current fields are averaged over the entire upwelling season. This shows that an equatorward meandering current offshore, an equatorward coastal jet, a poleward undercurrent, eddies, and filaments appear as regular features of the CCS during the upwelling season (Figures 12a and 12b). The surface equatorward current flows along the coast of northern IP until ~40° N where it impinges on Cabo de Roca splitting into two distinct flows, a coastal jet

and an offshore current. Both the offshore current and coastal jet meander cyclonically and anticyclonically. The offshore current has alongshore wavelengths of several hundred kilometers, cross-shore excursions of ~100-200 km, speeds of 15-35 cm/s, a vertical excursion to ~600-800 m depth, and seems to flow approximately along the 17° C isotherm. The coastal jet continues to flow alongshore of the Iberian coast continuing anticyclonically through the Gulf of Cadiz and down the coast of Africa. The coastal jet has speeds of ~25-40 cm/s with increases near areas of maximum upwelling and extends to ~1000 m depth. The filaments extend ~200 km offshore with widths of ~30-100 km. The eddies are on the order of 100-150 km in diameter and tend to extend below 1000 m depth. Below the coastal jet lies the poleward undercurrent which is present along the entire coast (e.g., Figure 12c) throughout the upwelling season. The undercurrent meanders within ~100 km of the coast at speeds of ~10-15 cm/s. Offshore of the undercurrent are eddies of O(100 km) diameter.

Figures 13a and 13b are horizontal maps of the upper layer MKE and EKE averaged over the upwelling season. As in experiment 1, MKE is found principally near the core of the surface currents, while EKE is preferentially found in areas of cyclonic meanders and eddies. In addition, MKE has larger values than EKE; however, the EKE extends over a larger region. Comparisons of Figures 8a and 13a show that the MKE is spread out over a larger region than in experiment 1, while the maximum MKE has shifted from northwest Africa to the IP. Comparing Figures 8b and 13b shows that the large region of EKE west of the Gulf of Cadiz in experiment 1 has shifted north in experiment 2

to west of the IP. In addition, a large region of EKE is found in experiment 2 along the northern portion of the IP to Cabo da Roca as well as off the southern coast of the IP. Large areas of EKE south of the Cape Beddouzza area are found in both experiments. The regions with the largest values of EKE can be interpreted as areas where eddies are likely to be generated during the upwelling season.

In the fall (Figure 11d), the coastal equatorward flow moves offshore of Iberia as the temperature front weakens and is displaced offshore. The eddies that formed inshore of the current earlier also begin to propagate westward. Further offshore, a stronger equatorward flow is present (~30-40 cm/s) embedded with numerous cyclonic and anticyclonic eddies. To the south off Cape Beddouzza and Cape Ghir a strong filament forms with a cold core eddy at its western extent and a warm core anticyclonic eddy to the northeast.

In the winter (Figure 11e) the coastal jet is displaced even farther offshore by the continuing westward propagation of the nearshore eddies. By November a poleward flow (~20 cm/s) is established in the wake of the westward flow of the surface current and eddies (Figure 11g). This flow lasts through December and is likely due to forcing by the weak poleward winds of November (Figure 2d) and December.

Experiment 2 shows that irregularities in the coastal geometry are key elements for "anchoring" upwelling and filaments to geographical features. It also shows that coastline irregularities aid in the development and growth of meanders and eddies.

C. COMPARISONS OF MODEL RESULTS WITH OBSERVATIONS

It is useful to do a comparison of model results with available field and satellite observations to ensure they are consistent with actual features of the CCS. Although direct comparisons are not valid since the studies are not hindcasts, but idealized process-oriented studies, it can be shown that the phenomenonological model behavior is qualitatively similar to the observed data. General features of the Canary Current are apparent from satellite images as well as measured current data. The discussion in the ensuing paragraphs details the general features, and then discusses the specific magnitudes and characteristics along the western coasts of the IP and Northwest Africa. Overall, the results of the model simulations of experiment 2 highlight the major characteristics of the CCS with impressive similarities to field observations.

1. Comparison of Ocean Currents

The major characteristics of the modeled Canary Current off western Iberia and northwestern Africa are consistent with the few field observations and studies available. Satellite imagery also reveals a system of meanders, eddies, and along-shelf jets, on a range of length scales that correspond closely with model output.

a. Equatorward Flow

In experiment 2, the numerical model, through the use of climatological wind data and a realistic coastline, develops an ocean current that contains many features

observed in the CCS. The existence of a mean broad equatorward flow throughout the entire model domain matches the general description of classical EBCs by Wooster and Reid (1963). In addition, the sustained magnitudes of the model's equatorward flow compares favorably with available data. For example, Figures 14a and 14b from DMAH/TC (1988) show a mean flow of 0.5 to 0.7 kts (~25-35 cm/s) with occasional jets reaching 2 to 2.5 kts (~100-125 cm/s), which are consistent with velocities found in the model simulations.

b. Poleward Flow

The model establishes a poleward undercurrent with a core at ~300-400 m depth but extending to over 1200 m depth, with magnitudes consistent with observations from current measurements noted by Haynes and Barton (1990) of ~20 cm/s with a core depth ranging between 100 and 600 m. Ambar (1982) discusses the existence of three separate cores (~400 m, 600-900 m, and 1100-1200 m depth) of poleward MO (with velocities of ~18-29 cm/s) existing along the southern coast of the IP in the Gulf of Cadiz and extending to the north along the entire western coast of the IP. The model depicts this deep poleward undercurrent (~10-15 cm/s) as well (Figures 5, 7b, 12b, and 12c).

The model also depicts a narrow (~50 km), weak (~15-20 cm/s) surface poleward flow, extending to ~400 m depth. The flow is found close to shore in the northern portion of the model domain during December (Figures 11e and 11g). This corresponds well to the shift in the climatological winds from northerly to southwesterly allowing the equatorward flow to diminish. Recent studies by Frouin *et al.*, (1990) and

Haynes and Barton (1990) using high resolution infra-red images from NOAA7 and NOAA9 and numerous in-situ measurements reveal the existence of a surface poleward flow off the northern coast of Portugal and northwestern Spain. These studies show a current ~25-40 km wide, with speeds ~25 cm/s, extending to ~200 m depth.

2. Comparison of Eddies

Observations by Fiuza (1984) show pairs of mesoscale eddies on the order of 100 km exist off the west coast of Iberia (Figure 15). This study, as well as new high resolution satellite imagery confirms the models generation of numerous eddies in the CCS.

In experiment 2, the onset of instabilities occurs at preferred locations. These locations are where the coastline significantly changes, i.e., near Porto, Cabo da Roca, Cabo de Sines, Cabo de Sao Vincent, the Gulf of Cadiz, and Cape Beddouzza/Cape Ghir (Figure 1). Figure 15 shows a satellite image that agrees with some of the west coast preferred locations for the formation of meanders and eddy positions, while Figure 16 shows that the model also forms eddies in similar locations.

3. Comparison of Upwelling

Because the currents are dependent on the winds and the winds have been shown to oscillate seasonally, upwelling off the coast of Portugal (Fiuza *et al.*, 1982) as well as along the coast of the rest of the model domain also varies with the seasons. Upwelling is observed off Portugal from ~43° N to Cabo de Sao Vincent in the south (Figure 17) and

along the southern coast of Portugal to Cabo de Santa Maria, ~8° W (Figure 18), which the model depicts quite well (e.g., Figure 11b). Observations of upwelling at its maximum during the summer and early autumn are shown in Figures 19 and 20, while Figure 21 shows the model depicting increased upwelling during this period as well. Weak to non-existent upwelling is observed to occur along the northern coast of Morocco, then increases again south of 33° N, near Cape Beddouzza (Figure 22)(Fiuza 1982). As the Azores High migrates north, the upwelling first appears off Cape Ghir/Cape Beddouzza in early May as seen in Figures 23a and 23b of Van Camp *et al.* (1991), then gradually moves north up the Moroccan coast. This is simulated by the model and depicted in Figures 11b, 21, and 24.

4. Comparison of Filaments

Several studies have been done that show the existence of cold filaments extending off the coasts depicted in our model: Fiuza (1983), Barton (1986), and Fiuza and Sousa (1989), off the northwest coast of Iberia; Folkard *et al.,* (1997) off the southern coasts of Portugal and Spain in the Gulf of Cadiz; and Van Camp *et al.,* (1991) and Hagen *et al.,* (1996) near Cape Ghir off northwest Africa.

a. West Coast of Iberia

Fiuza (1983) was the first study indicating the existence of filaments off the west coast of Iberia. Additional studies by Fiuza and Sousa (1989) confirmed the existence of filaments using CTD data and satellite imagery in which several filaments

appear including a large filament off Cabo da Roca (Figure 25). In addition, recent sea surface temperature (SST) observations show several good images of filaments occurring along the entire western coast of Iberia (Figure 19) with a particularly long filament near 40.5° N. The model depicts filaments in many of the same locations as well (Figure 21). A rather strong filament exists near ~40.5° N as well as one further south at ~39.5° N. A small filament is also evident at ~37.5° N. Figure 11a shows a filament off Cabo da Roca with a striking resemblance to the filament in Figure 25.

b. South Coast of Iberia/Gulf of Cadiz

Folkard *et al.*, (1997) investigated the waters of southern Iberia in the Gulf of Cadiz. In that study he observed filaments extending off the coast during March and October (Figures 26 and 27). The model depicts these filaments as well: a coastal jet deflected offshore near ~8° W, Cabo de Santa Maria, advects cold upwelled water offshore (Figures 28 and 29).

c. Cape Ghir/Northwest Africa

Consistent with satellite observations (Figure 23) of Van Camp *et al.*, (1991) and satellite observations (Figure 30) coupled with CTD surveys (Figure 31) from Hagen *et al.*, (1996), a filament of cold upwelled water extends off Cape Ghir near 31° N for about 200 km. The model depicts this filament as an equatorward meandering coastal jet which transports cold upwelled water offshore. Observations show that the coastal jet

and subsequent frontal zone caused by the advected cold water results in the generation of a cyclonic eddy-like feature on the cold water side, while an anticyclonic eddy forms on the warm water side (Figure 32). Most of the general features of the filament are depicted well in the model; however, the placement and orientation of the filament are slightly off. The model places the filament extending offshore at about 32° N with a northwest/southeast orientation. This discrepancy may be due to the lack of bottom topography in the model since topographic influence of the Cape Ghir Plateau on the actual formation of the filament has been demonstrated by Hagen *et al.* (1996).

The variety of length scales and life time scales, in conjunction with the differences in field observations themselves, emphasize the complex flow region of the CCS. Except for the slight disagreement with placement and orientation of the cold filament off Cape Ghir, the numerical model results of experiment 2 show striking similarities to the field observations.

IV. SUMMARY

This study was designed to investigate the role of wind forcing and coastal geometry in the formation of currents, eddies, and filaments in the Canary Current system. It was found that wind forcing can set up coastal currents, which can subsequently become unstable and lead to the formation of many of the observed features in the CCS. To demonstrate that wind forcing can create both a surface current and an opposing undercurrent, a high resolution, multi-level, PE model was forced from rest with spatially and temporally varying winds. The major components of the currents developed quite rapidly, generating both horizontal (barotropic instability) and vertical (baroclinic instability) shears which caused the currents to become unstable, resulting in the formation of meanders. As the meanders grew, eddies developed along with areas of increased upwelling. In time, filaments also formed as the meanders intensified and advected cold upwelled water offshore.

A seasonal cycle was also identified, as was expected due to the temporal nature of the seasonal winds. Obviously there is a distinct upwelling season tied to the migration of the Azores High. In addition to this, however, is the generation of a seasonal surface equatorward coastal jet overlying a poleward undercurrent that occurs during the upwelling season. The eddy formation along the coast also appears to be seasonal, forming during the height of the upwelling season, when the coastal jet is at its maximum strength. In addition, filaments appear to be seasonal, occurring during and just after the

upwelling season; however, some filaments do occur during other seasons, especially off Iberia where cold water exists nearshore throughout the year.

The meanders and some eddies appear as quasi-permanent features. A relatively large anticyclonic eddy develops in the Gulf of Cadiz and remains there year-round. Additional quasi-permanent meanders and eddies play a significant role in the modification of the coastal current, upwelling, and filament formation.

Irregularities in the coastal geometry also appear to be significant factors in the formation of certain features as well as for enhancing the growth of meanders, eddies and filaments. Specifically, capes are significant in the location and formation of filaments, providing an area of enhanced upwelling as well as acting a barrier to force the coastal jet offshore.

A comparison of model results with available observations show that while both experiments successfully simulate most of the features of the CCS, experiment 2 shows better agreement between current velocities and feature placements. Although experiment 2 simulated most features well, some discrepancies existed. For example, the positioning of the Cape Ghir Filament placement in the model run is approximately half a degree north of its actual position. This may be due to the lack of bottom topography in the model, since Hagen *et al.* (1996) suggests that the Cape Ghir Plateau influences the formation of the filament. Another example of placement error due to lack of bottom topography is the

placement of the poleward surface current off northern Iberia. The model places the current approximately one degree closer to the coast than available observations show.

Besides the lack of bottom topography the model also does not include the effects of salinity forcing or an opening of the boundary to the Mediterranean Sea. Several variable salinity inputs exist in the area, including the Mediterranean Sea influence, as well as several large river inflows off northern Iberia and numerous smaller rivers along Morocco. Opening the boundary to the Mediterranean Sea would allow the existence of MO, which would then result in a density-driven component to the undercurrent (in addition to the model-simulated wind driven component). In addition, incorporation of bottom topography, salinity forcing, and MO could result in the proper simulation of other cores of the undercurrent, which have been observed in the region (e. g., Ambar, 1982).

While this study focused on the role of seasonal wind forcing and used the relatively coarse spatial resolution of ECMWF winds, it would be of interest to investigate the role of higher resolution spatial and temporal wind forcing. Fine spatial resolution down to ~1 km combined with fine temporal resolution of ~1 day would allow the oceanic response to wind events, relaxations, and reversals to be studied. Observations have shown that, depending on the prevailing wind direction, an inflow or outflow through the Strait of Gibraltar can exist, which could affect the flow in the Gulf of Cadiz (e.g., Folkard *et al.*, 1997).

Of concern to studies such as this one is the lack of readily available data along both the Moroccan coast and the IP. Few observations exist of the equatorward flow, including velocities and structure. Some data exists on the relatively deep poleward MO and the upwelling along Iberia, and more recently several studies have discussed the poleward surface current located off northern Iberia. In addition, several studies discuss briefly the surface temperature, salinity, and density patterns off northwest Africa and of the Cape Ghir Filament, but little discussion is available about the basics. This area is a prime candidate for a refreshing update of the generalization given the Canary Current by Wooster and Reed (1963).

Nevertheless, the results from these model runs show surprising similarities to the large-scale observational data available in the area studied. This supports the hypothesis that wind forcing coupled with irregular coastal geometry are key issues in the generation, evolution, and sustainment of the currents, and other unique feature including meanders, eddies, and filament structures of the CSS.

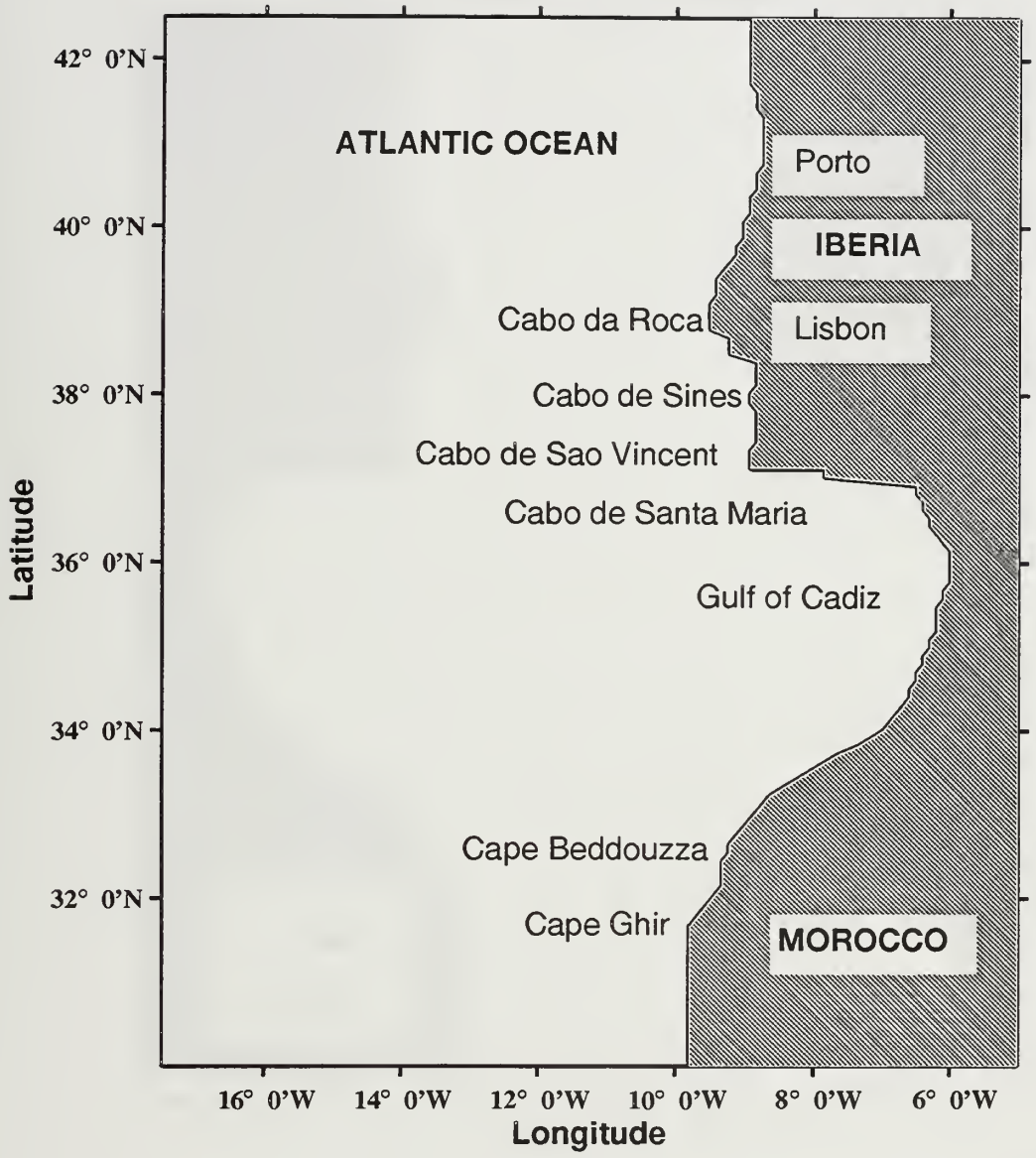

Figure 1. Domain of the model for the Canary Current System (CCS) off the western coast of the Iberian peninsula and northwest Africa. The domain is bounded by 30° N to 42.5° N, 5° W to 17.5° W. The figure also shows the major geographical features.

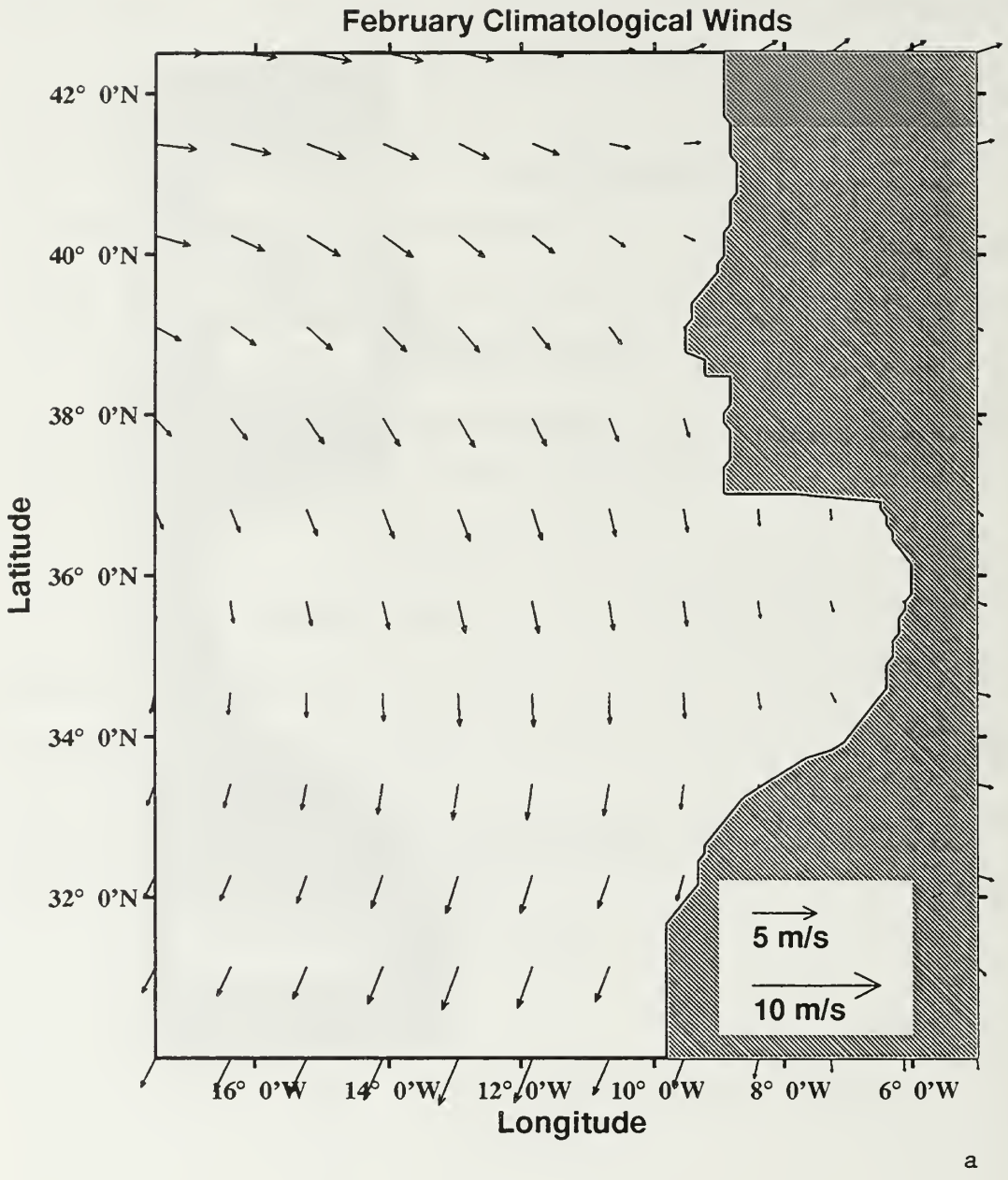

Figure 2. Climatological (1980-1989) ECMWF winds in m/s used in experiments 1 and 2: (a) February, (b) July, (c) September, (d) November.

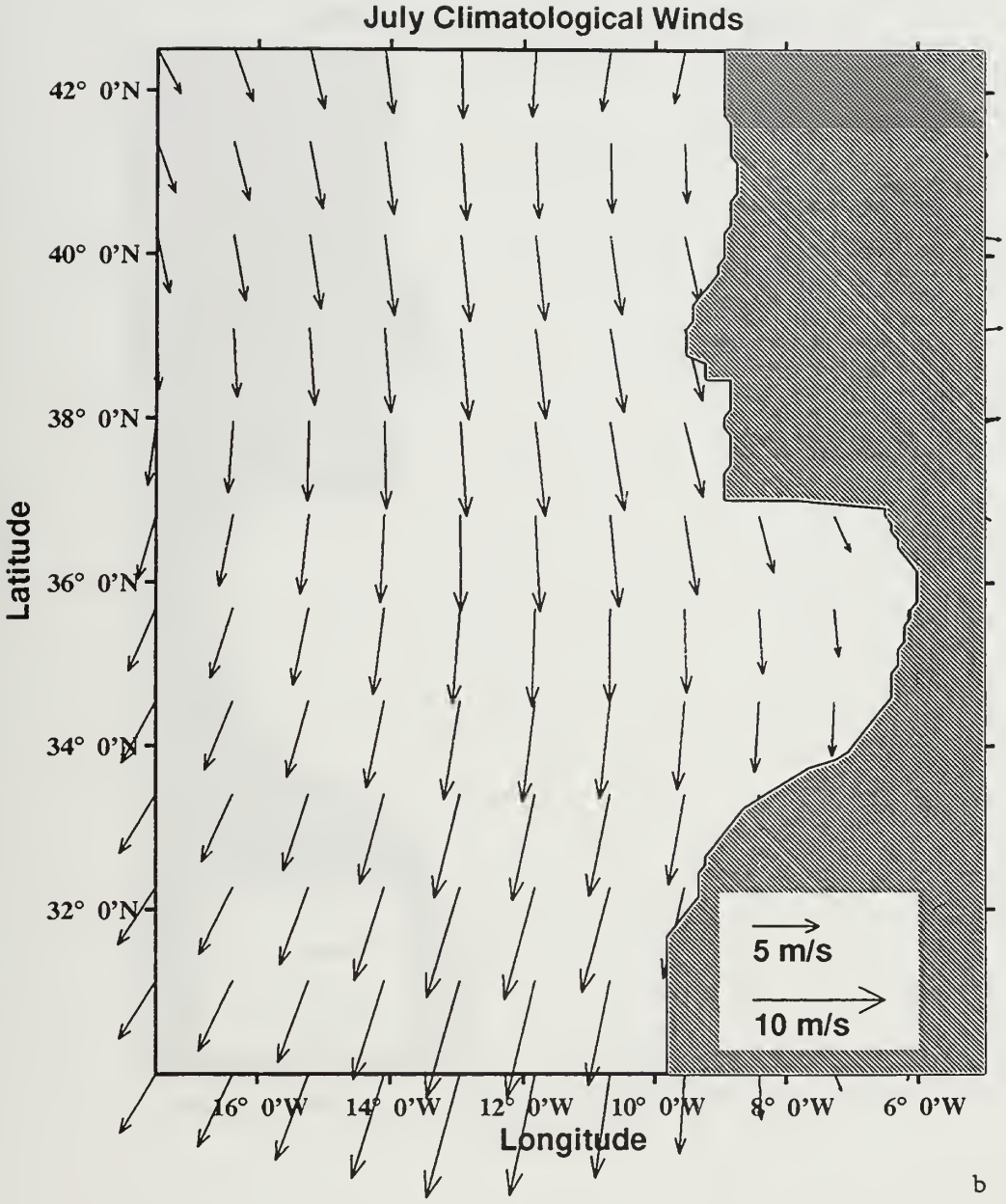
July Climatological Winds
42° 0'N
40° 0'N
38° 0'N
36° 0'N
34° 0'N
32° 0'N
Latitude
16° 0'W
14° 0'W
12° 0'W
10° 0'W
8° 0'W
6° 0'W
Longitude
5 m/s
10 m/s

b

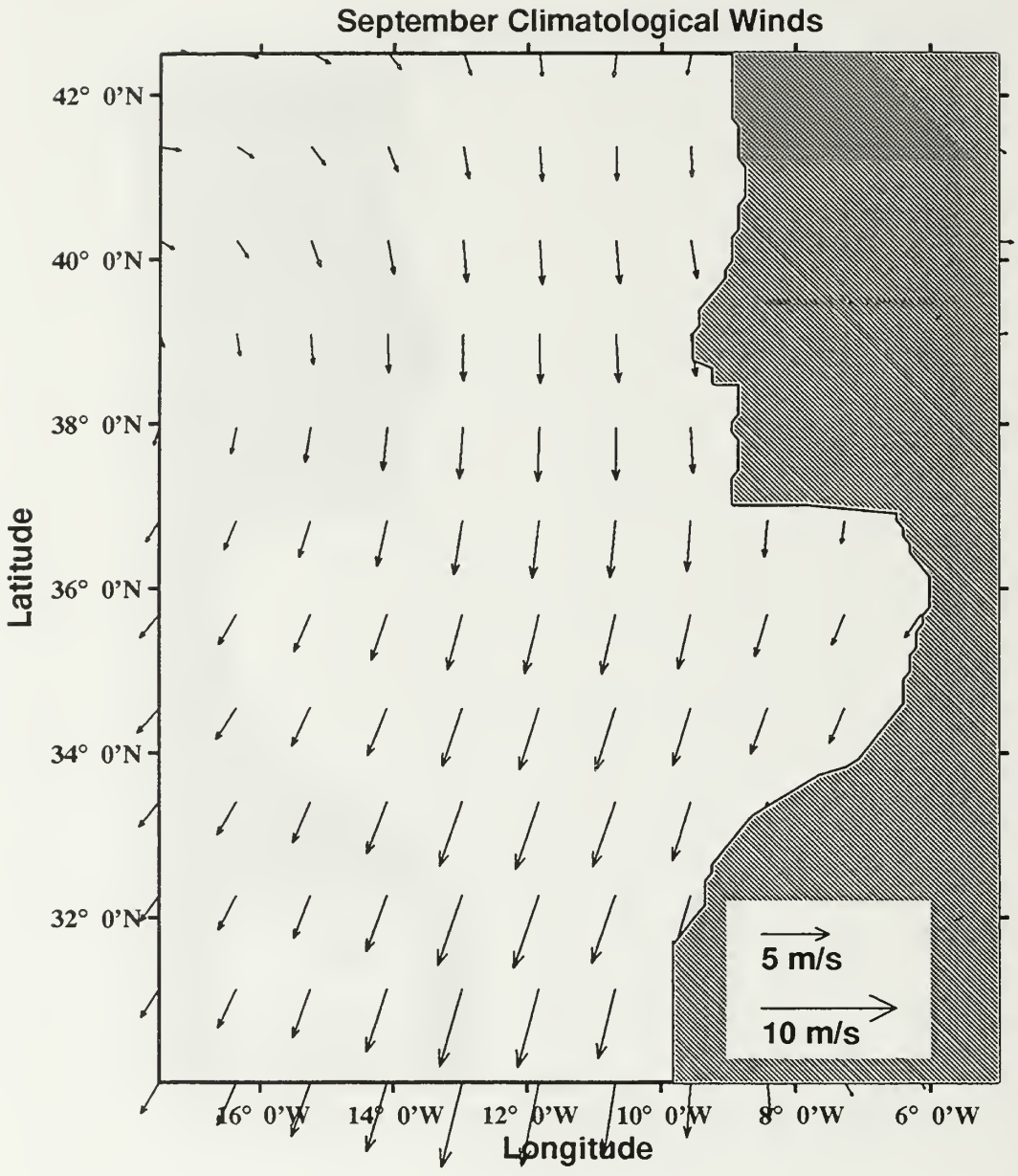
September Climatological Winds
42° 0'N
40° 0'N
38° 0'N
36° 0'N
34° 0'N
32° 0'N
Latitude
16° 0'W
14° 0'W
12° 0'W
10° 0'W
8° 0'W
6° 0'W
Longitude
5 m/s
10 m/s

c

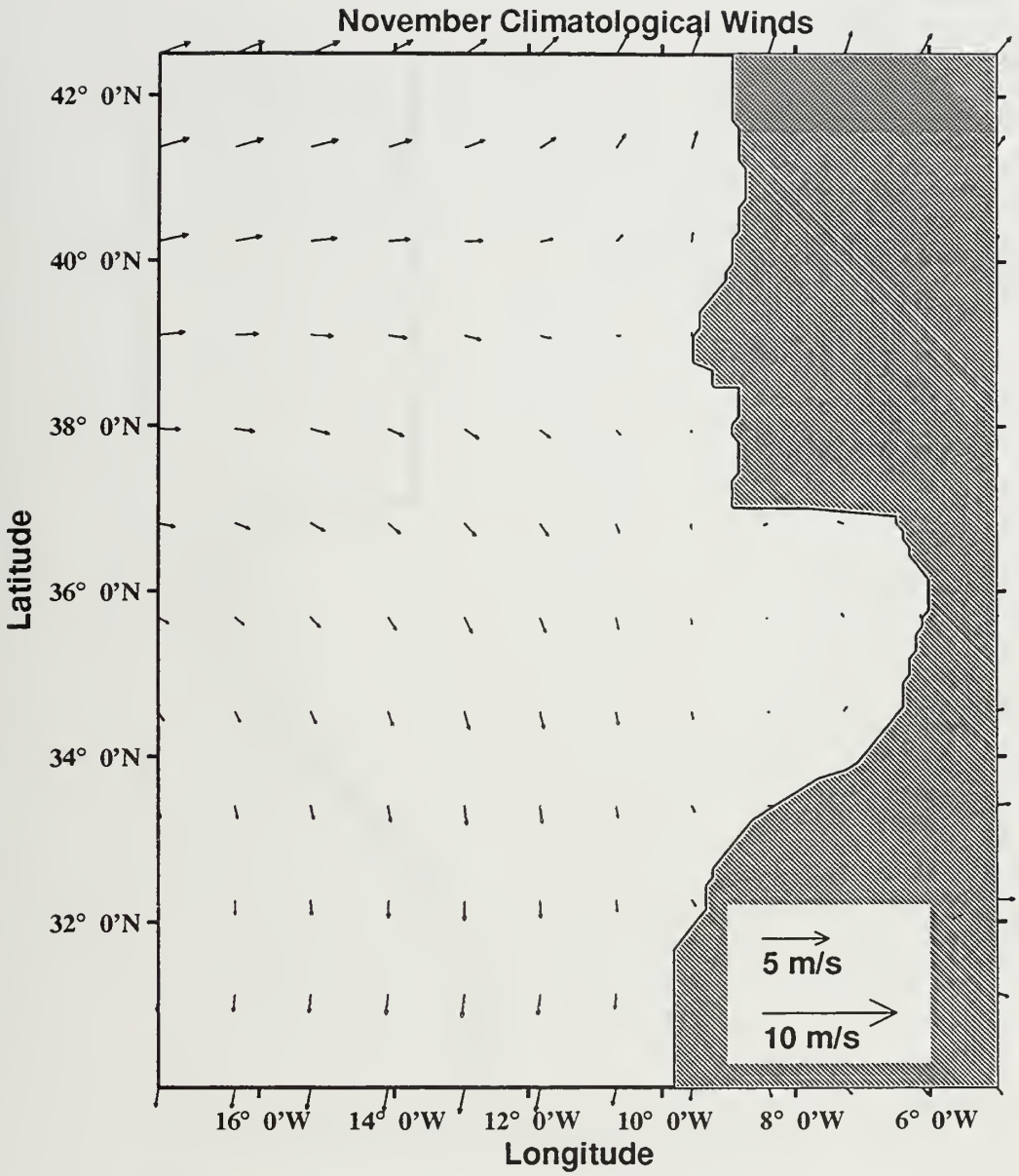
November Climatological Winds
42° 0'N
40° 0'N
38° 0'N
36° 0'N
34° 0'N
32° 0'N
Latitude
5 m/s
10 m/s
16° 0'W
14° 0'W
12° 0'W
10° 0'W
8° 0'W
6° 0'W
Longitude

d

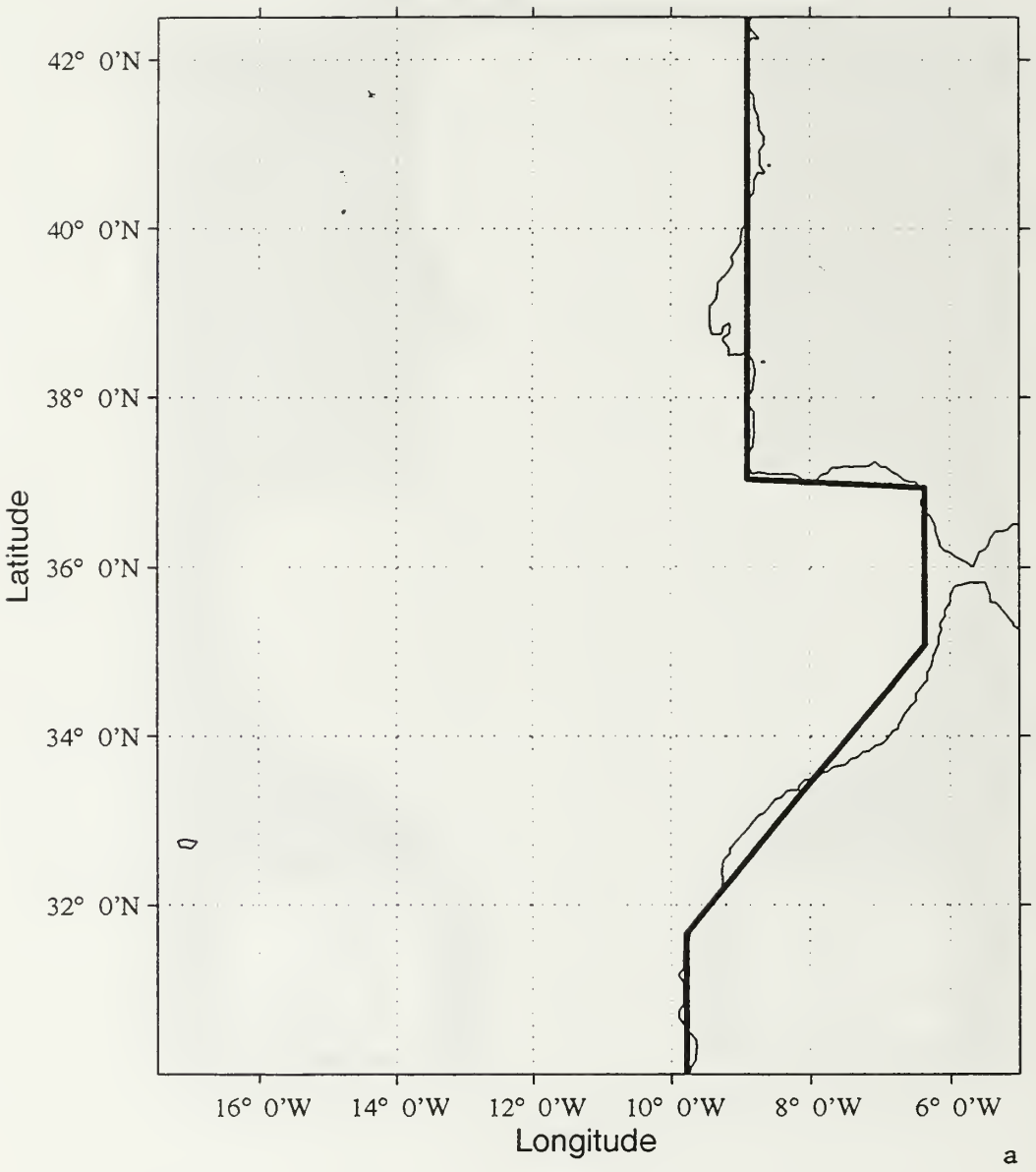

Figure 3. Coastlines used in experiments 1 and 2: (a) The idealized or "straightened" coastline uses a straight coast for the Iberian Peninsula with a 90 corner depicting Cabo de Sao Vincent. The Gulf of Cadiz is then depicted with a straight coast for southern Iberia as well as a portion near the Strait of Gibraltar, and then a sloping straight coast south to an angle depicting the Cape Beddouzza area. (b) The irregular or "realistic" coastline which features the general characteristics and irregularities of the coast in the model domain as described in Figure 1.

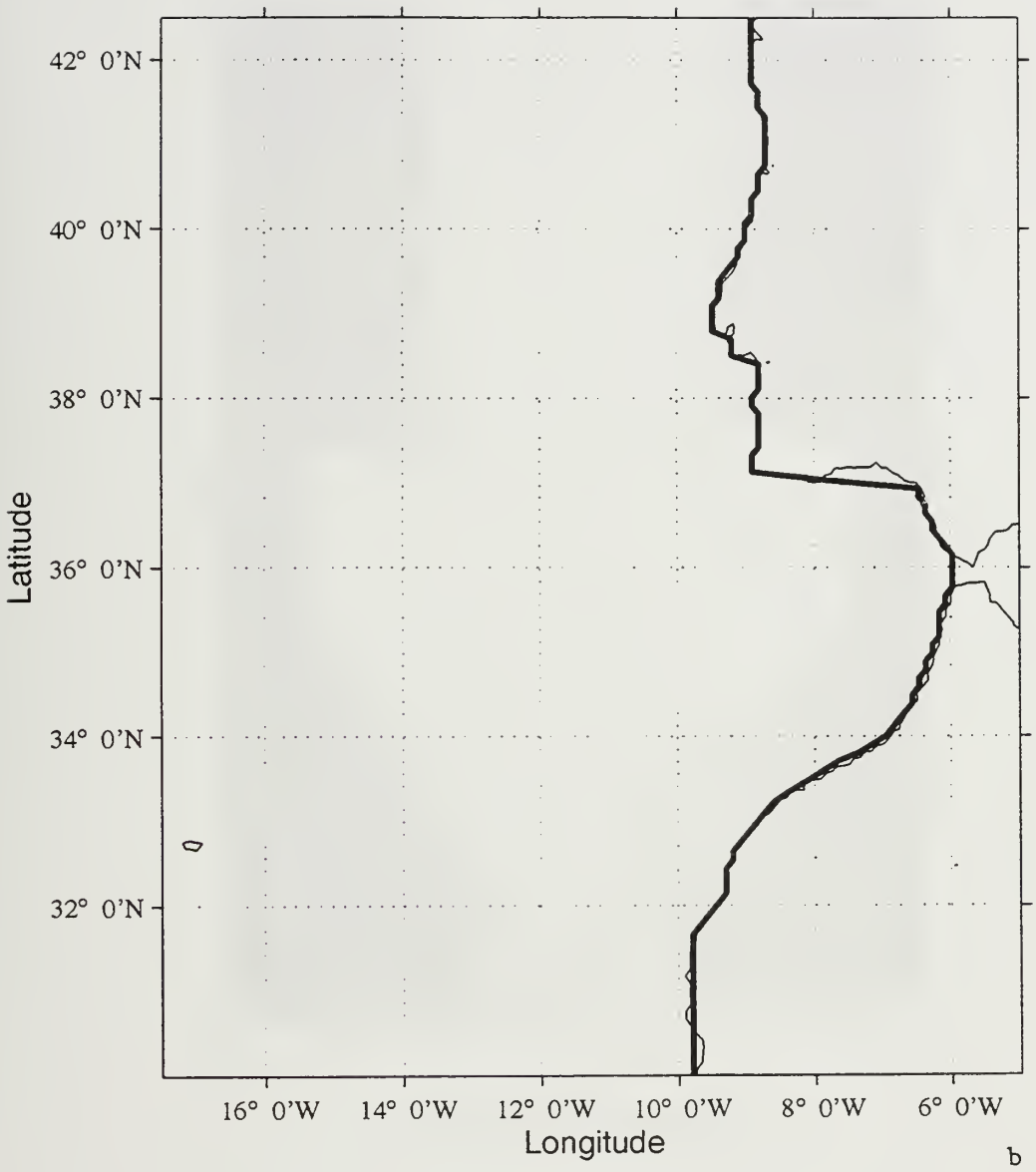
42° 0'N
40° 0'N
38° 0'N
36° 0'N
34° 0'N
32° 0'N
Latitude
16° 0'W
14° 0'W
12° 0'W
10° 0'W
8° 0'W
6° 0'W
Longitude
b

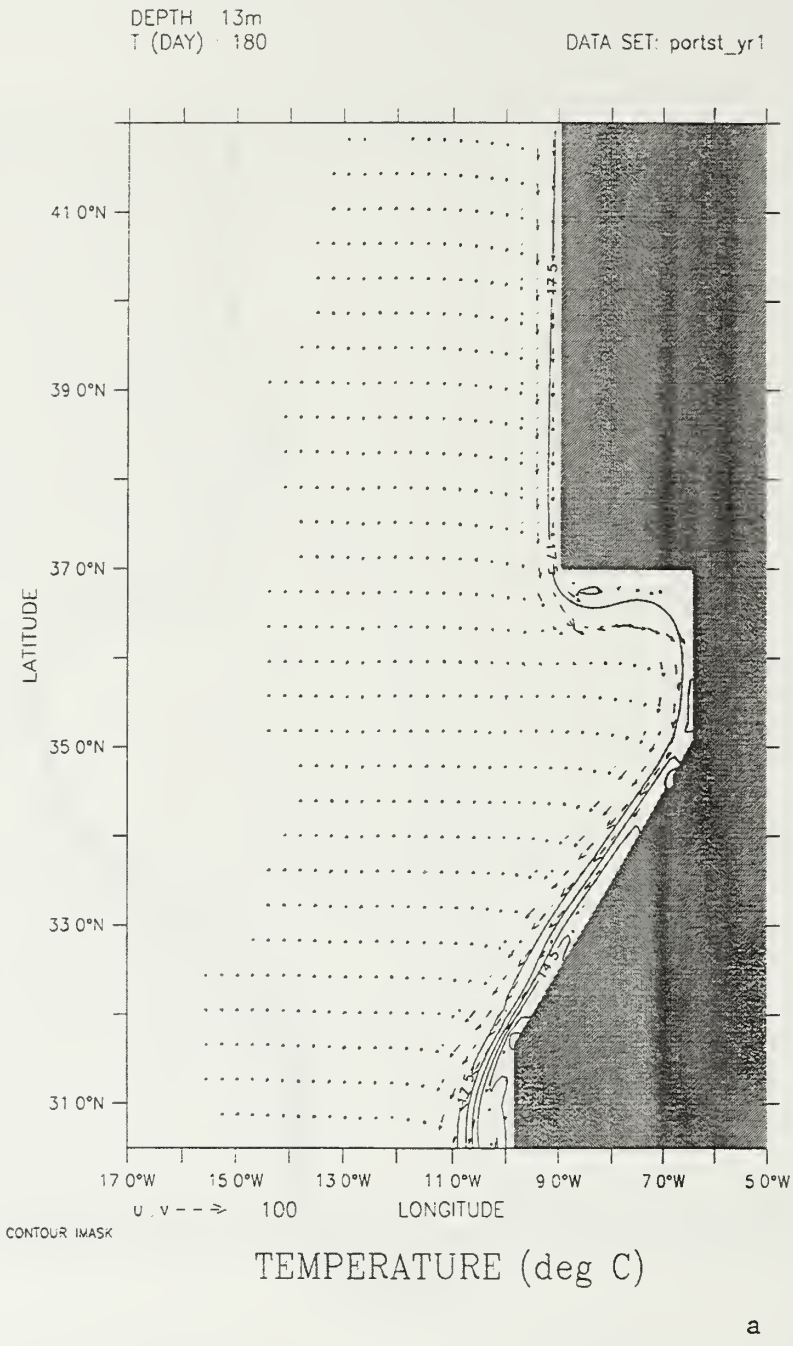

Figure 4. Experiment 1: Temperature contours and velocity vectors at 13 m depth at days (a) 180, (b) 255, (c) 270, (d) 330, (e) 336, and (f) 501 (day 136 of year 2). The contour interval is 1°C. To avoid clutter, the velocity vectors are plotted every third grid point in the cross-shore direction and every fourth grid point in the along-shore direction. Maximum current velocity is 100 cm/s.

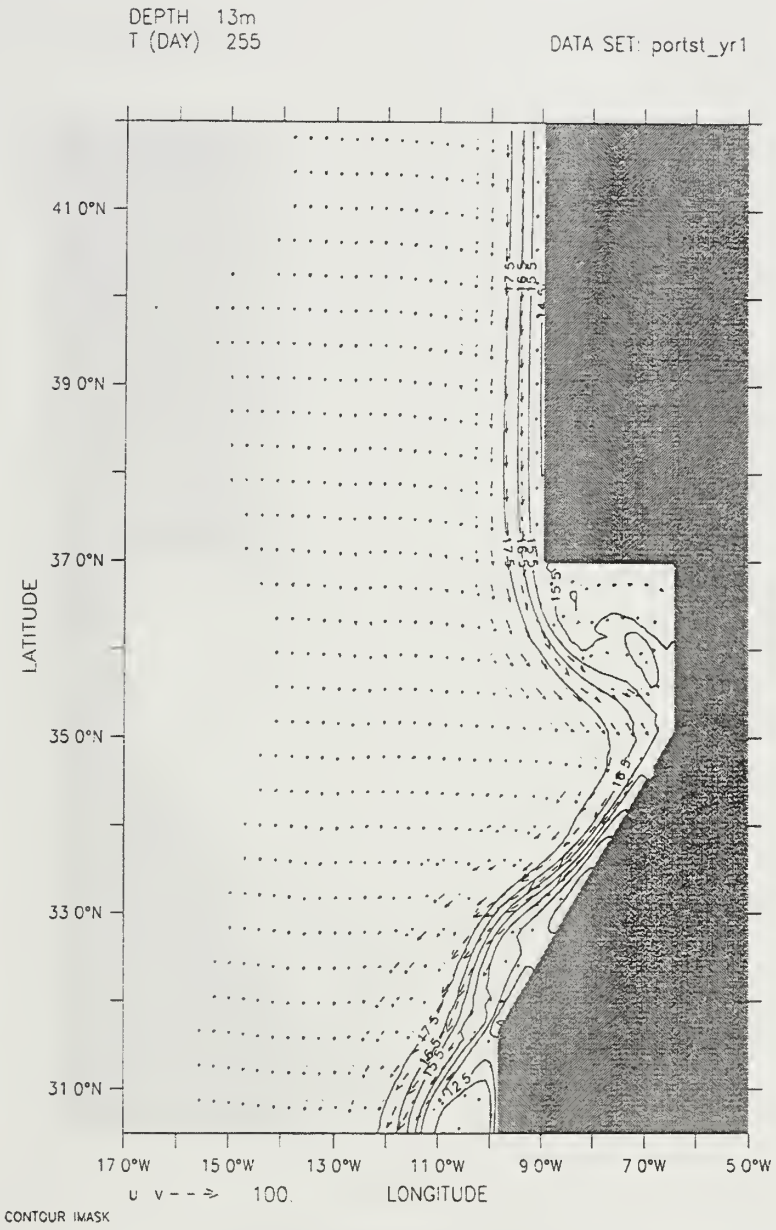
DEPTH 13m
T (DAY) 255
DATA SET: portst_yr1
41 0°N
39 0°N
37 0°N
35 0°N
33 0°N
31 0°N
LATITUDE
17 5
16 5
15 5
14 5
17 0°W
15 0°W
13 0°W
11 0°W
9 0°W
7 0°W
5 0°W
LONGITUDE
u v - - > 100.
CONTOUR IMASK
TEMPERATURE (deg C)

b

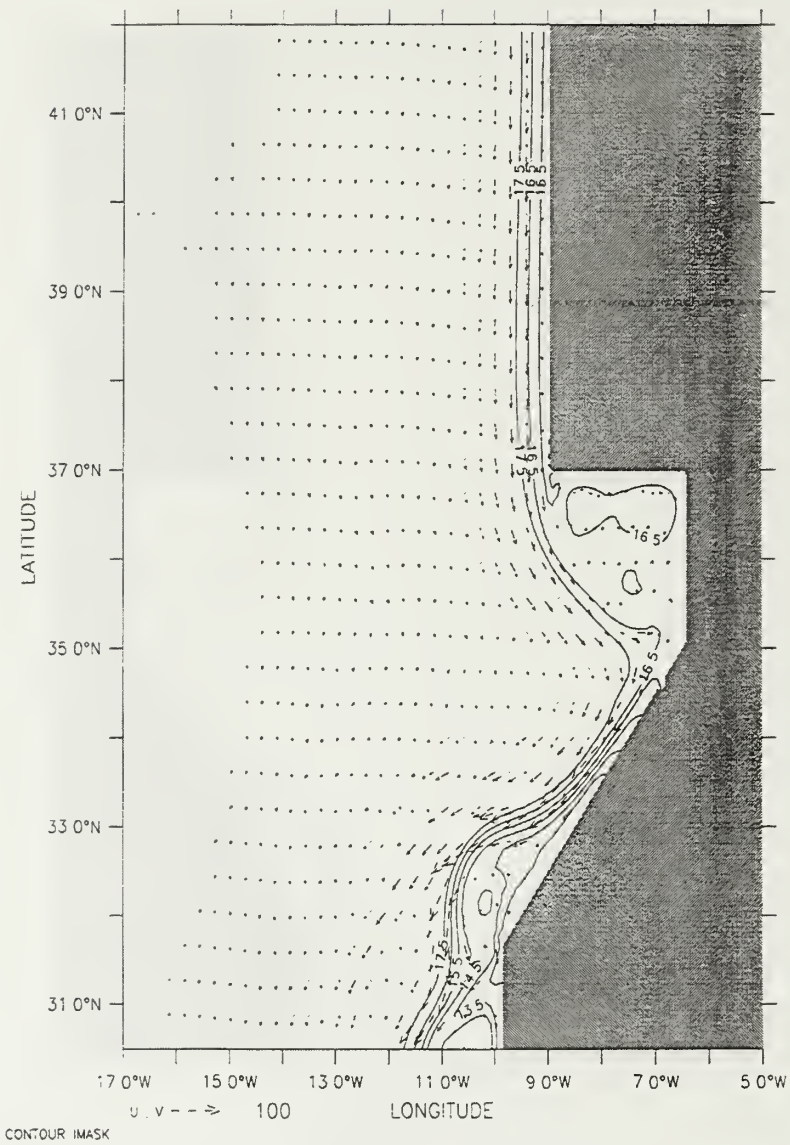
DEPTH : 13m
T (DAY) : 270
DATA SET: portst_yr1
41 0°N
39 0°N
37 0°N
35 0°N
33 0°N
31 0°N
LATITUDE
17 0°W
15 0°W
13 0°W
11 0°W
9 0°W
7 0°W
5 0°W
LONGITUDE
u , v - - > 100
CONTOUR IMASK
TEMPERATURE (deg C)

c

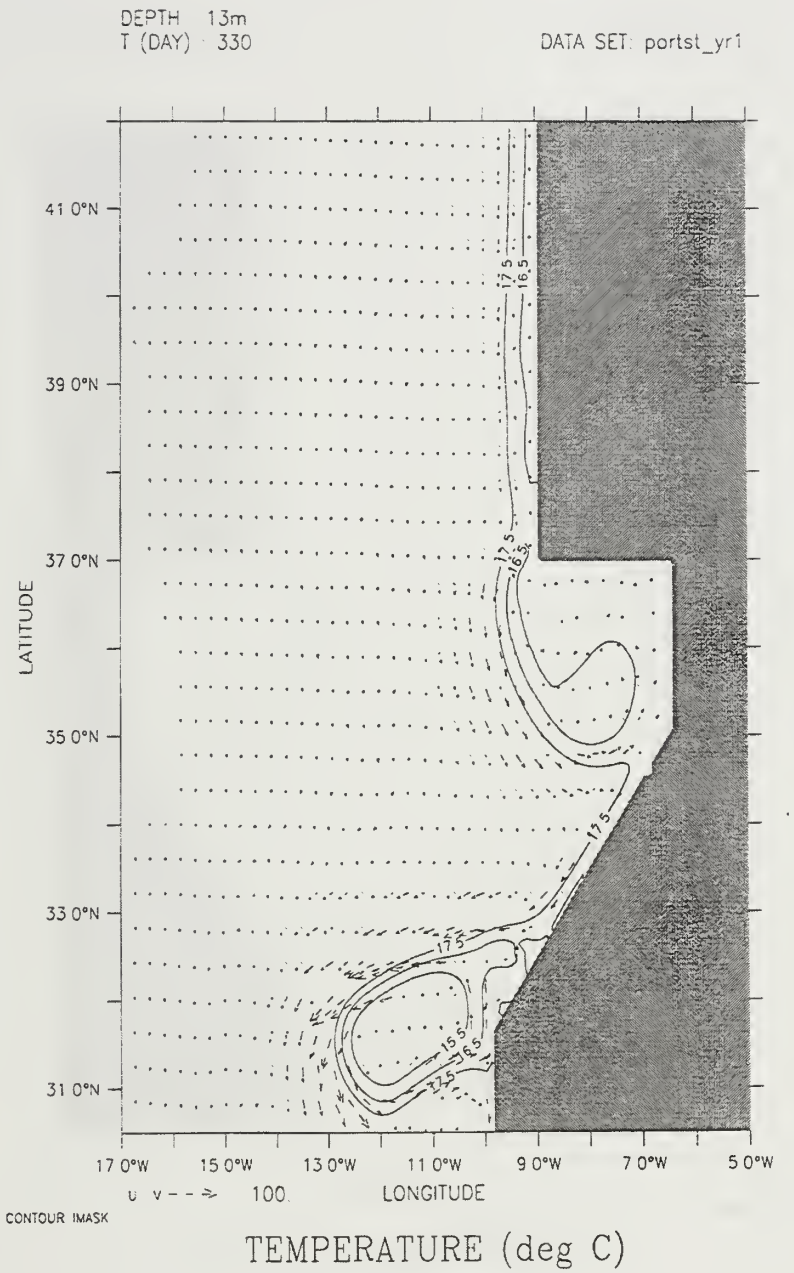
DEPTH 13m
T (DAY) 330
DATA SET: portst_yr1
41 0°N
39 0°N
37 0°N
35 0°N
33 0°N
31 0°N
LATITUDE
17 5
16 5
15 5
17 0°W
15 0°W
13 0°W
11 0°W
9 0°W
7 0°W
5 0°W
LONGITUDE
u v 100
CONTOUR IMASK
TEMPERATURE (deg C)

d

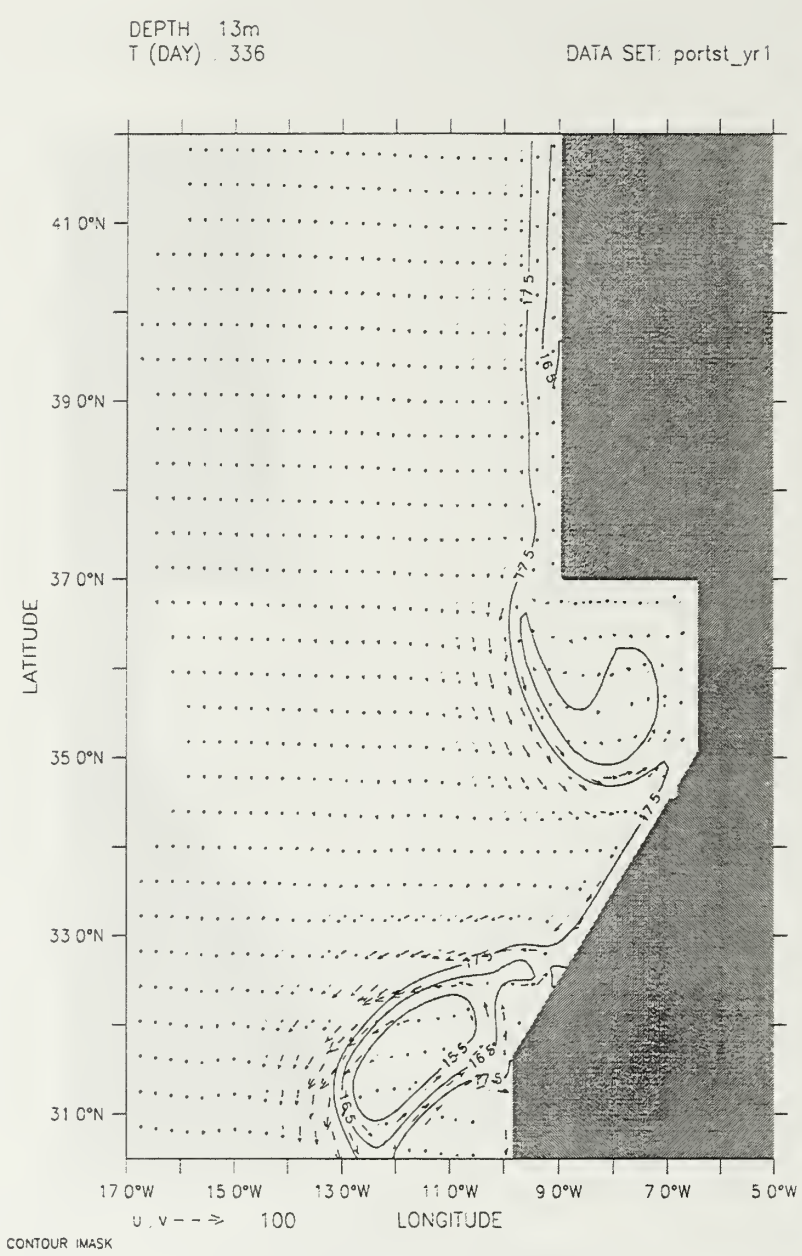

TEMPERATURE (deg C)

e

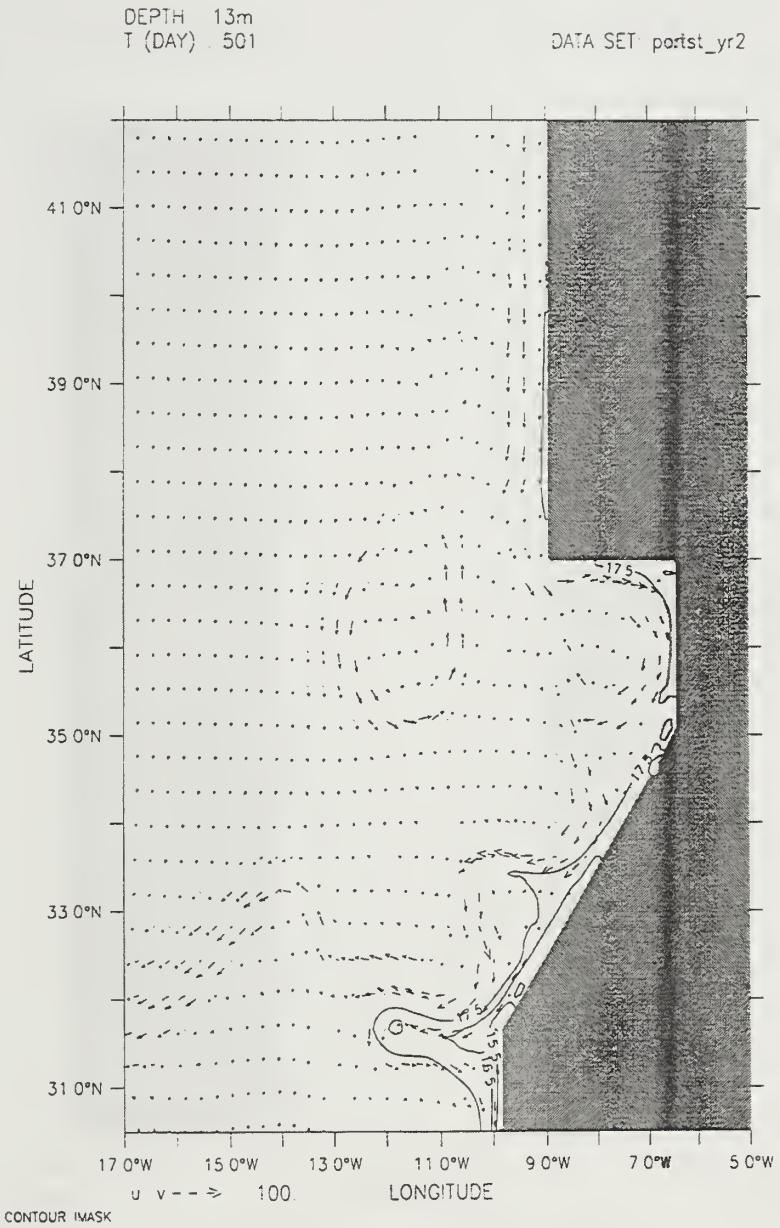
DEPTH 13m
T (DAY) 501
DATA SET portst_yr2
41 0°N
39 0°N
37 0°N
35 0°N
33 0°N
31 0°N
LATITUDE
17 5
17 0
16 5
16 0
15 5
15 0
17 0°W
15 0°W
13 0°W
11 0°W
9 0°W
7 0°W
5 0°W
LONGITUDE
u v - - > 100
CONTOUR IMASK
TEMPERATURE (deg C)

f

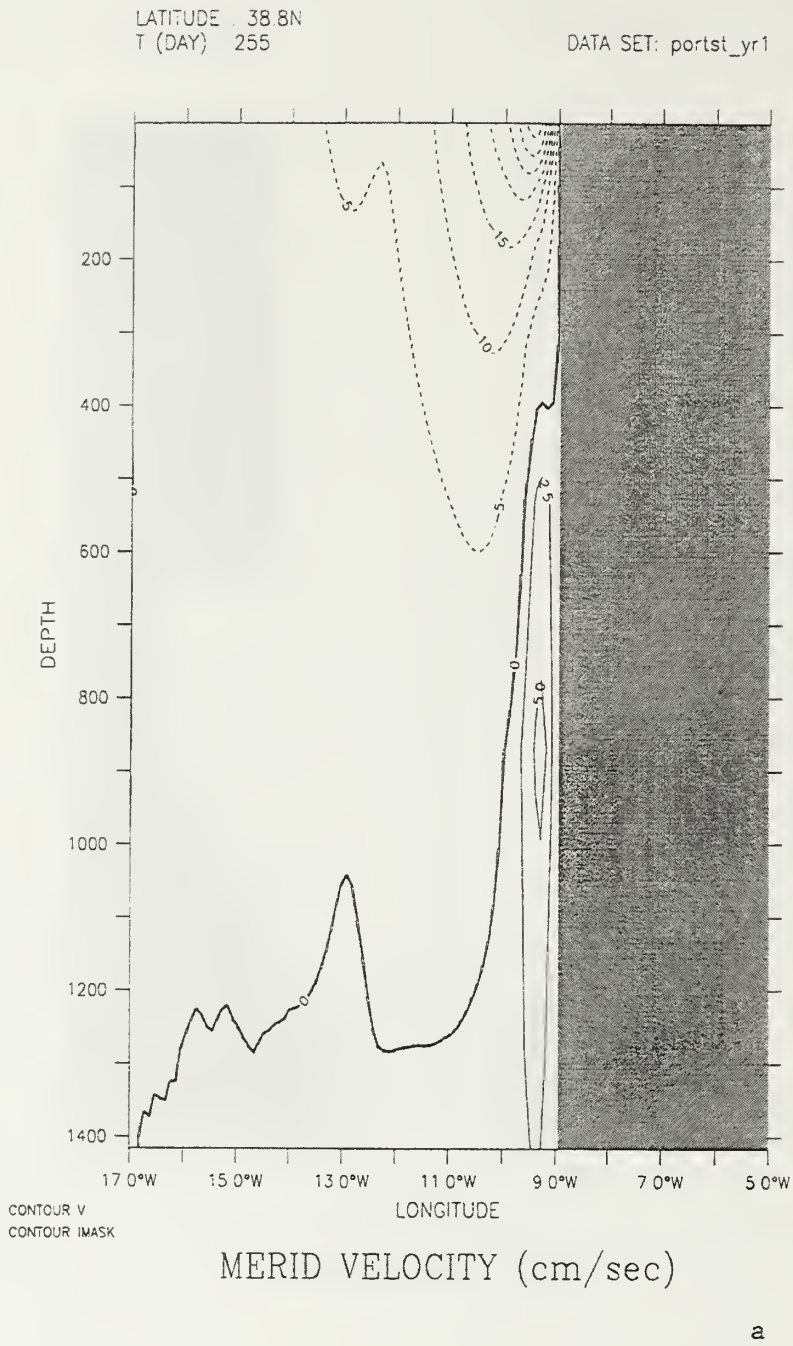

Figure 5. Experiment 1: Cross-shore section at 38.8° N of the meridional component of velocity (v) in the coastal region at days (a) 255 and (b) 309. Solid lines indicate poleward flow, while dashed lines indicate equatorward flow. The contour interval is 2.5 cm/s for poleward flow and 5 cm/s for equatorward flow.

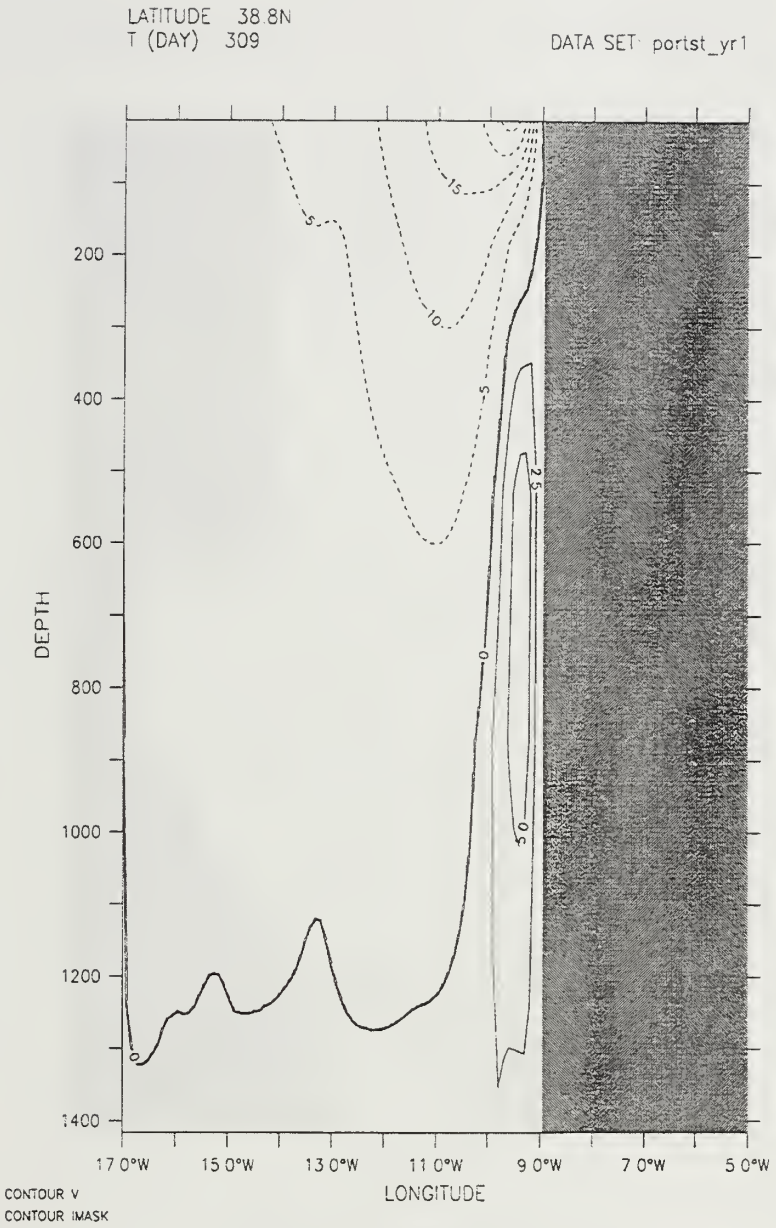
LATITUDE 38.8N
T (DAY) 309
DATA SET: portst_yr1
DEPTH
200
400
600
800
1000
1200
1400
17.0°W
15.0°W
13.0°W
11.0°W
9.0°W
7.0°W
5.0°W
LONGITUDE
CONTOUR V
CONTOUR IMASK
MERID VELOCITY (cm/sec)

b

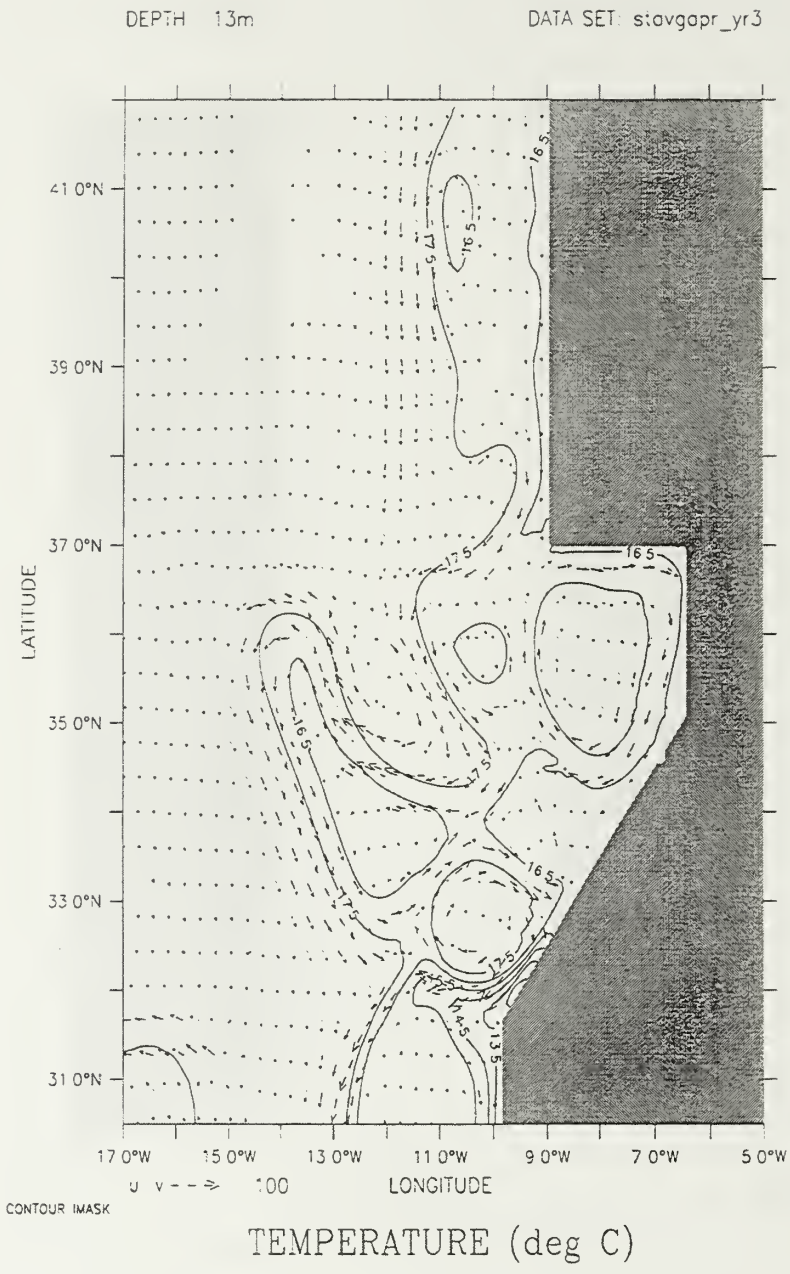

Figure 6. Experiment 1: Temperature contours and velocity vectors at 13 m depth in the third year of the model simulation time-averaged over the months of (a) April, (b) August, and (c) November. The contour interval is 1° C. Maximum current velocity is 100 cm/s.

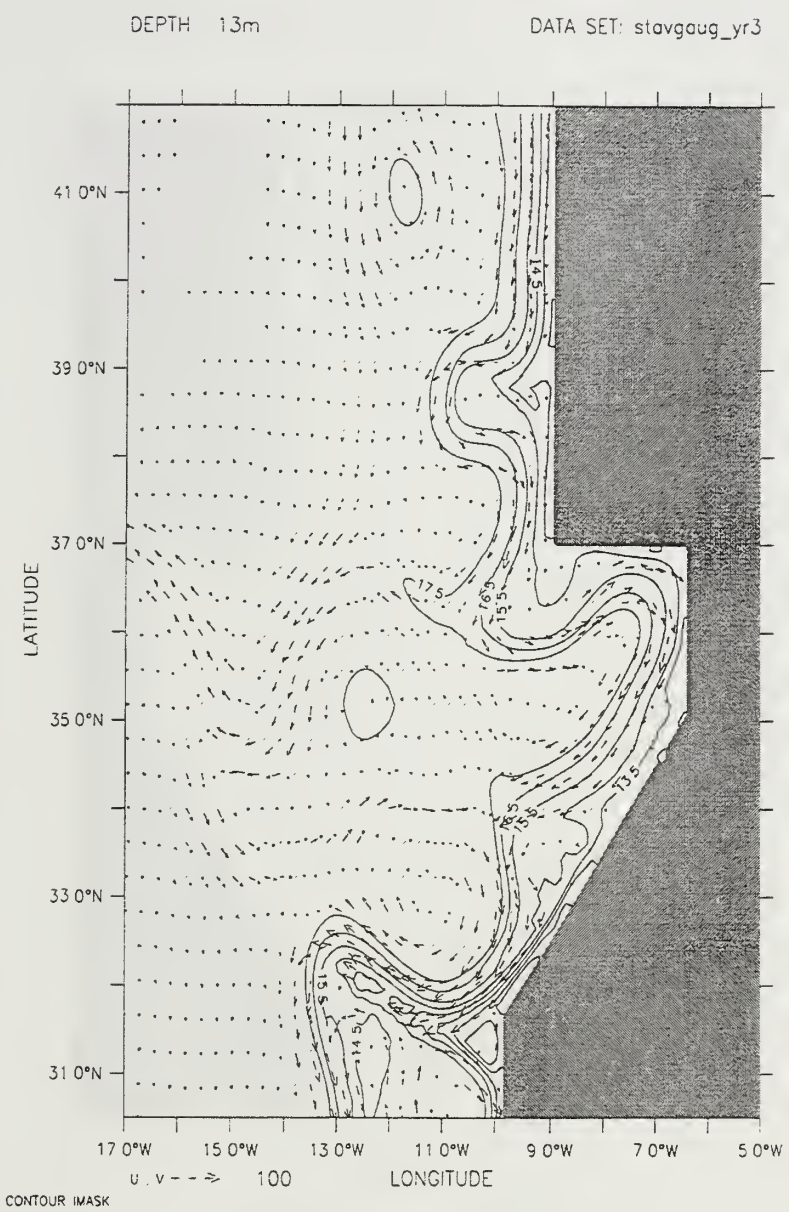

TEMPERATURE (deg C)

b

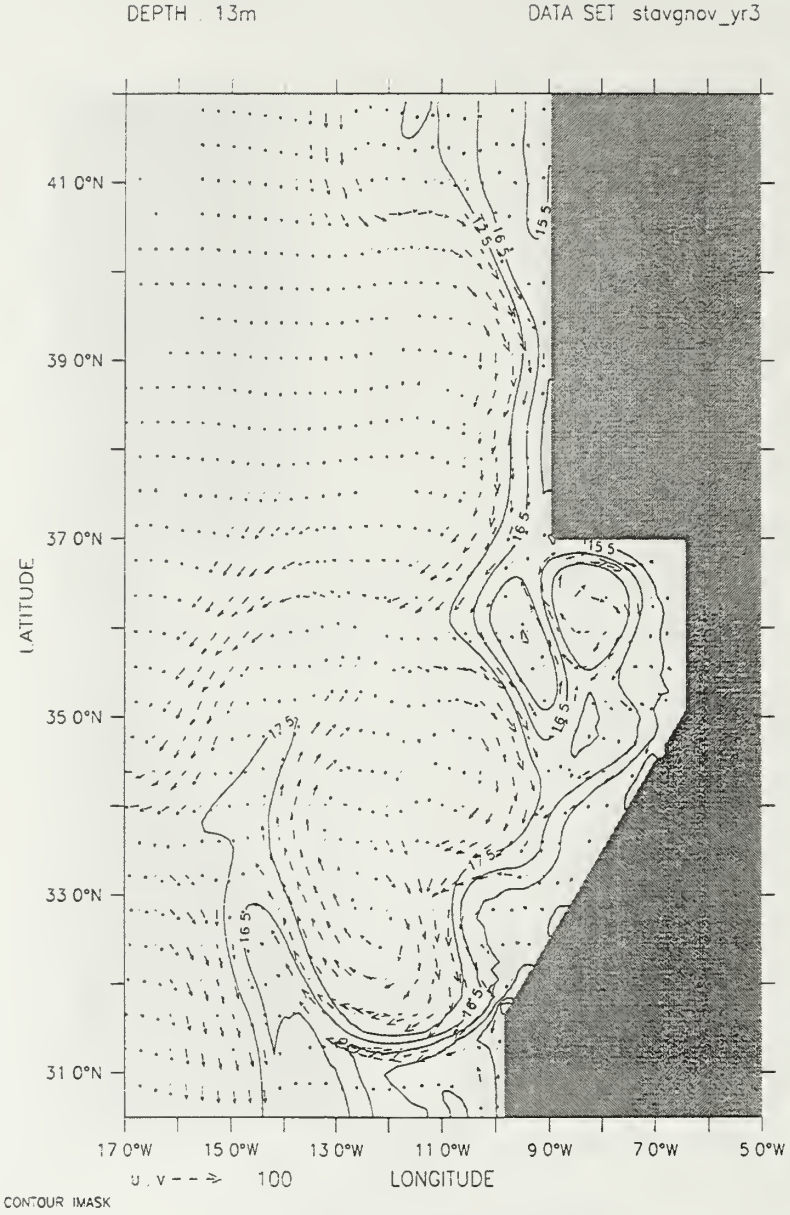
DEPTH . 13m
DATA SET stavgnov_yr3
41 0°N
39 0°N
37 0°N
35 0°N
33 0°N
31 0°N
LATITUDE
17 0°W
15 0°W
13 0°W
11 0°W
9 0°W
7 0°W
5 0°W
LONGITUDE
u , v - - > 100
CONTOUR IMASK
TEMPERATURE (deg C)

c

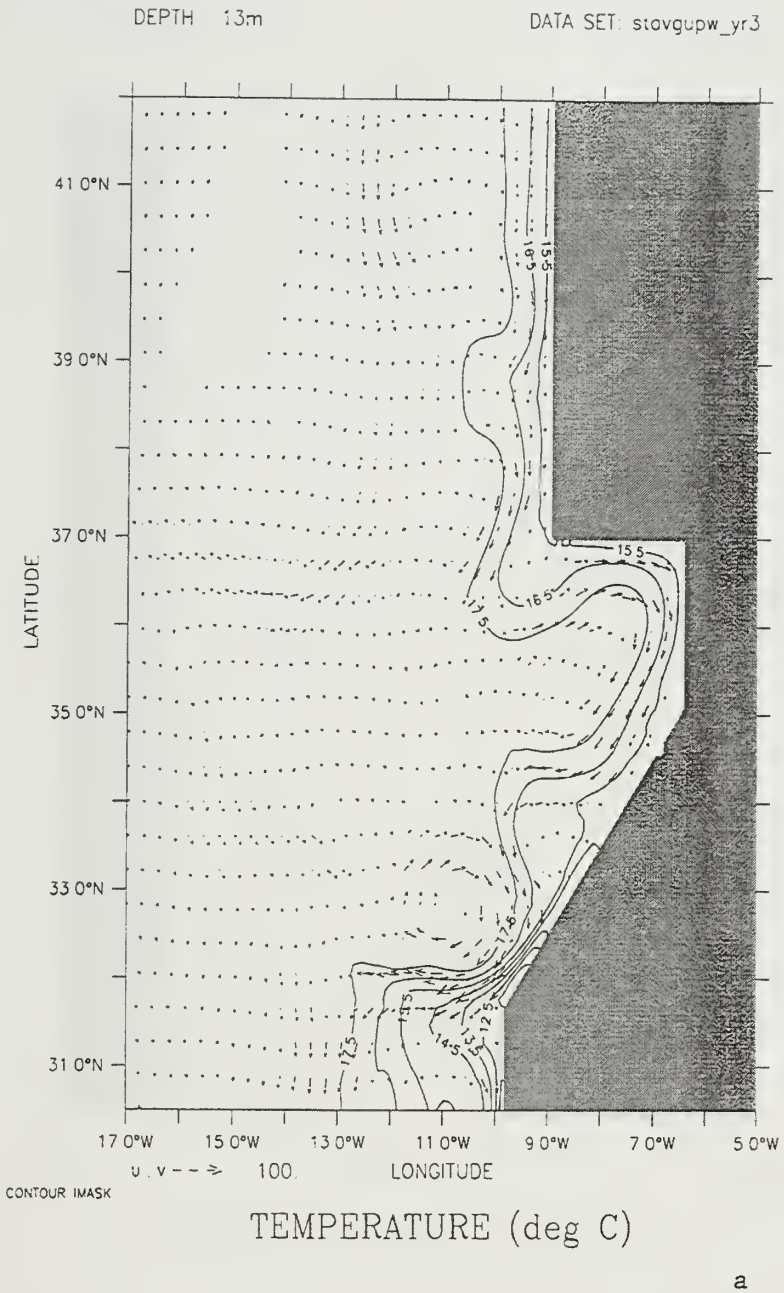

Figure 7. Experiment 1: Time-averaged plots for the upwelling season (April-September) of year 3 of (a) temperature contours and velocity vectors at 13 m depth, and (b) cross-shore section of velocity (v) at 37.7° N. The contour interval is 1° C in (a) and 2.5 cm/s for poleward flow and 5 cm/s for equatorward flow in (b). Maximum current velocity is 100 cm/s.

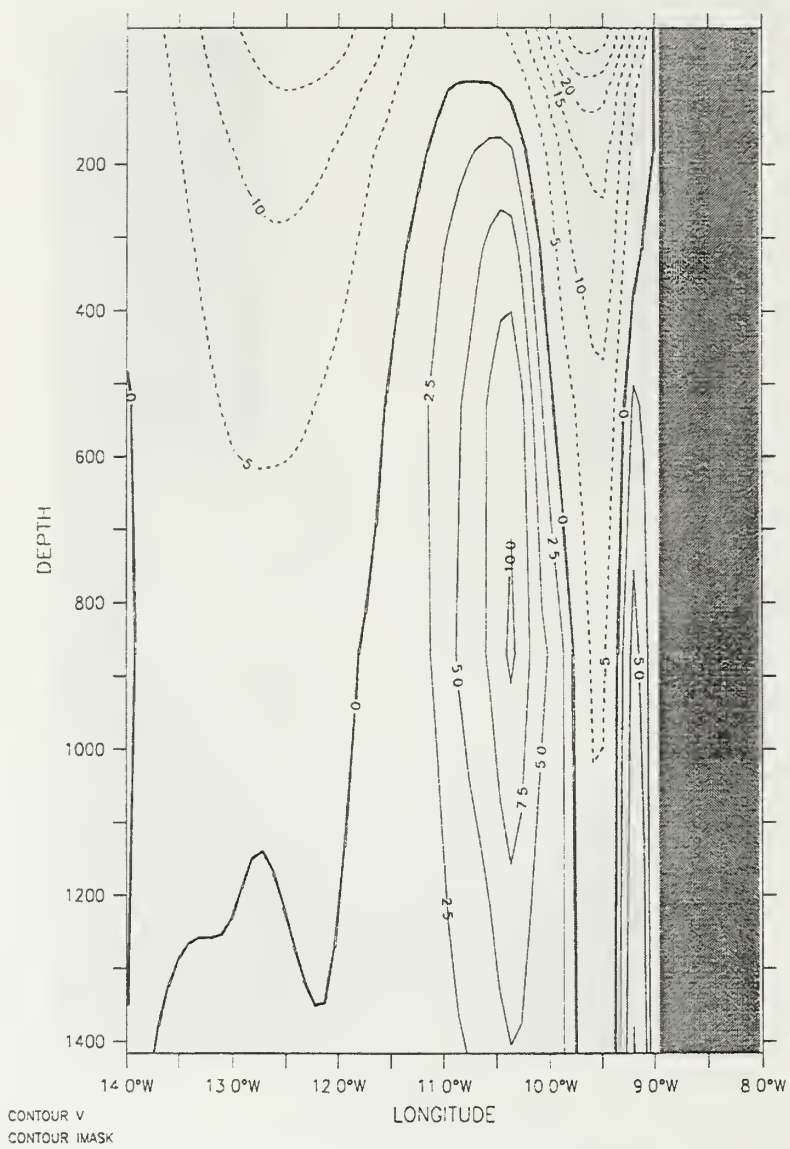
LATITUDE 37.7N
DATA SET: stavgupw_yr3
DEPTH
200
400
600
800
1000
1200
1400
14.0°W
13.0°W
12.0°W
11.0°W
10.0°W
9.0°W
8.0°W
LONGITUDE
CONTOUR V
CONTOUR IMASK
MERID VELOCITY (cm/sec)

b

Figure 8. Experiment 1: (a) Mean and (b) eddy kinetic energy at 13 m depth. Contour interval is 100 cm^2/s^2.


DEPTH 13m
DATA SET: meanupw_yr3
41.0°N
39.0°N
37.0°N
35.0°N
33.0°N
31.0°N
LATITUDE
17.0°W
15.0°W
13.0°W
11.0°W
9.0°W
7.0°W
5.0°W
LONGITUDE
CONTOUR IMASK
EDDY KINETIC ENERGY ((cm/sec)**2)

b

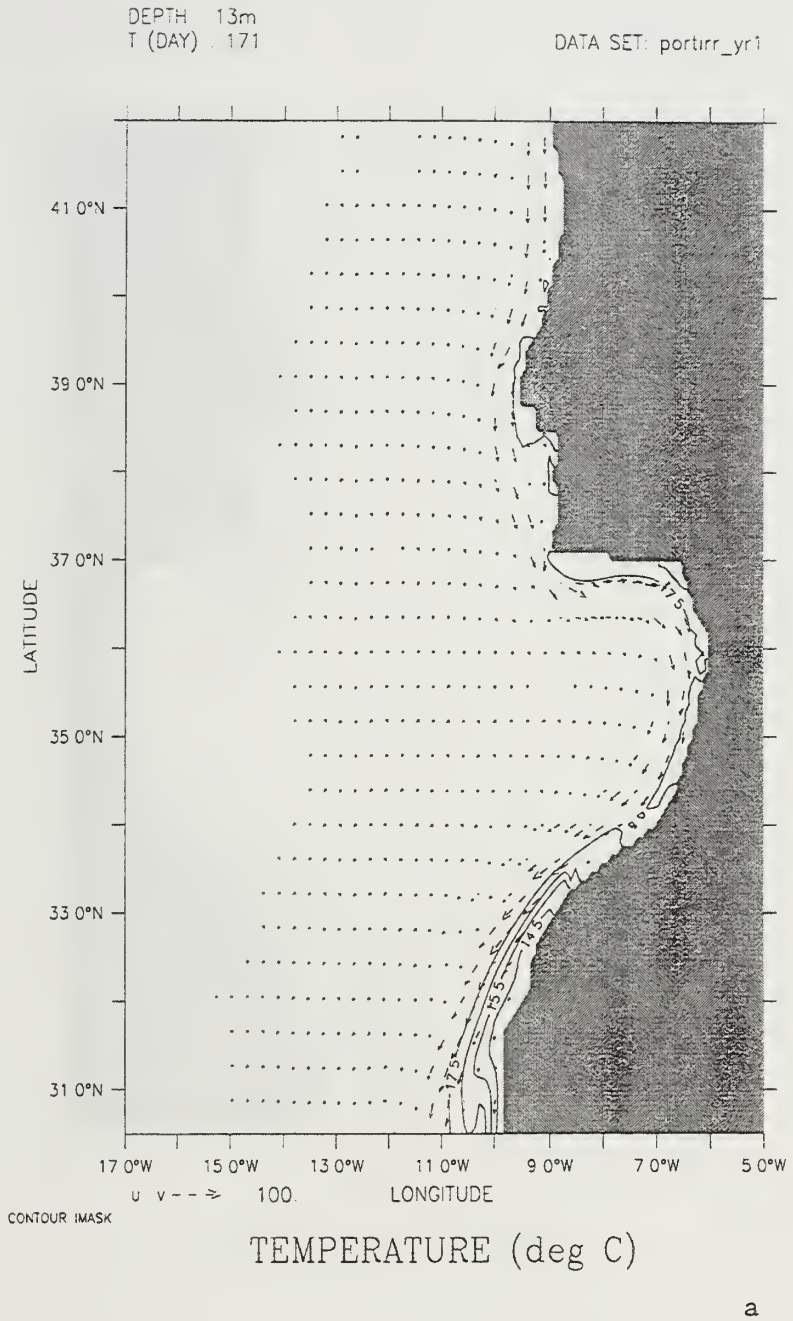

Figure 9. Experiment 2: Temperature contours and velocity vectors at 13 m depth at days (a) 171, (b) 240, (c) 300, and (d) 360. The contour interval is 1° C. Maximum current velocity is 100 cm/s.

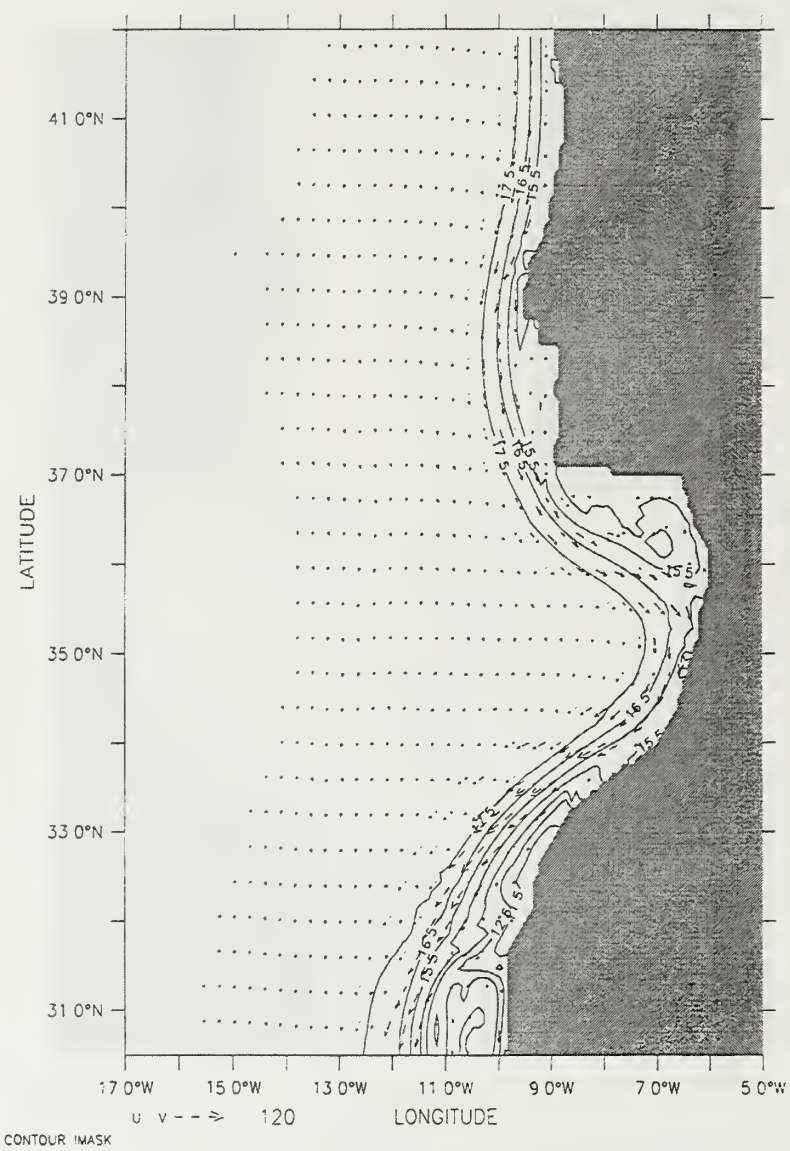
DEPTH 13m
T (DAY) : 240
DATA SET: portirr_yr1
41 0°N
39 0°N
37 0°N
35 0°N
33 0°N
31 0°N
LATITUDE
17 0°W
15 0°W
13 0°W
11 0°W
9 0°W
7 0°W
5 0°W
LONGITUDE
U V - - > 120
CONTOUR !MASK
TEMPERATURE (deg C)

b

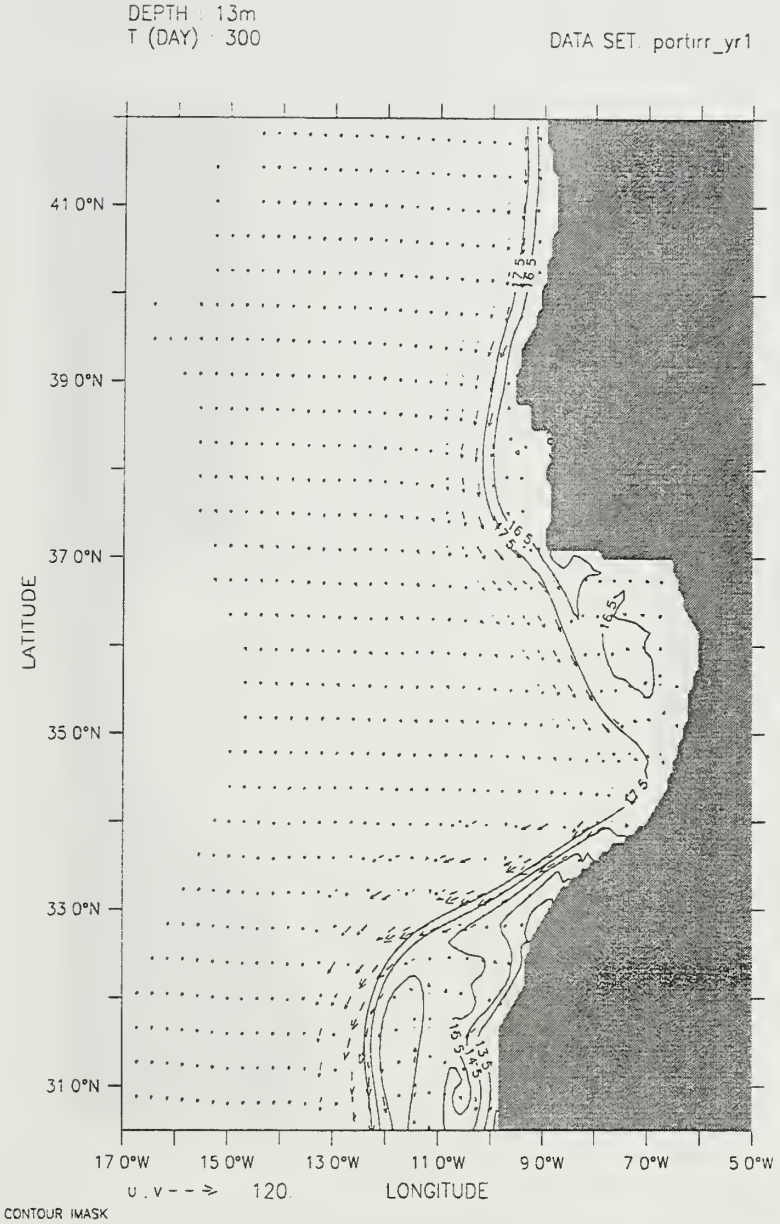

TEMPERATURE (deg C)

c

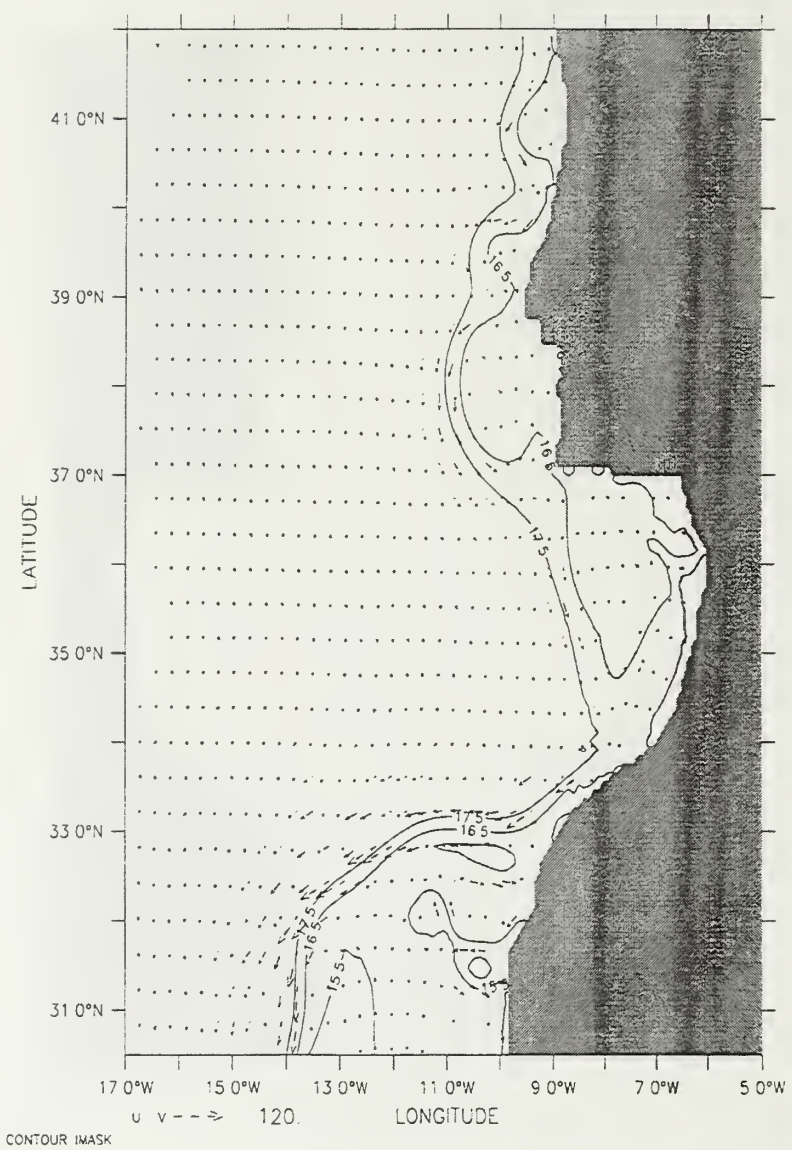

TEMPERATURE (deg C)

d

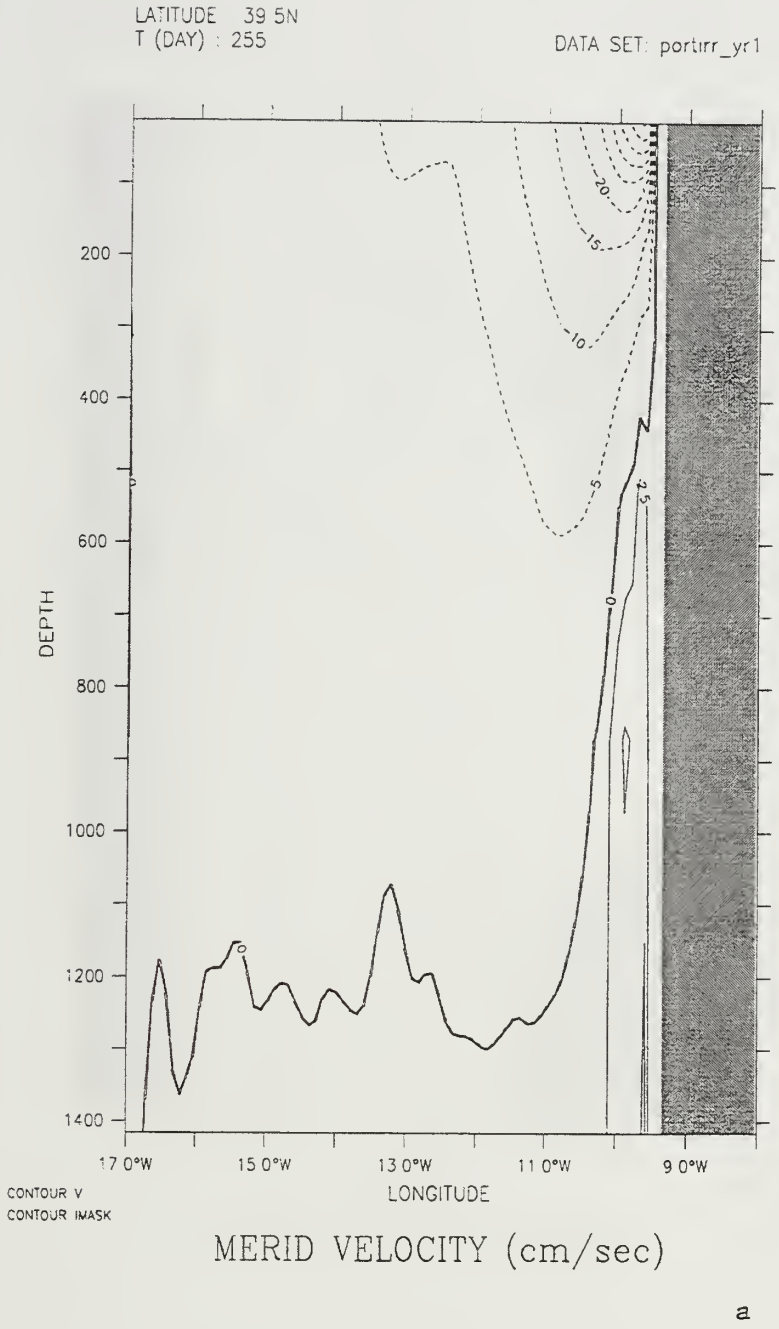

Figure 10. Experiment 2: Cross-shore section at 39.5° N of the meridional component of velocity (v) in the coastal region at days (a) 255 and (b) 309. Solid lines indicate poleward flow, while dashed lines indicate equatorward flow. The contour interval is 2.5 cm/s for poleward flow and 5 cm/s for equatorward flow.

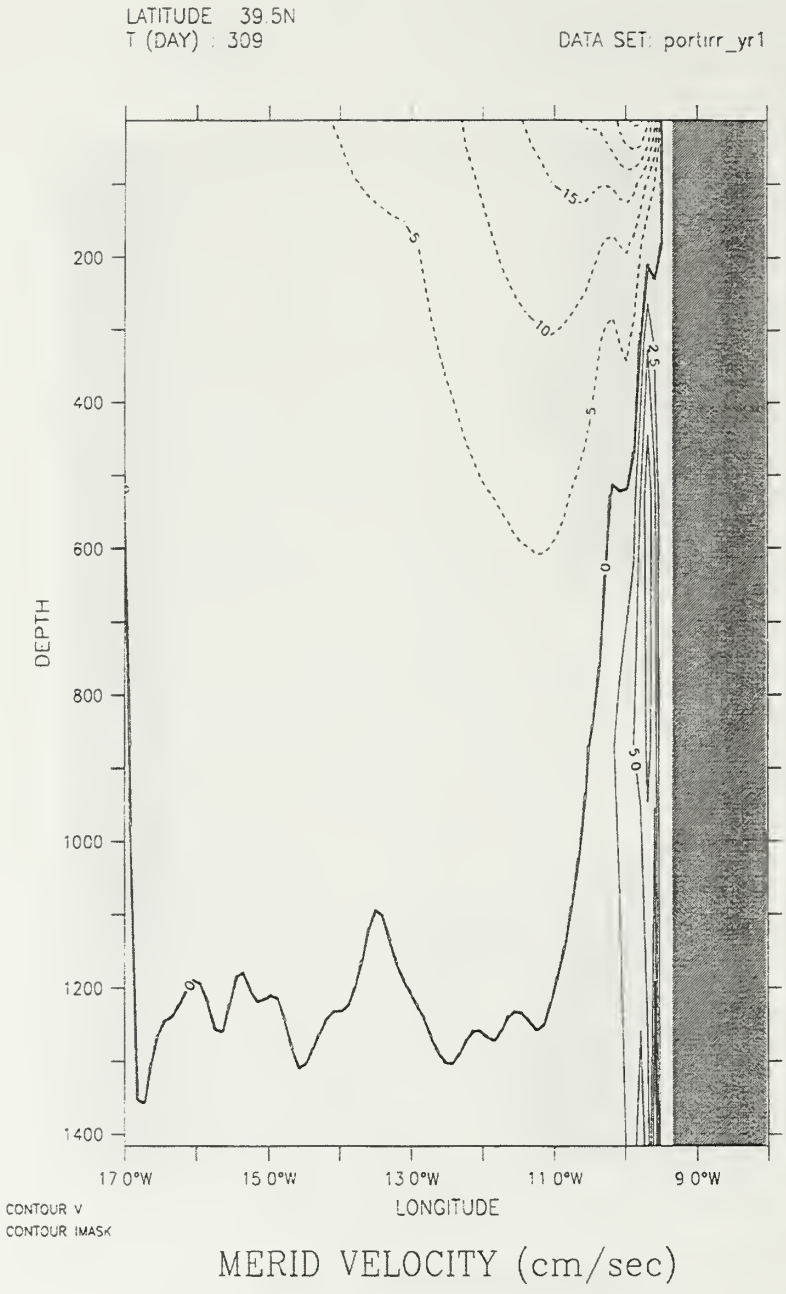
LATITUDE 39.5N
T (DAY) : 309
DATA SET: portirr_yr1
DEPTH
200
400
600
800
1000
1200
1400
17.0°W
15.0°W
13.0°W
11.0°W
9.0°W
LONGITUDE
CONTOUR V
CONTOUR IMASK
MERID VELOCITY (cm/sec)

b

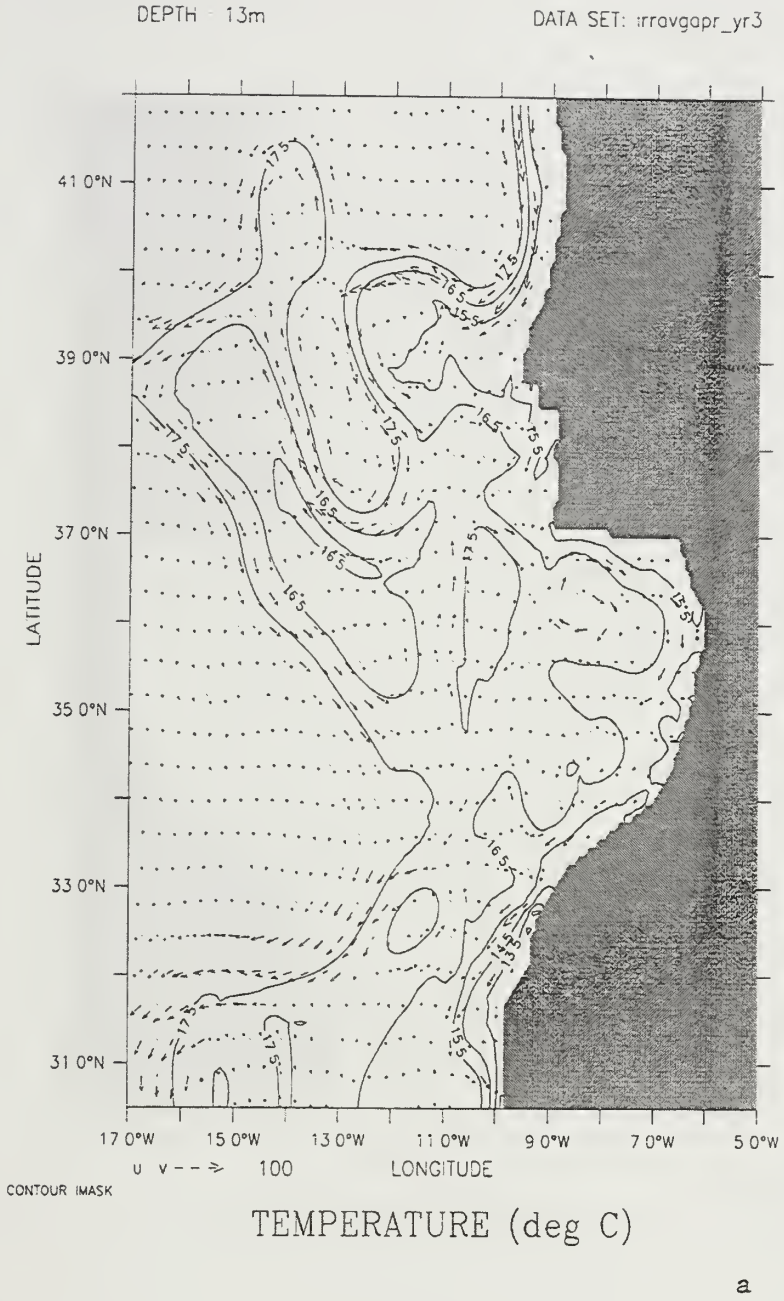

Figure 11. Experiment 2: Temperature contours and velocity vectors at 13 m depth in the third year of the model simulation time-averaged over the months of (a) April, (b) June, (c) August, (d) October, (e) December, and cross-shore section of velocity (v) at (f) 37.8° N time-averaged over June and (g) 41.1° N time-averaged over December. The contour interval is 1° C in (a) - (e), 2.5 cm/s for poleward flow and 5 cm/s for equatorward flow in (f) and 5 cm/s for (g). Maximum current velocity is 100 cm/s.

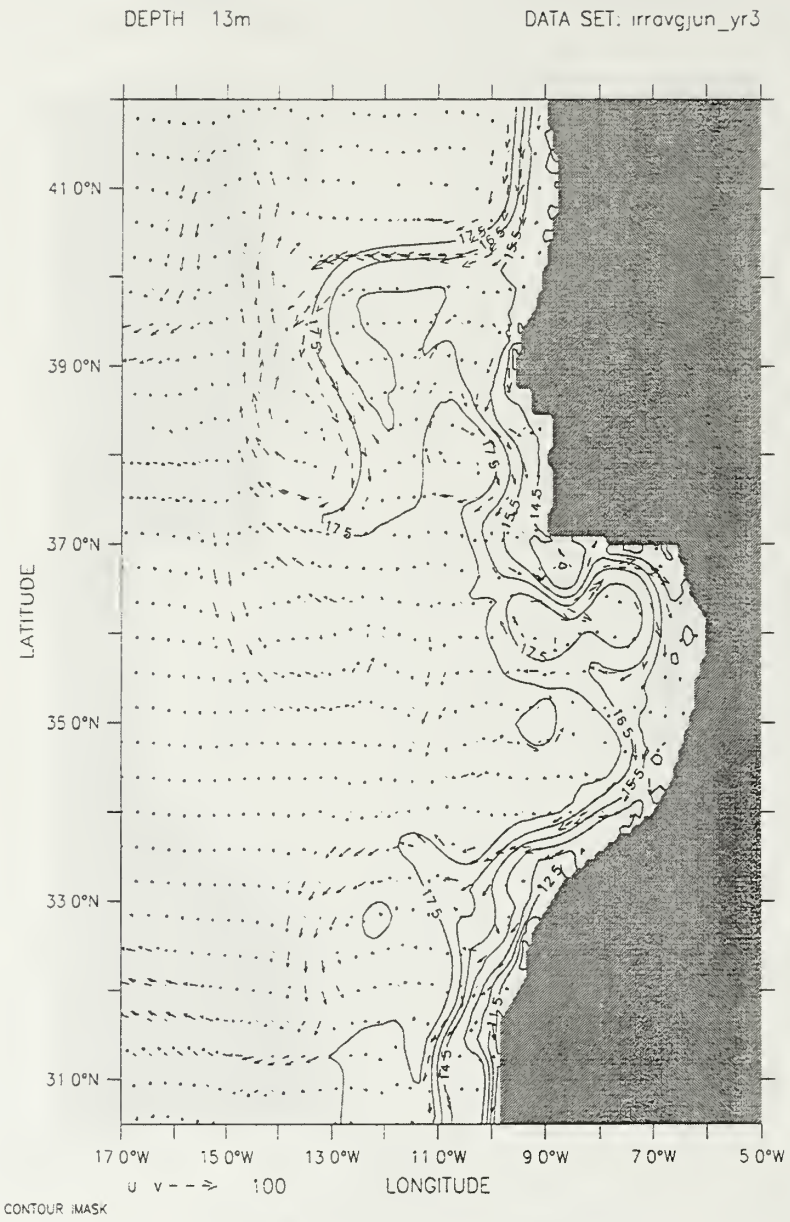

TEMPERATURE (deg C)

b

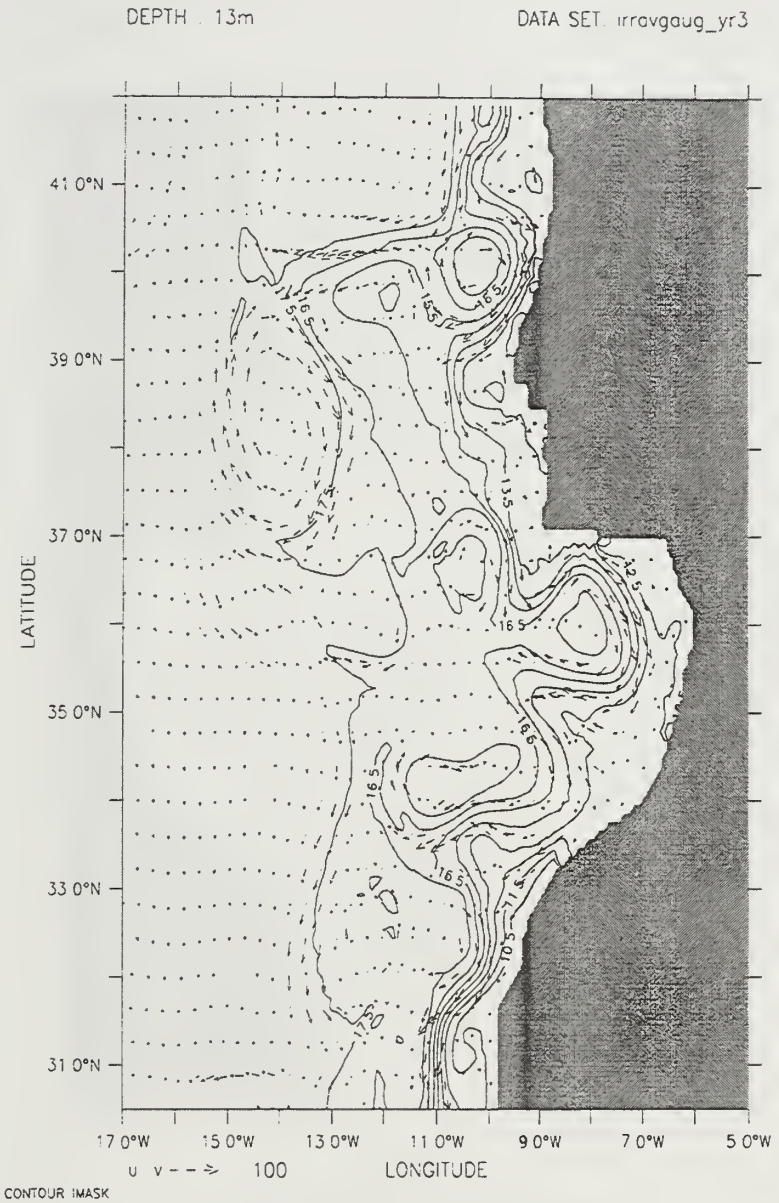
DEPTH . 13m
DATA SET. irravgaug_yr3
41 0°N
39 0°N
37 0°N
35 0°N
33 0°N
31 0°N
LATITUDE
17 0°W
15 0°W
13 0°W
11 0°W
9 0°W
7 0°W
5 0°W
LONGITUDE
u v - - > 100
CONTOUR IMASK
TEMPERATURE (deg C)

c

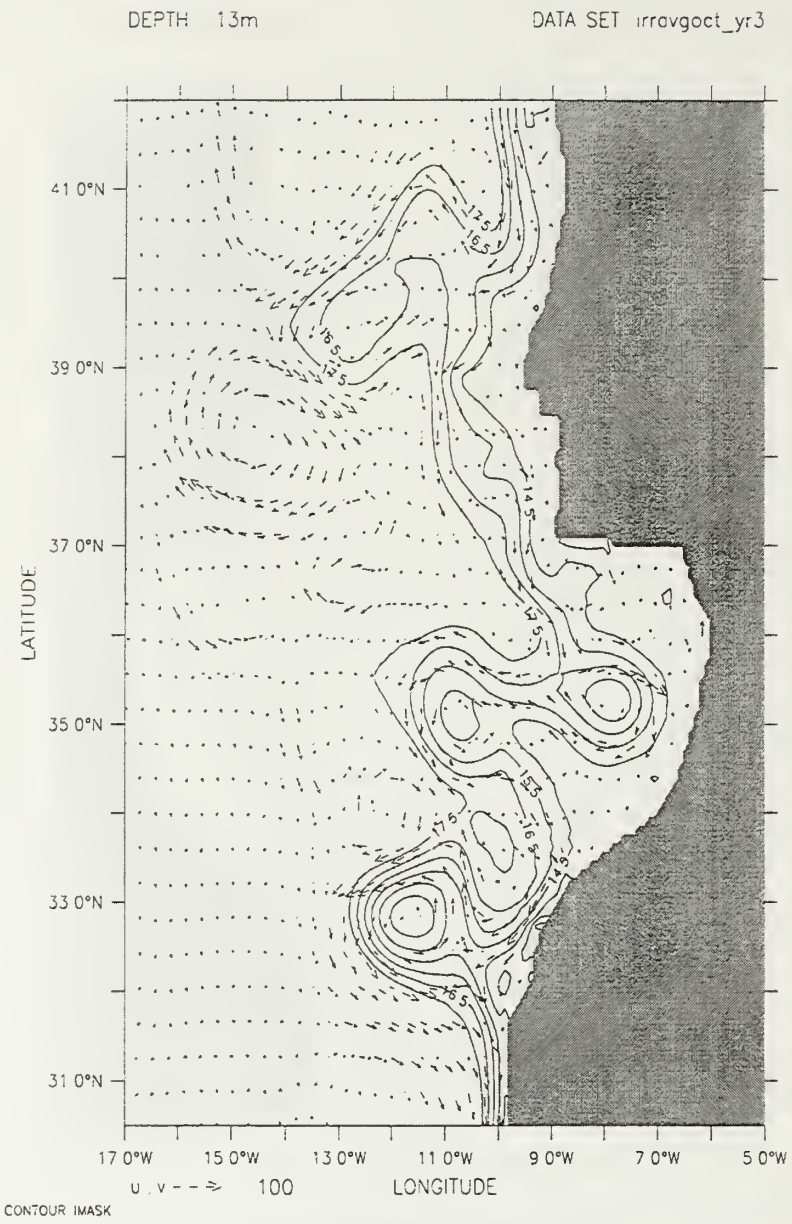
DEPTH 13m
DATA SET irravgoct_yr3
41 0°N
39 0°N
37 0°N
35 0°N
33 0°N
31 0°N
LATITUDE
17 5
16 5
15 5
14 5
17 0°W
15 0°W
13 0°W
11 0°W
9 0°W
7 0°W
5 0°W
LONGITUDE
U , V - - - > 100
CONTOUR IMASK
TEMPERATURE (deg C)

d

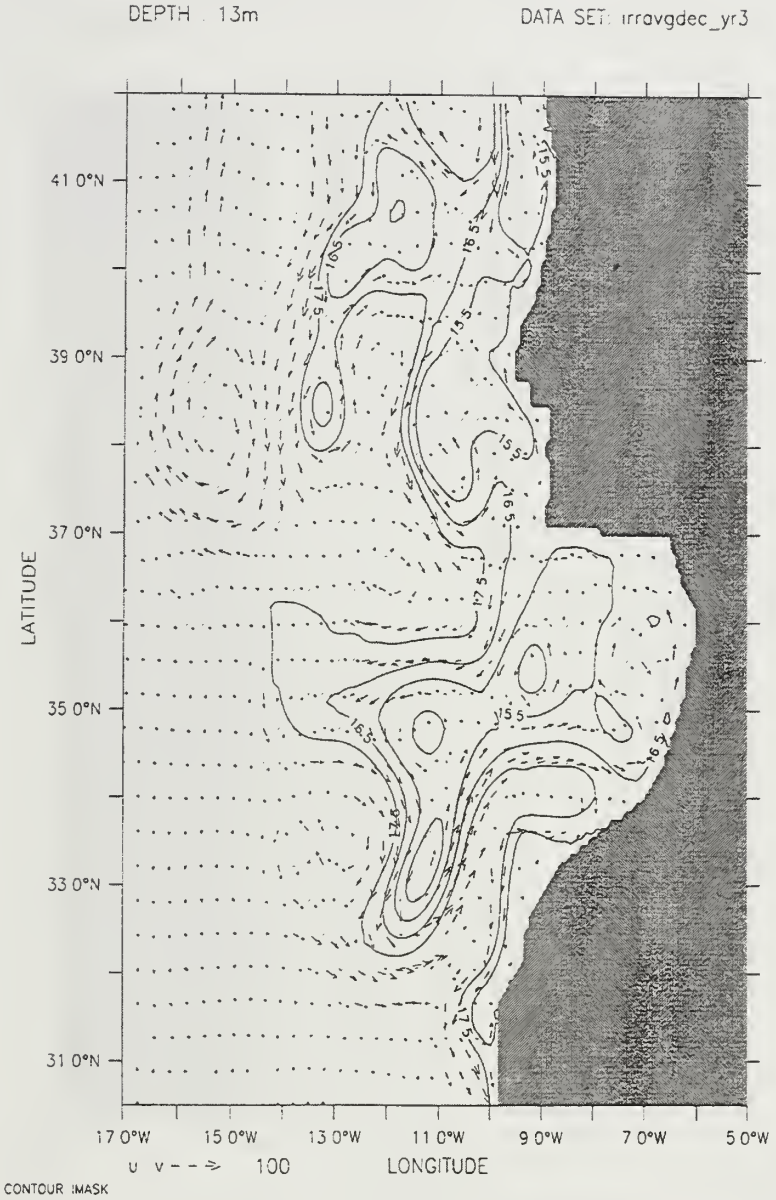
DEPTH . 13m
DATA SET: irravgdec_yr3
41 0°N
39 0°N
37 0°N
35 0°N
33 0°N
31 0°N
LATITUDE
17 0°W
15 0°W
13 0°W
11 0°W
9 0°W
7 0°W
5 0°W
LONGITUDE
u v - - > 100
CONTOUR :MASK
TEMPERATURE (deg C)

e

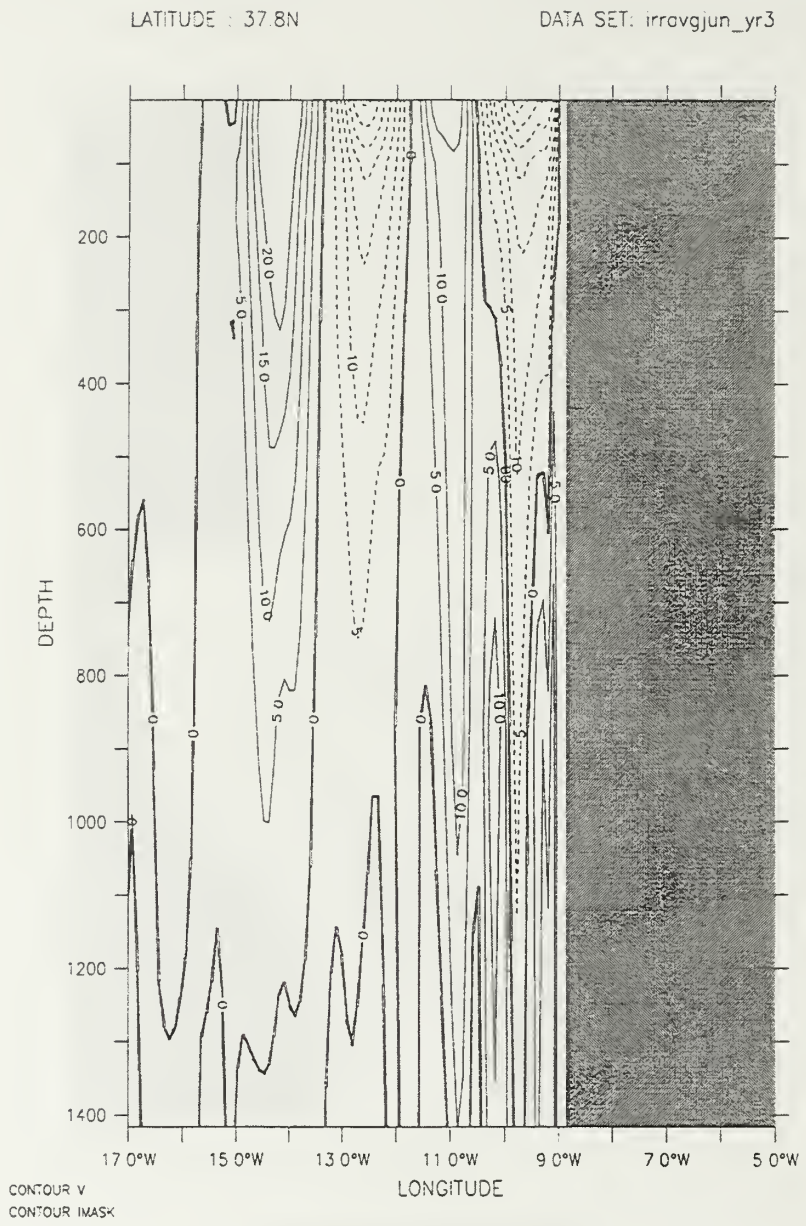

MERID VELOCITY (cm/sec)

f

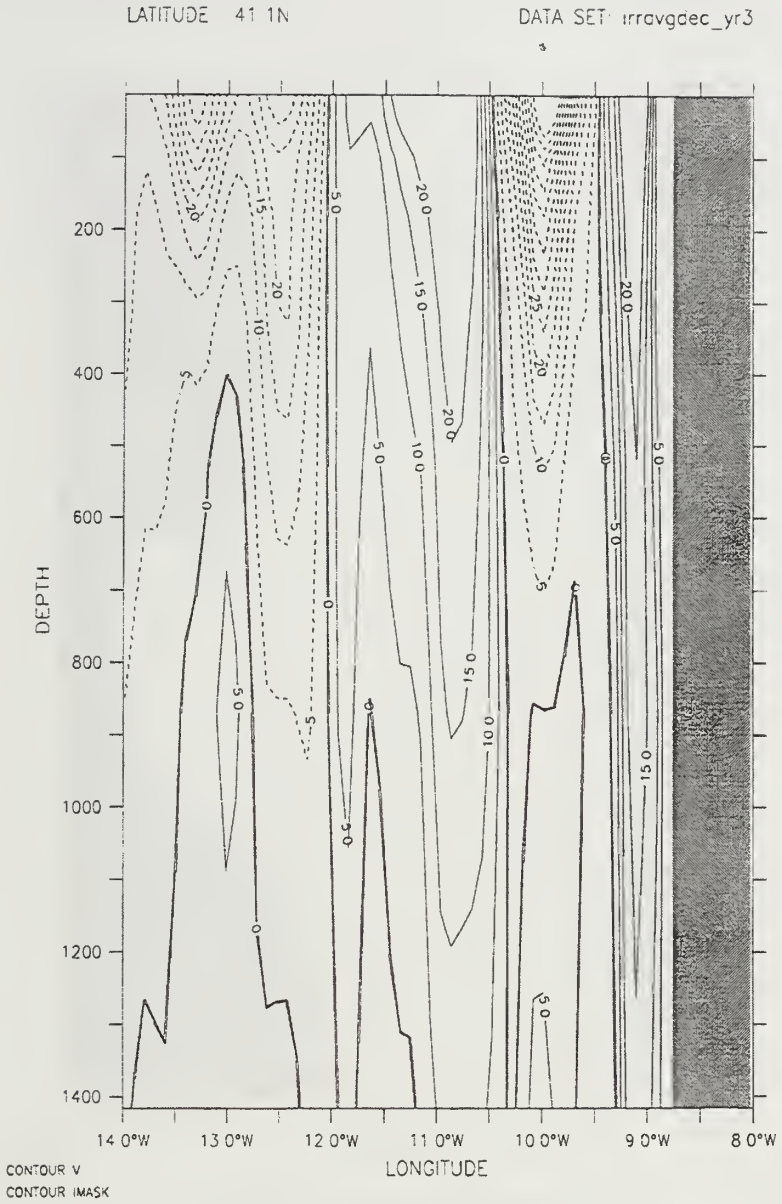

MERID VELOCITY (cm/sec)

g

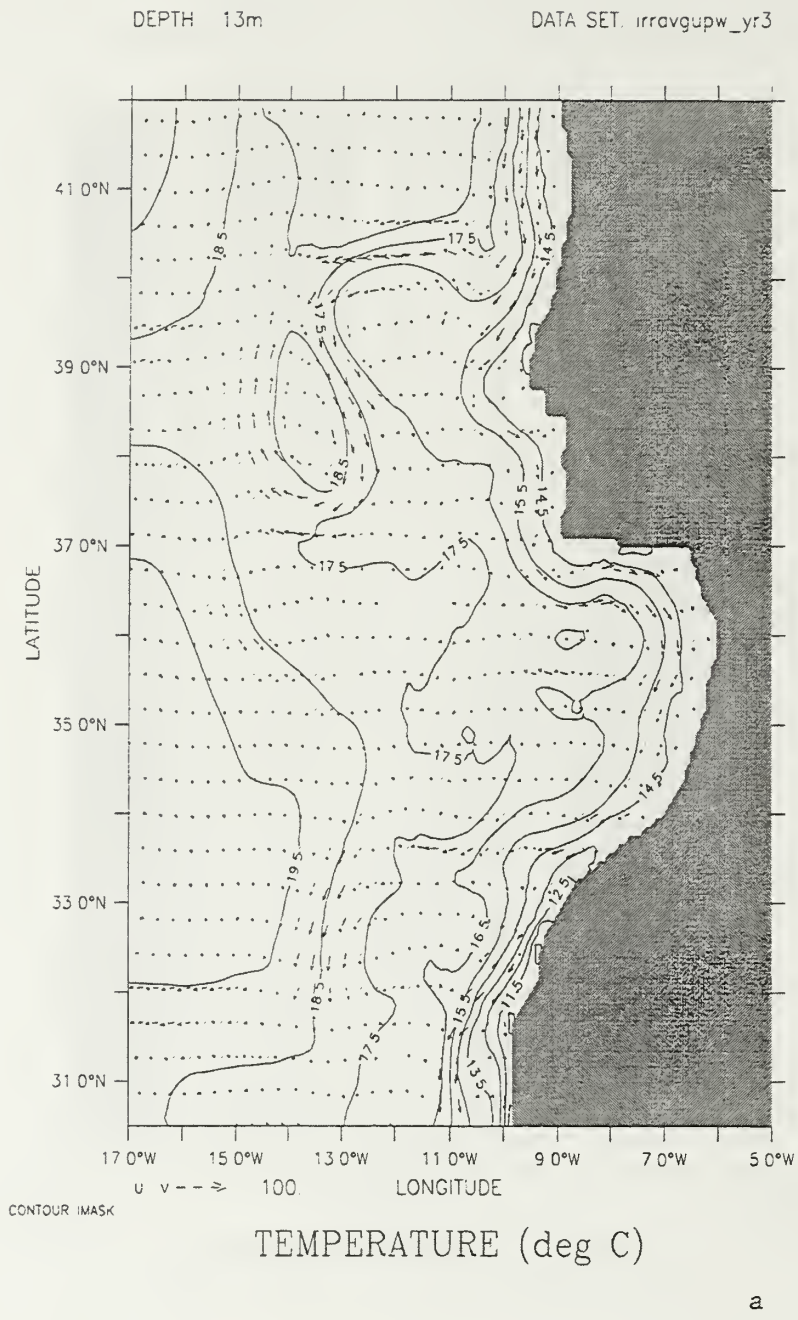

Figure 12. Experiment 2: Time-averaged plots for the upwelling season (April-September) of (a) temperature contours and velocity vectors at 13 m depth, (b) cross-shore section of velocity (v) at 32.1° N, and (c) temperature contours and velocity vectors at 870 m depth. The contour interval is 1° C in (a) and 2.5 cm/s for poleward flow and 5 cm/s for equatorward flow in (b). Maximum current velocity is 100 cm/s in (a) and 50 cm/s in (c).

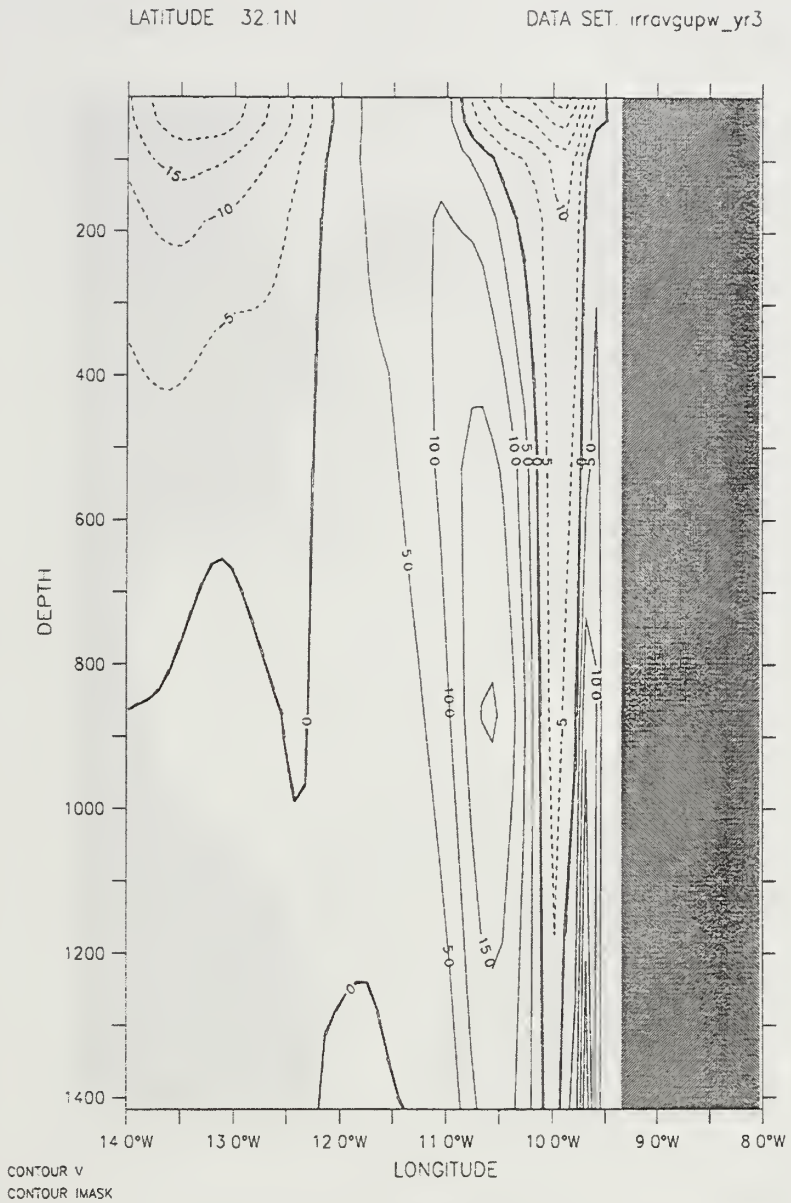
LATITUDE 32.1N
DATA SET: irravgupw_yr3
DEPTH
200
400
600
800
1000
1200
1400
14.0°W
13.0°W
12.0°W
11.0°W
10.0°W
9.0°W
8.0°W
LONGITUDE
CONTOUR V
CONTOUR IMASK
MERID VELOCITY (cm/sec)

b

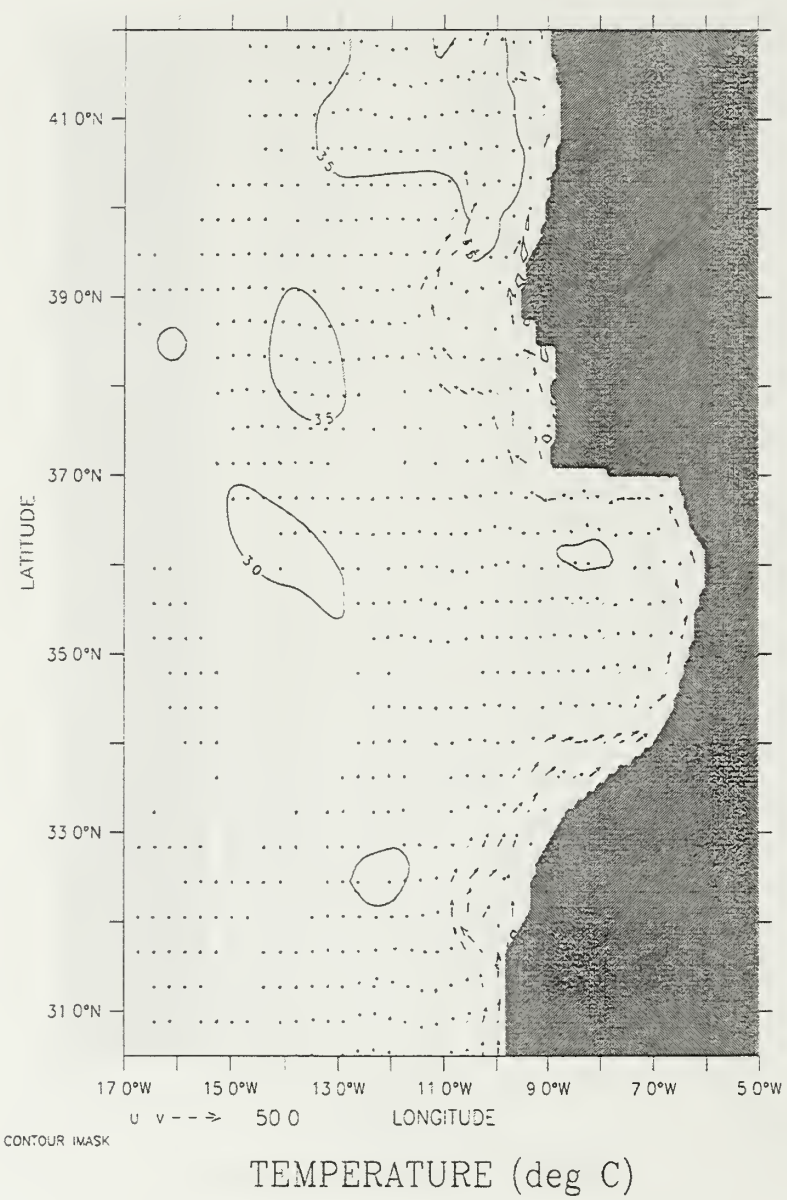
DEPTH 870m
DATA SET irravgupw_yr3
41 0°N
39 0°N
37 0°N
35 0°N
33 0°N
31 0°N
LATITUDE
35
35
30
17 0°W
15 0°W
13 0°W
11 0°W
9 0°W
7 0°W
5 0°W
u v - - > 50 0
LONGITUDE
CONTOUR IMASK
TEMPERATURE (deg C)

c

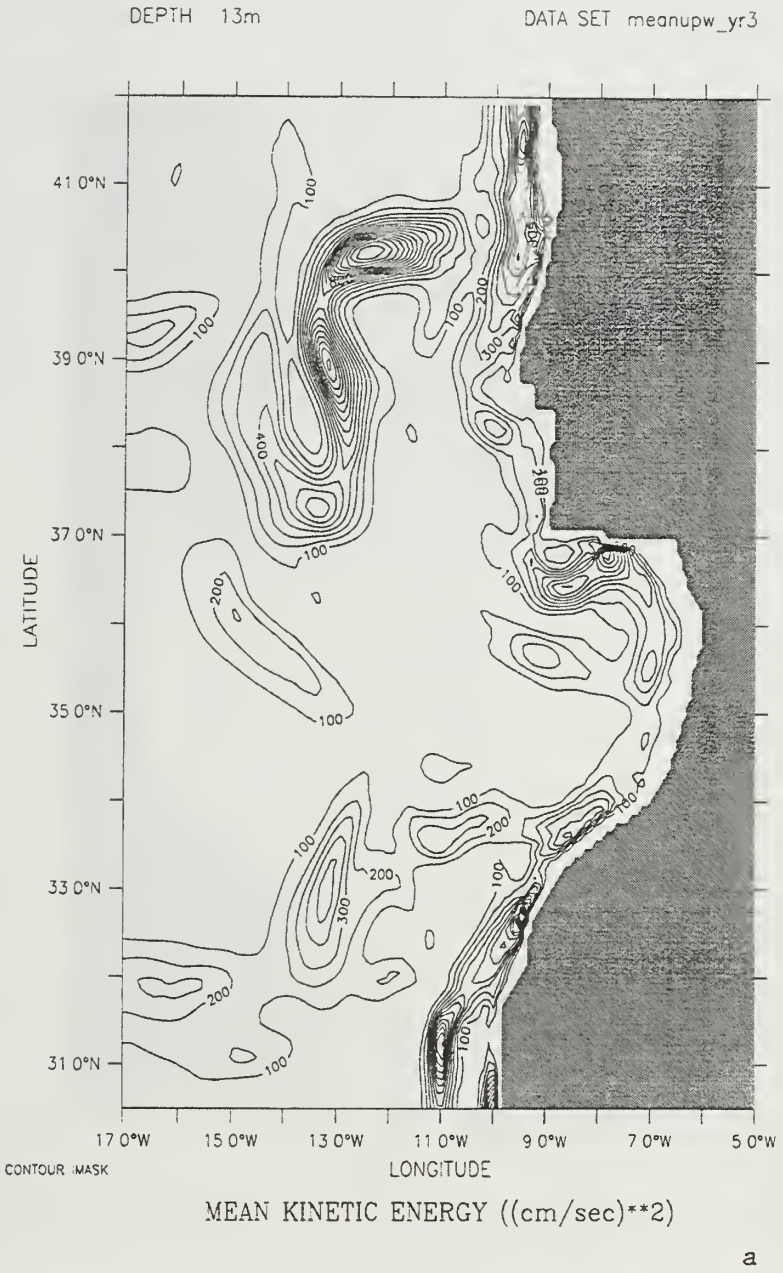

Figure 13. Experiment 2: (a) Mean and (b) eddy kinetic energy at 13 m depth. Contour interval is 100 cm^2/s^2.

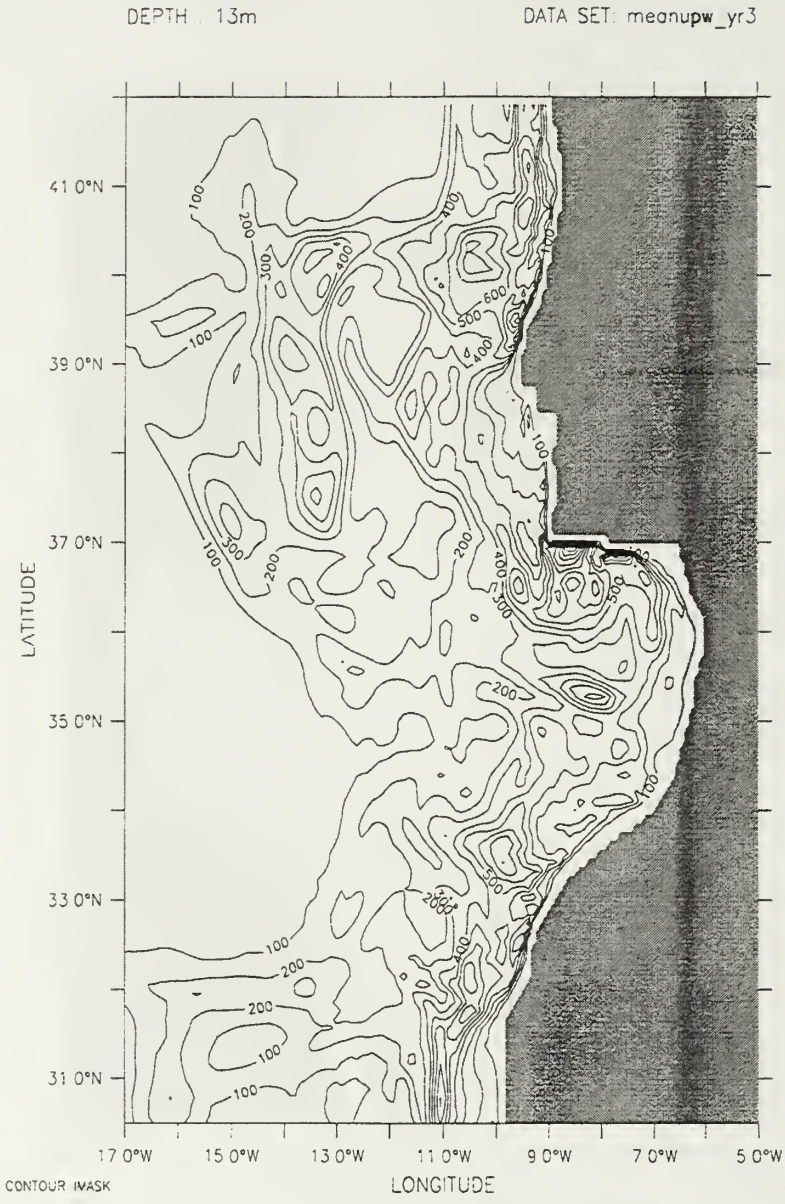
DEPTH : 13m
DATA SET: meanupw_yr3
41.0°N
39.0°N
37.0°N
35.0°N
33.0°N
31.0°N
LATITUDE
17.0°W
15.0°W
13.0°W
11.0°W
9.0°W
7.0°W
5.0°W
LONGITUDE
CONTOUR MASK
EDDY KINETIC ENERGY ((cm/sec)**2)

b

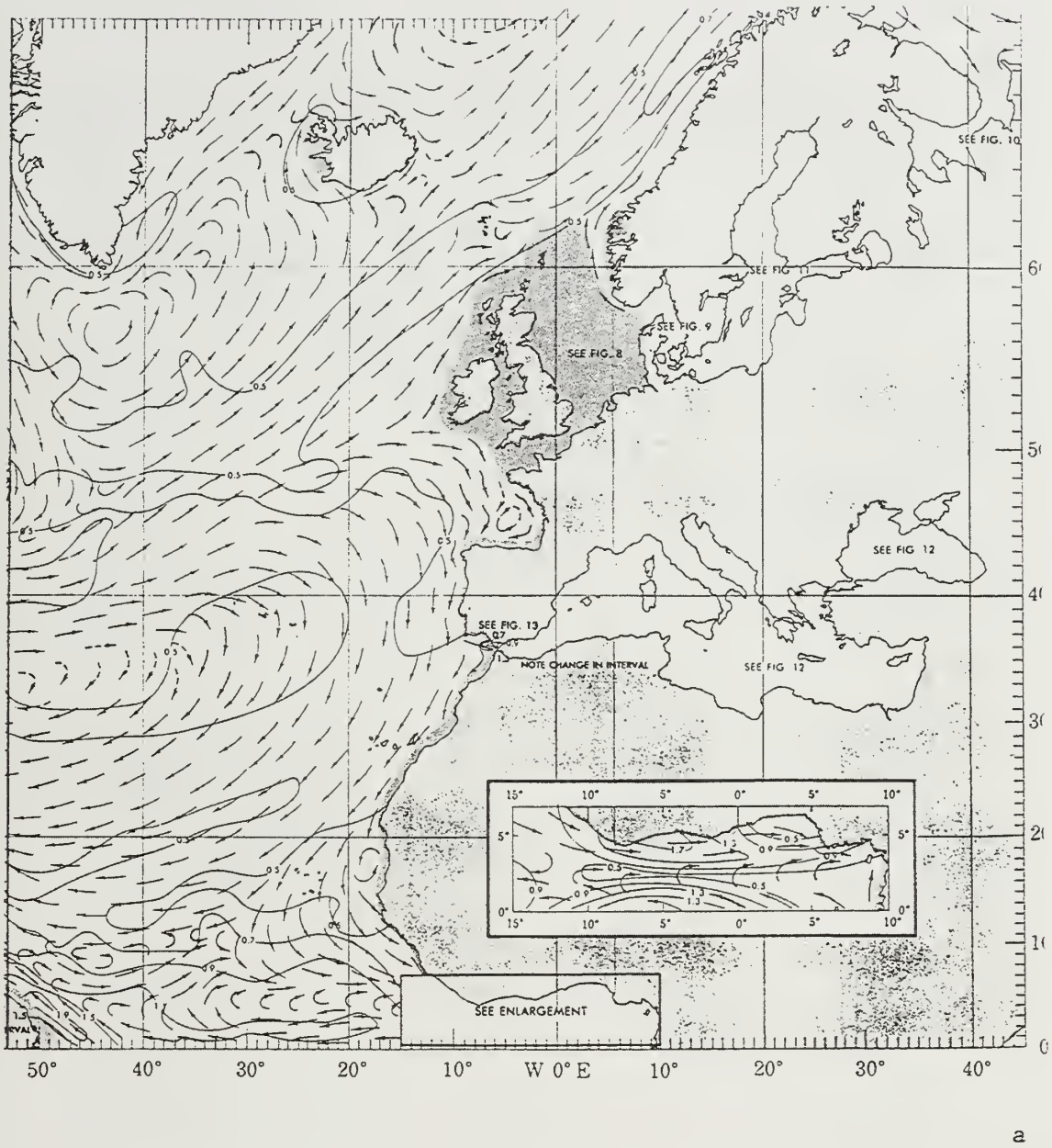

Figure 14. Mean surface current speeds in knots and prevailing direction for (a) winter (January, February, March), for (b) summer (July, August, September). "After DMAH/TC, 1988."

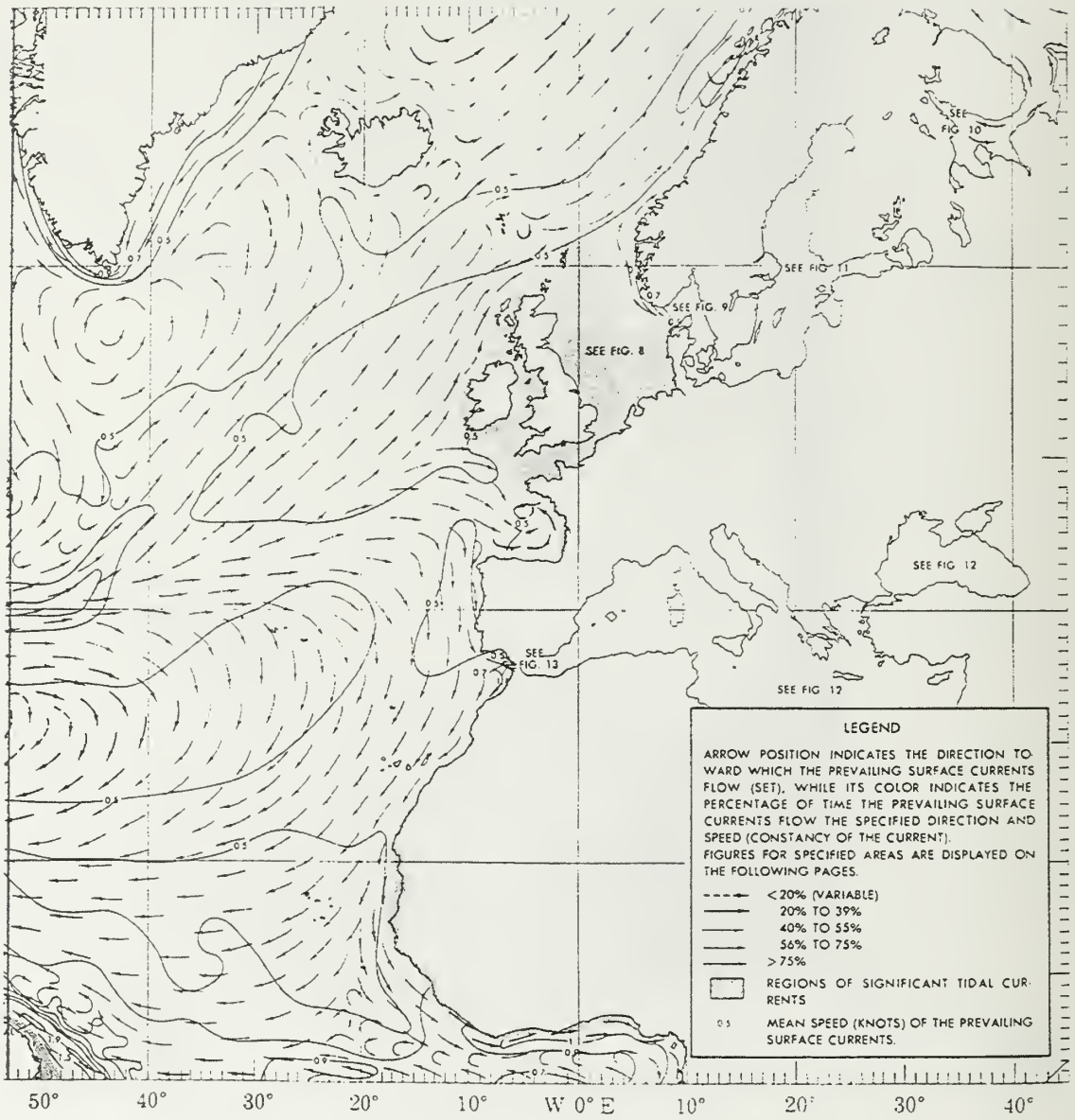
SEE FIG. 10
SEE FIG. 11
SEE FIG. 9
SEE FIG. 8
SEE FIG. 12
SEE FIG. 13
SEE FIG. 12
LEGEND
ARROW POSITION INDICATES THE DIRECTION TOWARD WHICH THE PREVAILING SURFACE CURRENTS FLOW (SET), WHILE ITS COLOR INDICATES THE PERCENTAGE OF TIME THE PREVAILING SURFACE CURRENTS FLOW THE SPECIFIED DIRECTION AND SPEED (CONSTANCY OF THE CURRENT).
FIGURES FOR SPECIFIED AREAS ARE DISPLAYED ON THE FOLLOWING PAGES.
<20% (VARIABLE)
20% TO 39%
40% TO 55%
56% TO 75%
>75%
REGIONS OF SIGNIFICANT TIDAL CURRENTS
0.5 MEAN SPEED (KNOTS) OF THE PREVAILING SURFACE CURRENTS.
50° 40° 30° 20° 10° W 0° E 10° 20° 30° 40°

b

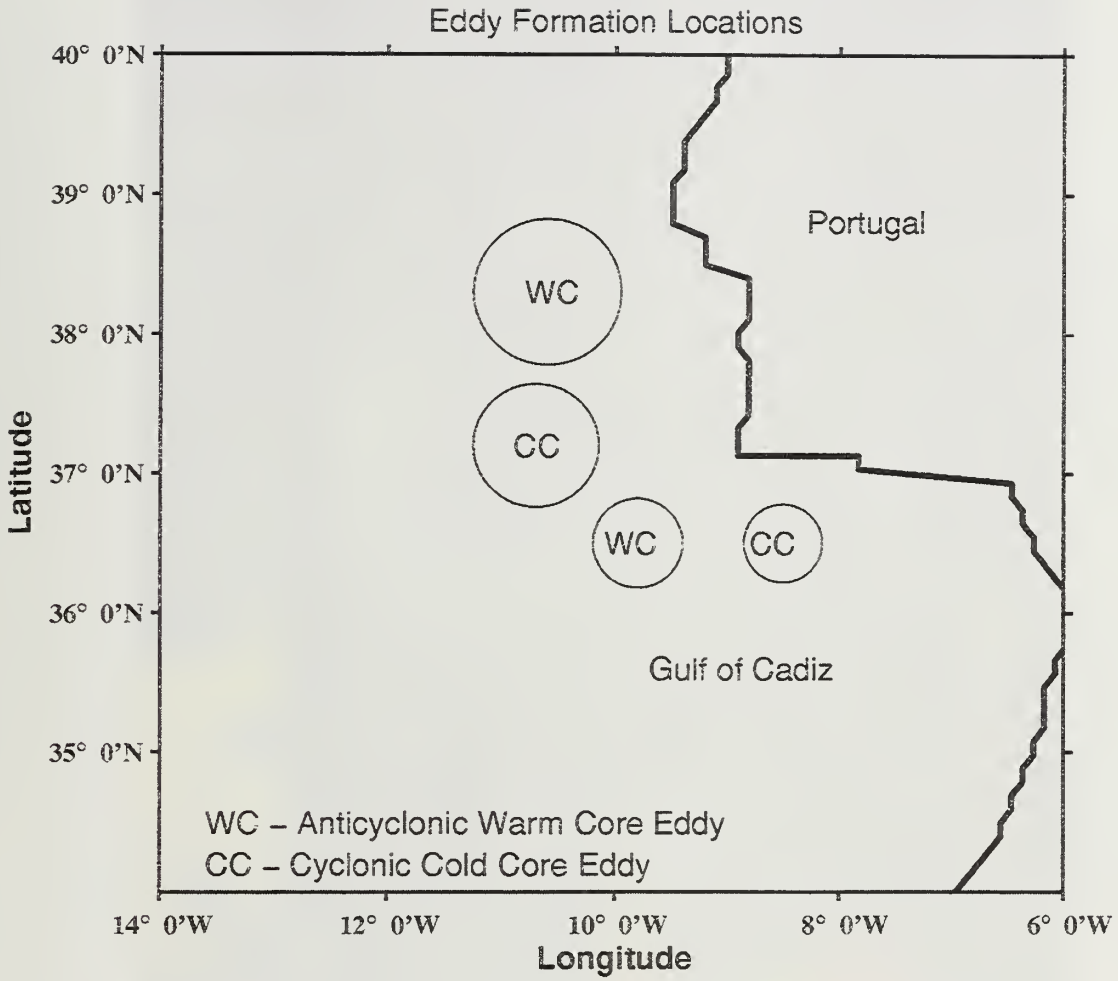

Figure 15. Computer representation of AVHRR NOAA7 Sea Surface Temperatures (SST) with observed eddy formations from 5 August 1982. "After Fiuza 1984."

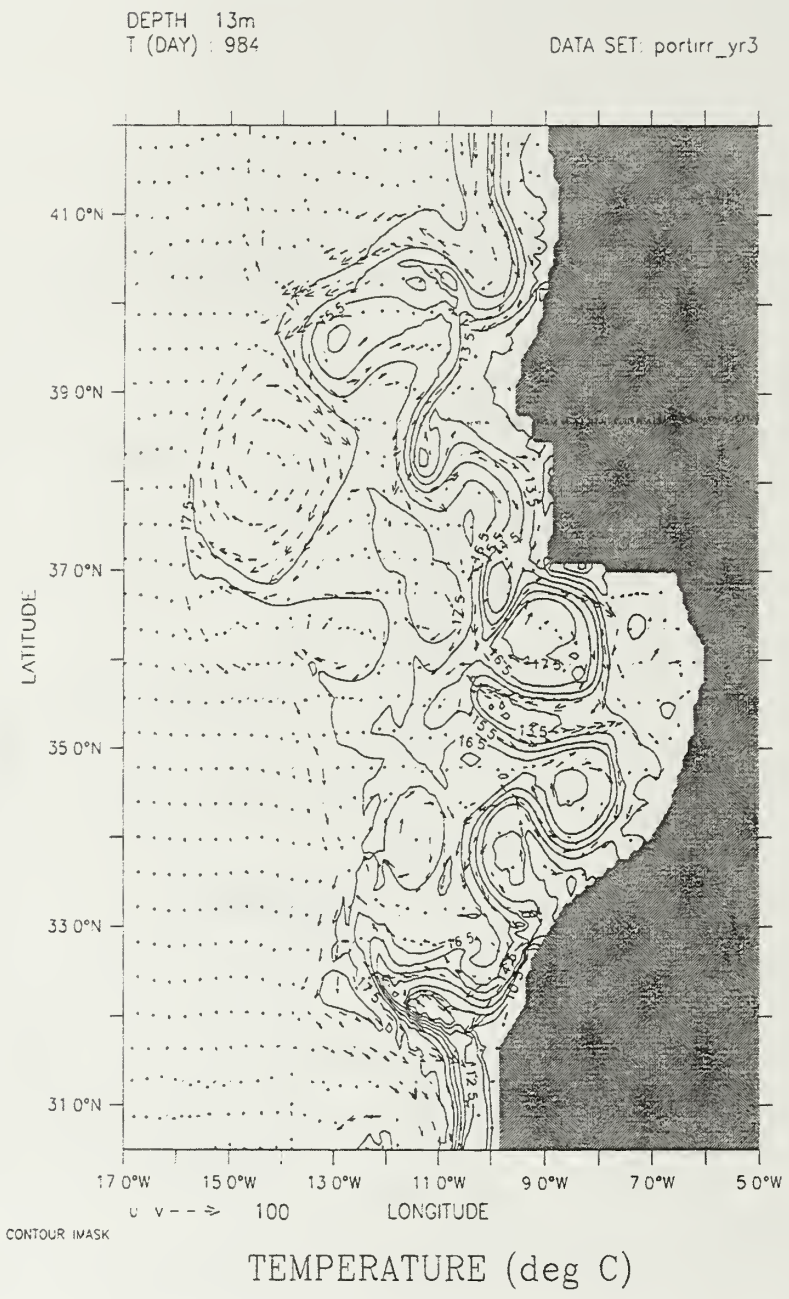

Figure 16. Experiment 2: Temperature contours and velocity vectors at 13 m depth at day 984 showing preferred eddy formation locations. The contour interval is 1° C. Maximum current velocity is 100 cm/s.

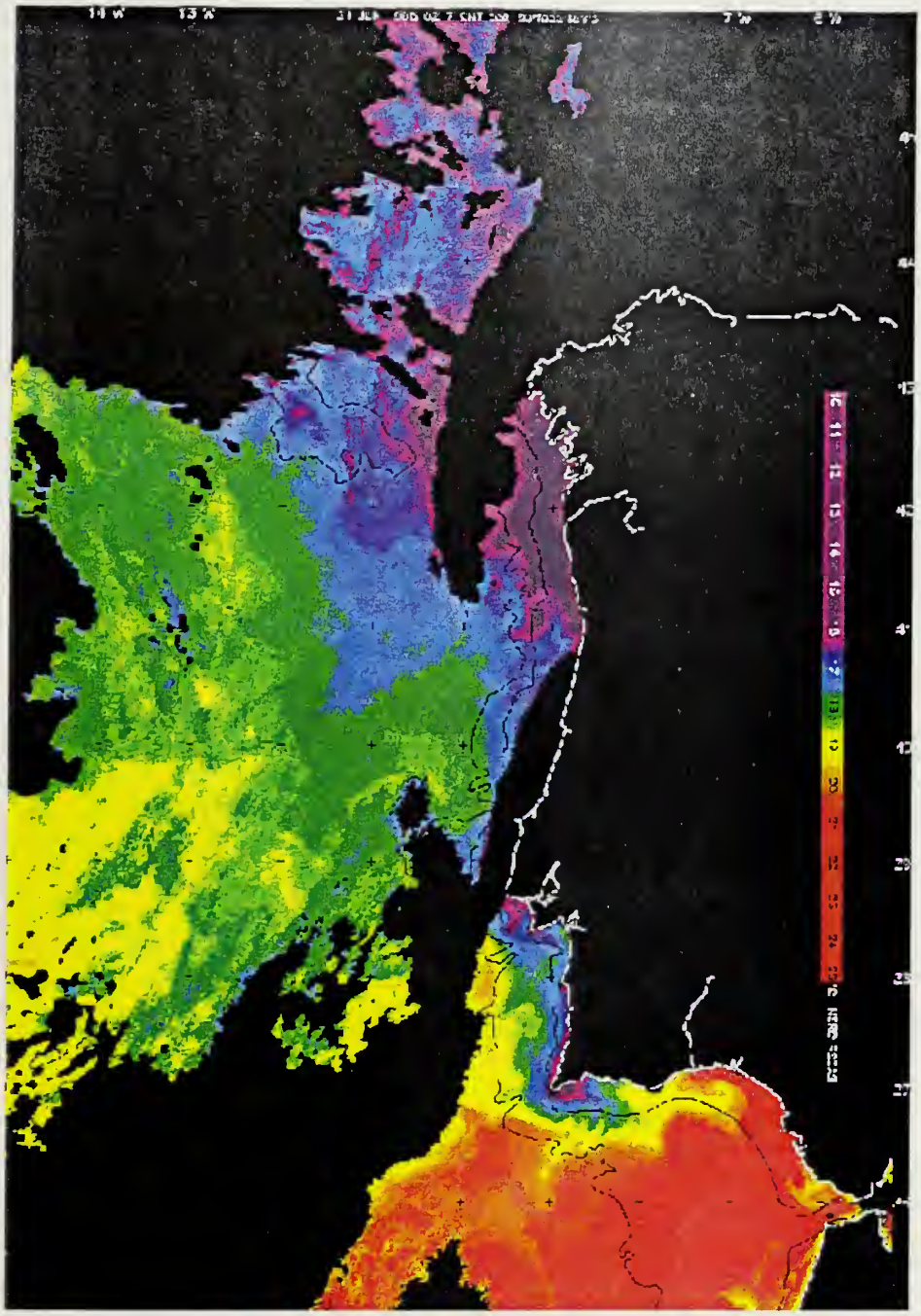

Figure 17. AVHRR SST from 21 June 1995 showing increased cold SST southwest of Cabo de Sao Vincent caused by intensified upwelling and advection of upwelled water around the cape. "From The Remote Sensing Data Analysis Service (RSDAS), Plymouth Marine Laboratory, UK."

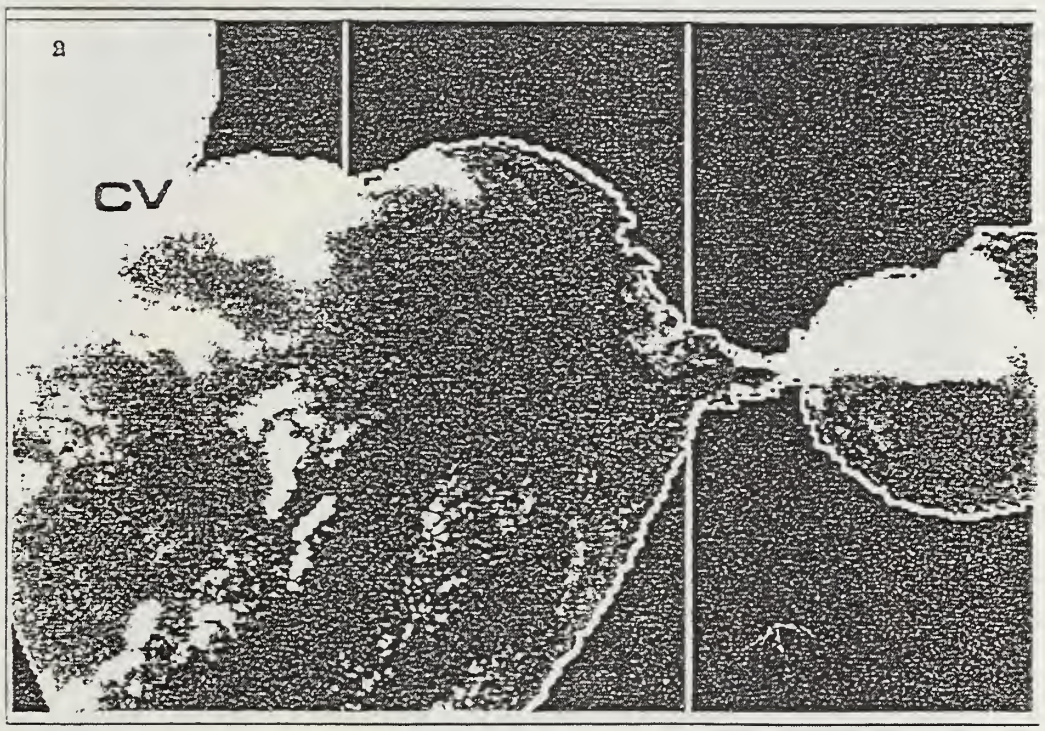

Figure 18. AVHRR thermal image from 7 July 1989, showing effects of westerly winds on the surface temperature fields in southern Iberian coastal waters during the summer. "From Folkard *et al.*, 1997."

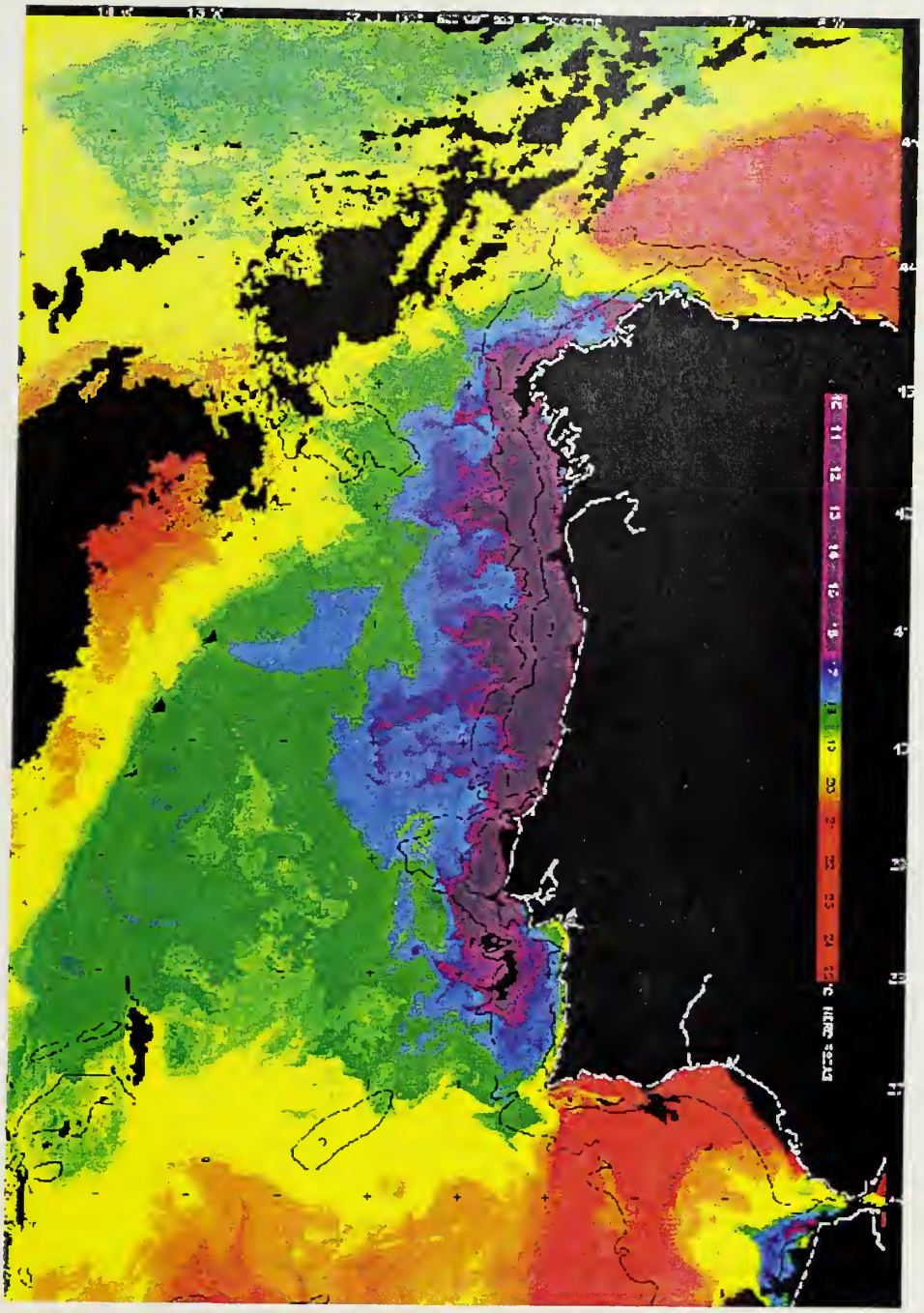

Figure 19. AVHRR SST from 27 July 1993 showing strong upwelling and numerous filaments off the west coast of the IP. "From The Remote Sensing Data Analysis Service (RSDAS), Plymouth Marine Laboratory, UK."

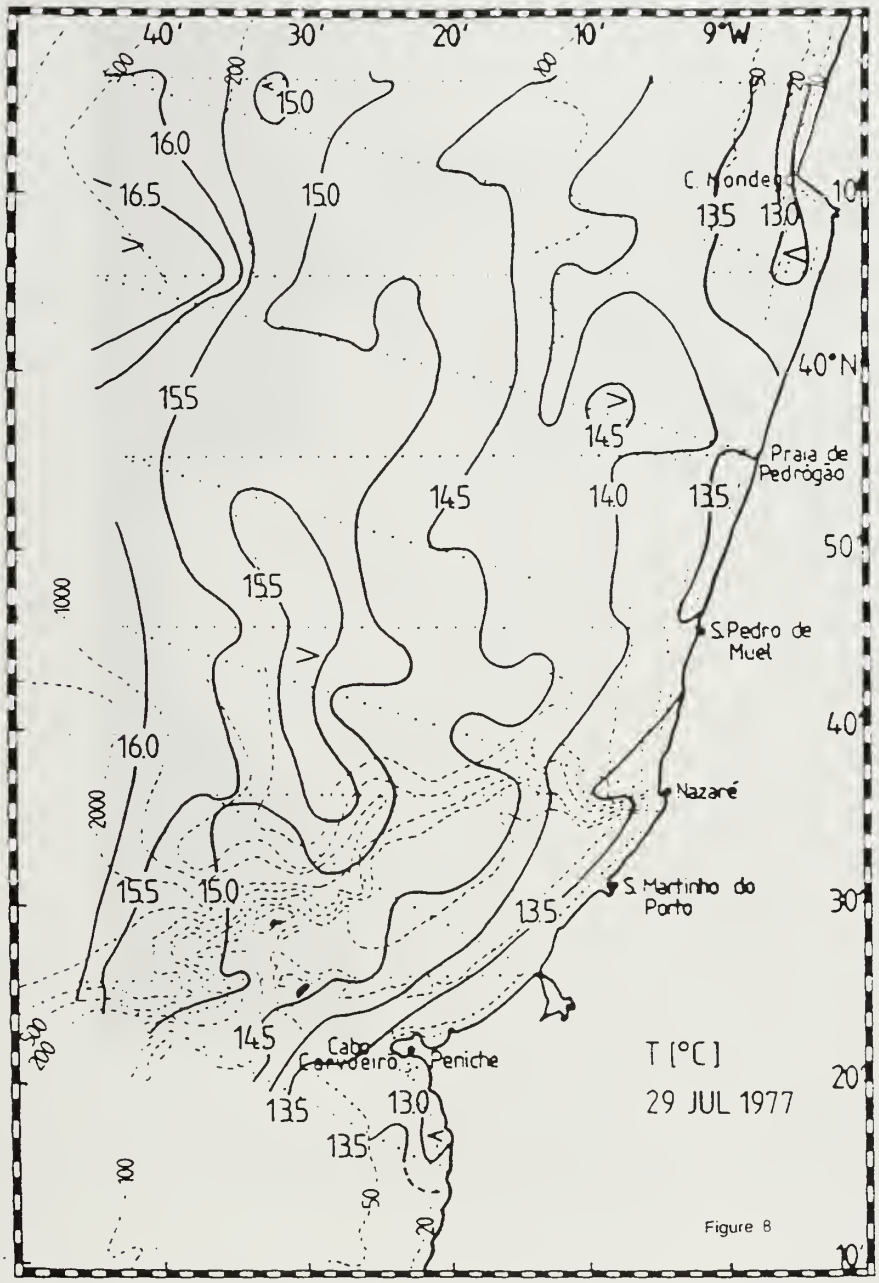

Figure 20. Sea Surface Temperatures (SST) showing intense upwelling north of Cabo da Roca from 29 July 1977. "From Fiuza 1982."

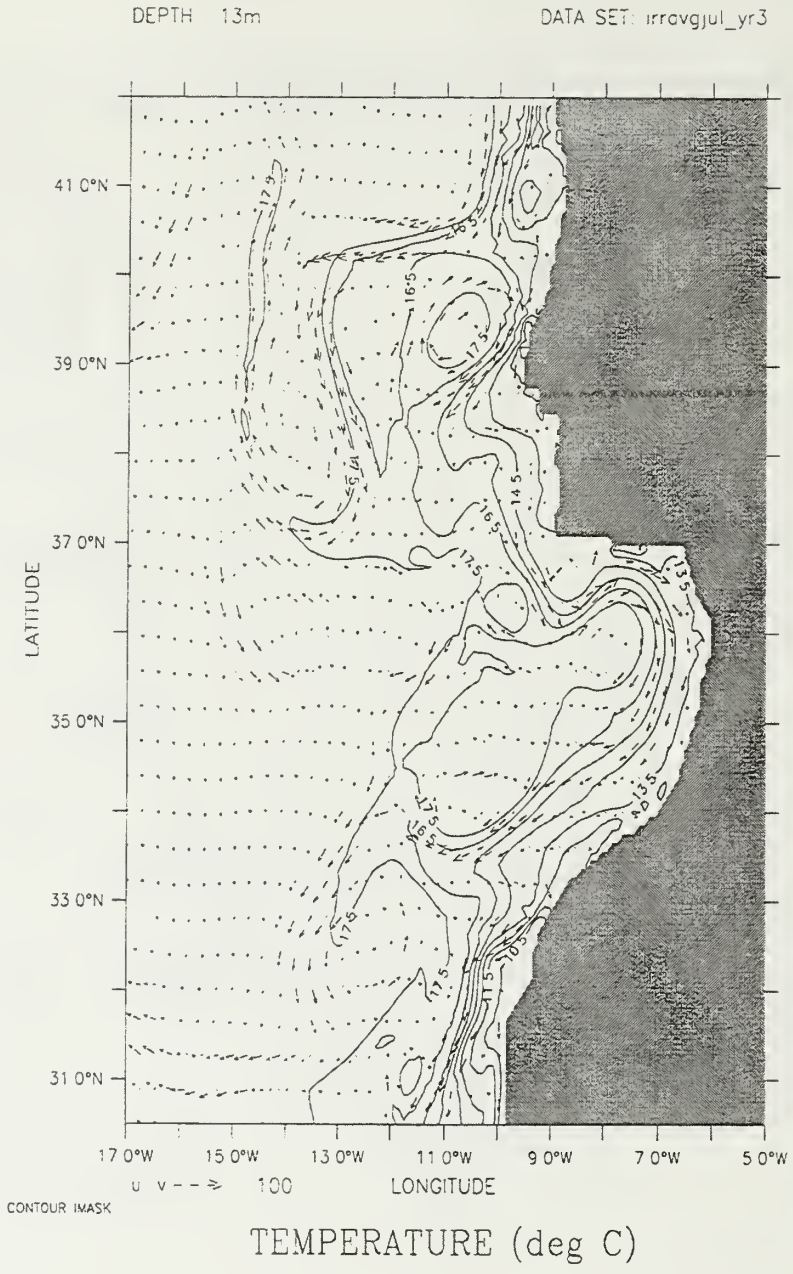

Figure 21. Experiment 2: Temperature contours and velocity vectors at 13 m depth in the third year of the model simulation time-averaged over the month of July shows the increased upwelling during the summer. The contour interval is 1° C. Maximum current velocity is 100 cm/s.

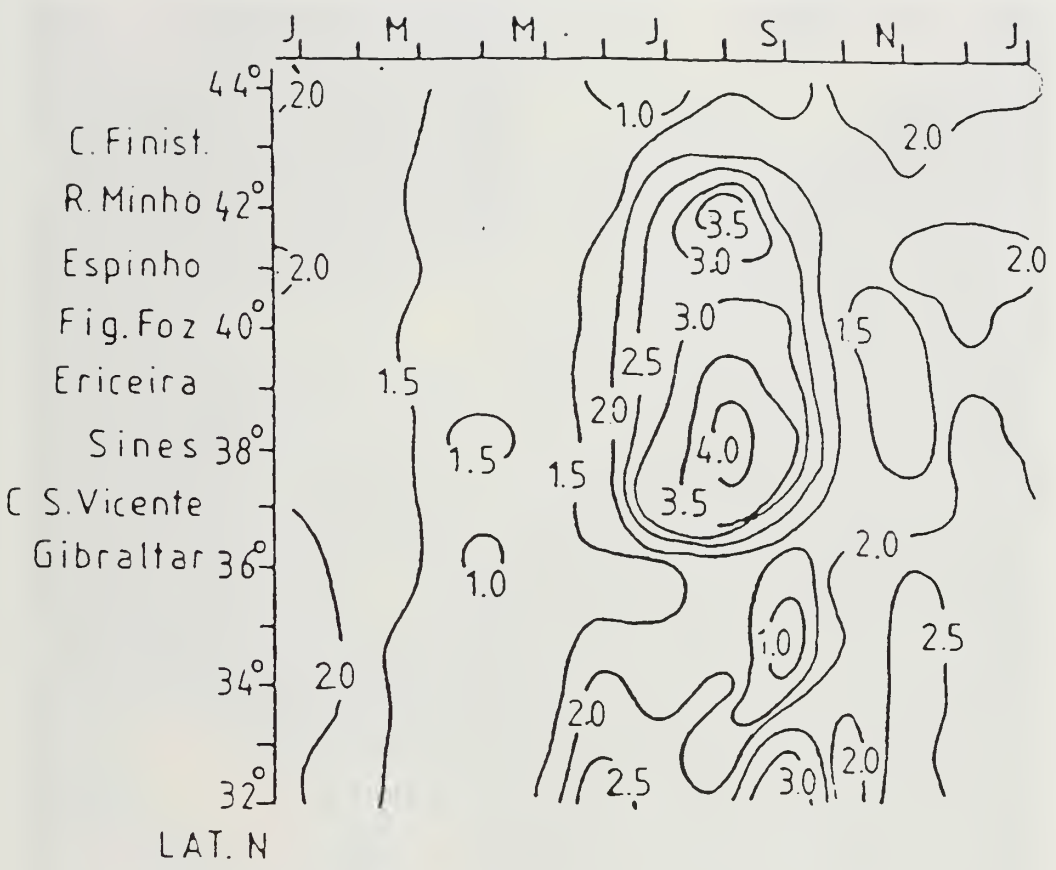

Figure 22. Seasonal cycle of thermal anomalies along the western coasts of Portugal and northwestern Africa between 32° N and 44° N. The thermal anomalies are computed from the climatological sea surface temperatures of Crowe (1949) and from observations from the period 1959-1969. The contour interval is 0.5° C. "After Fiuza 1982."

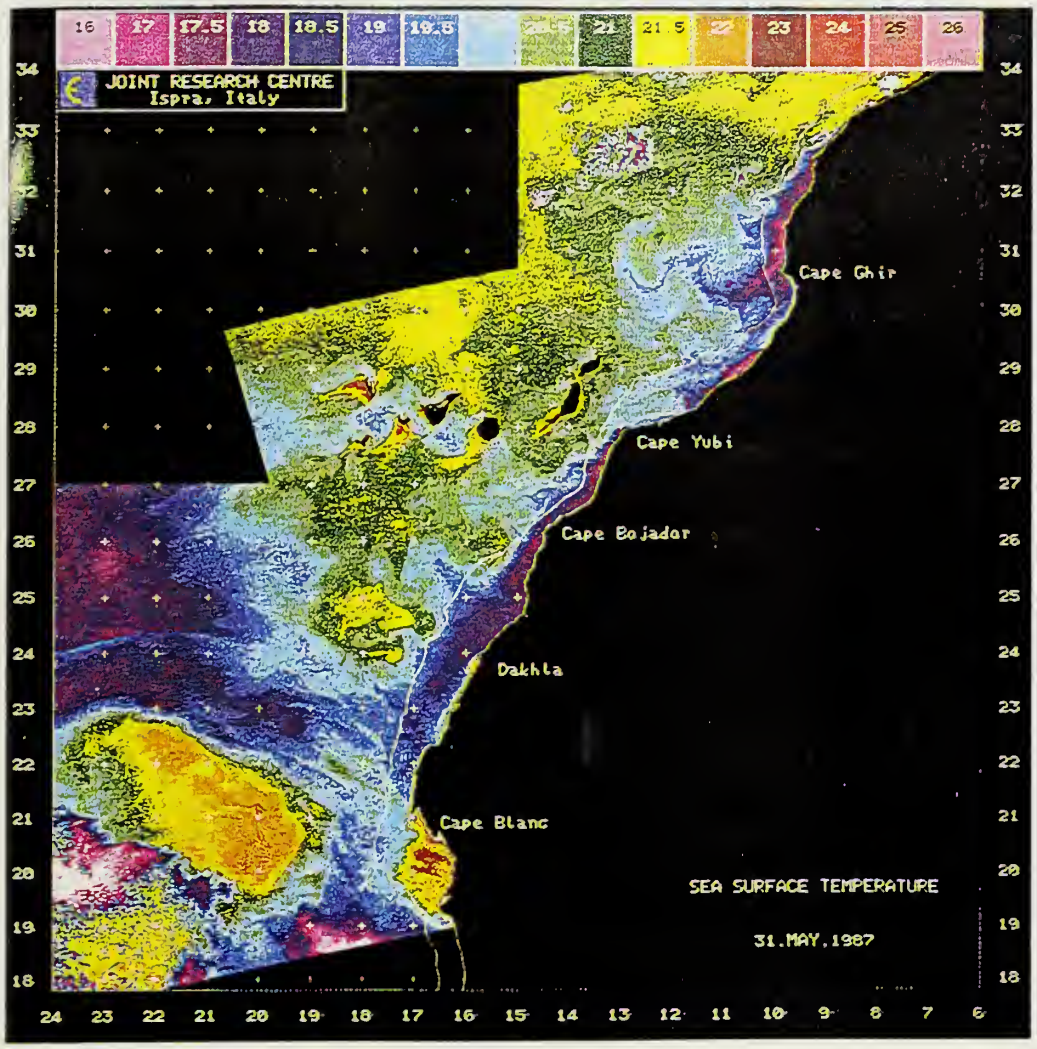

a

Figure 23. SST from (a) 31 May 1987 and (b) 9 June 1987 showing strong upwelling progressing north up the western coast of Northwest Africe and the development of the Cape Ghir filament. "From Van Camp *et al.*, 1991."

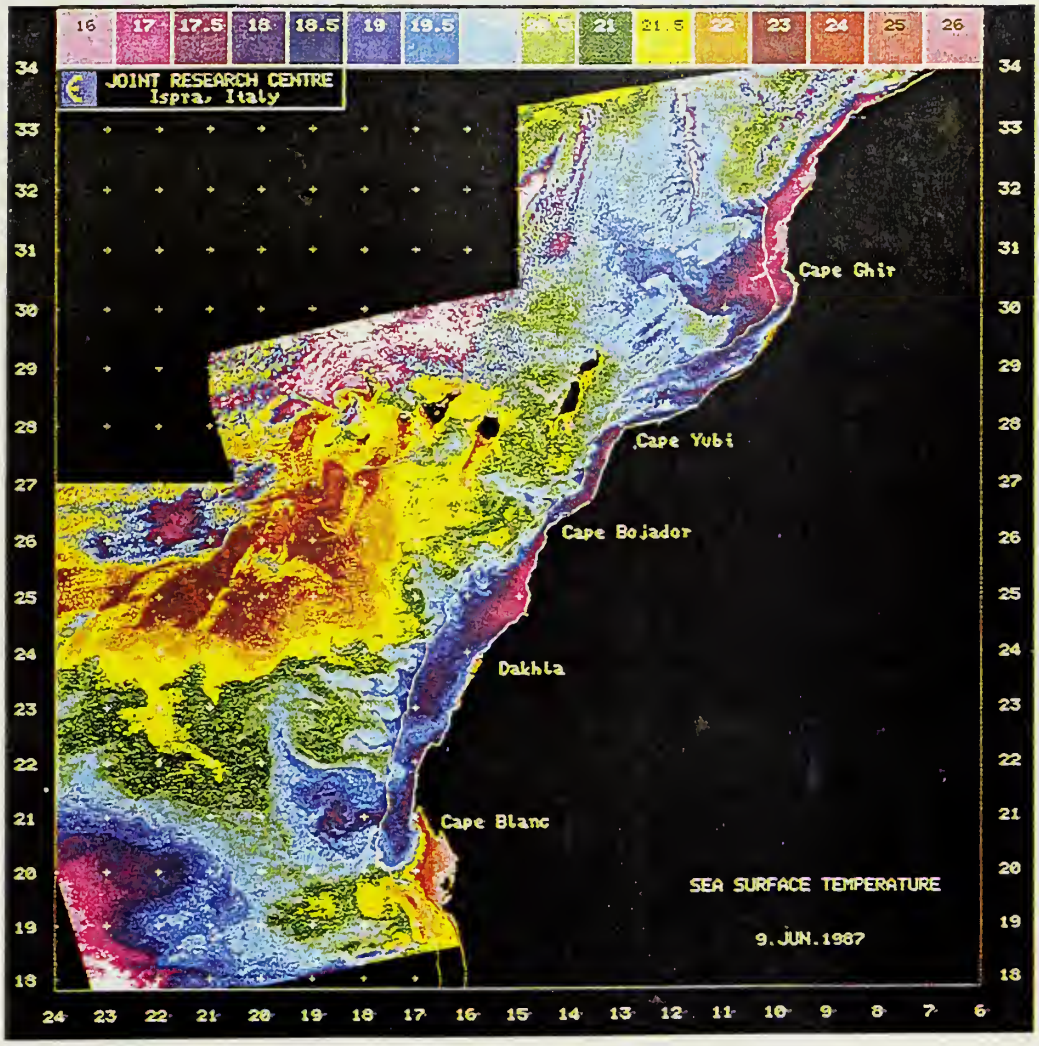
16
17
17.5
18
18.5
19
19.5
21
21.5
22
23
24
25
26
JOINT RESEARCH CENTRE
Ispra, Italy
Cape Ghir
Cape Yubi
Cape Bojador
Dakhla
Cape Blanc
SEA SURFACE TEMPERATURE
9.JUN.1987
34
33
32
31
30
29
28
27
26
25
24
23
22
21
20
19
18
24 23 22 21 20 19 18 17 16 15 14 13 12 11 10 9 8 7 6

b

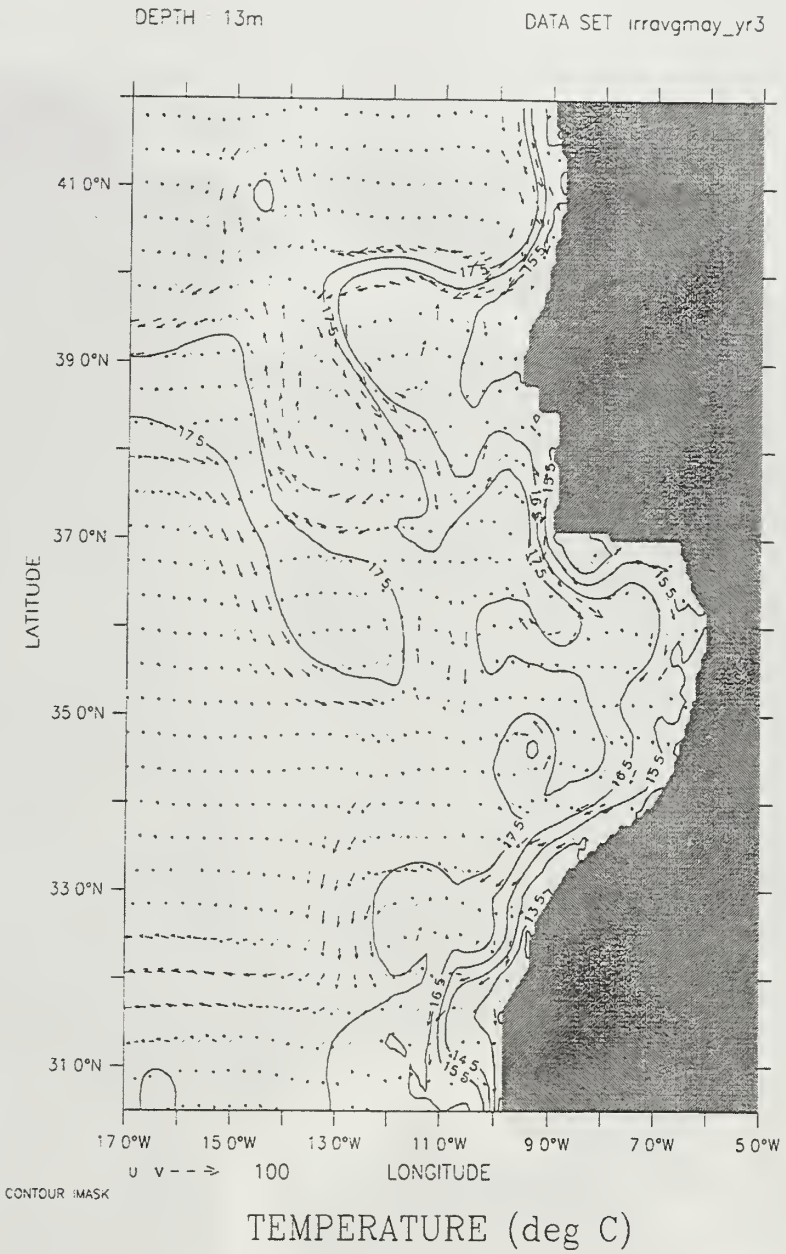

Figure 24. Experiment 2: Temperature contours and velocity vectors at 13 m depth in the third year of the model simulation time-averaged over the month of May shows the upwelling beginning to the south off Cape Ghir/Cape Beddouzza in the spring. The contour interval is 1° C. Maximum current velocity is 100 cm/s.

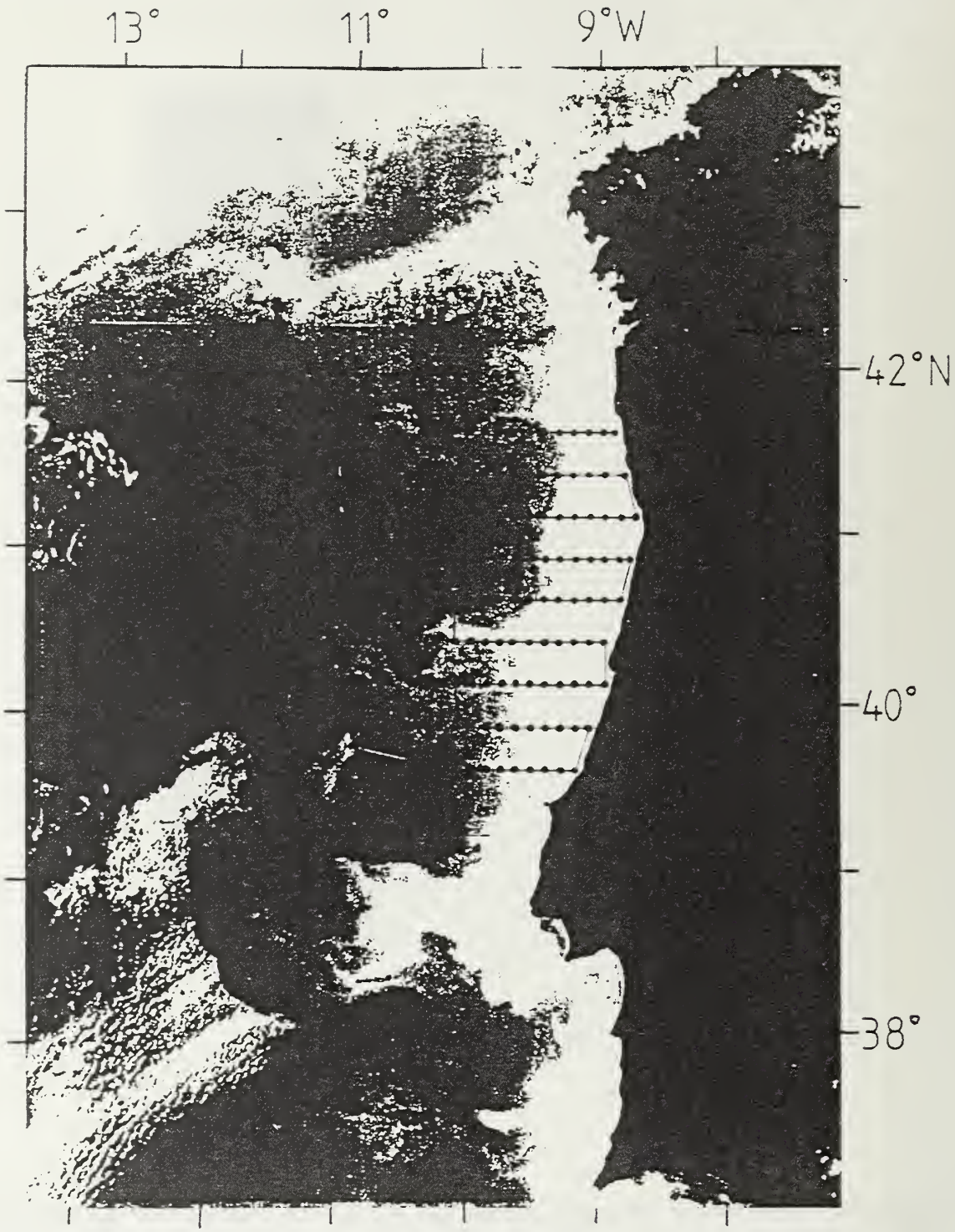

Figure 25. Satellite image of the SST off the west coast of Portugal and Spain, at 1611 UT 5 September from the University of Dundee ground receiving station. White tones nearshore correspond to cold, upwelled water with a distinct filament extending off Cabo da Roca. "From Fiuza and Sousa 1989."

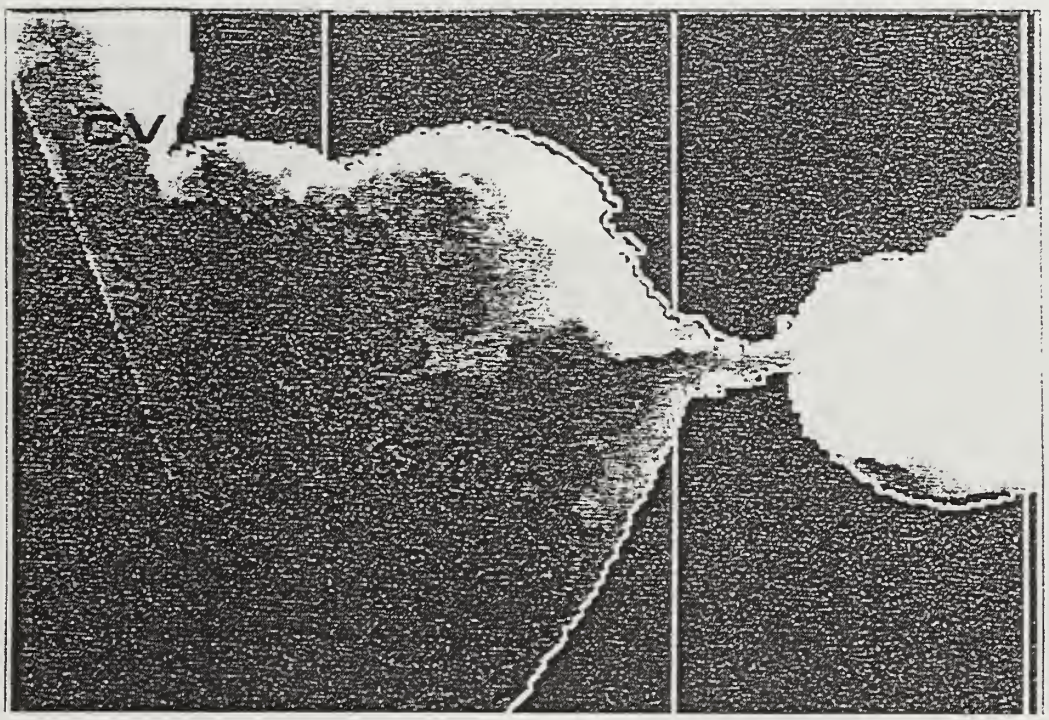

Figure 26. AVHRR image from 7 March 1988, showing a typical surface thermal pattern for spring. "From Folkard *et al.*, 1997."

Figure 27. AVHRR image from 8 October 1984, showing a typical surface thermal pattern for autumn. "From Folkard *et al.*, 1997."

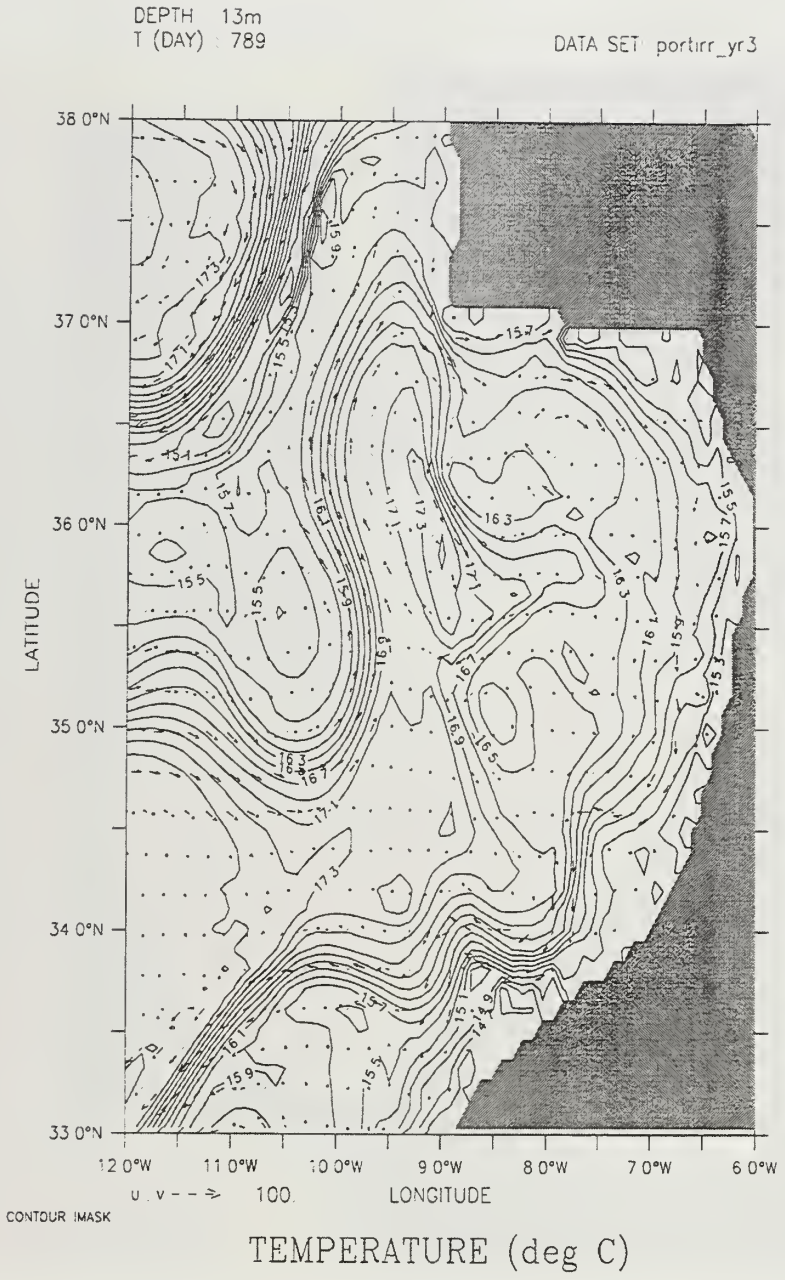

Figure 28. Experiment 2: Temperature contours and velocity vectors at 13 m depth in the third year of the model simulation time-averaged over the month of March shows the filament developing southwest of Cabo de Santa Maria. The contour interval is 0.2° C. Maximum current velocity is 100 cm/s.

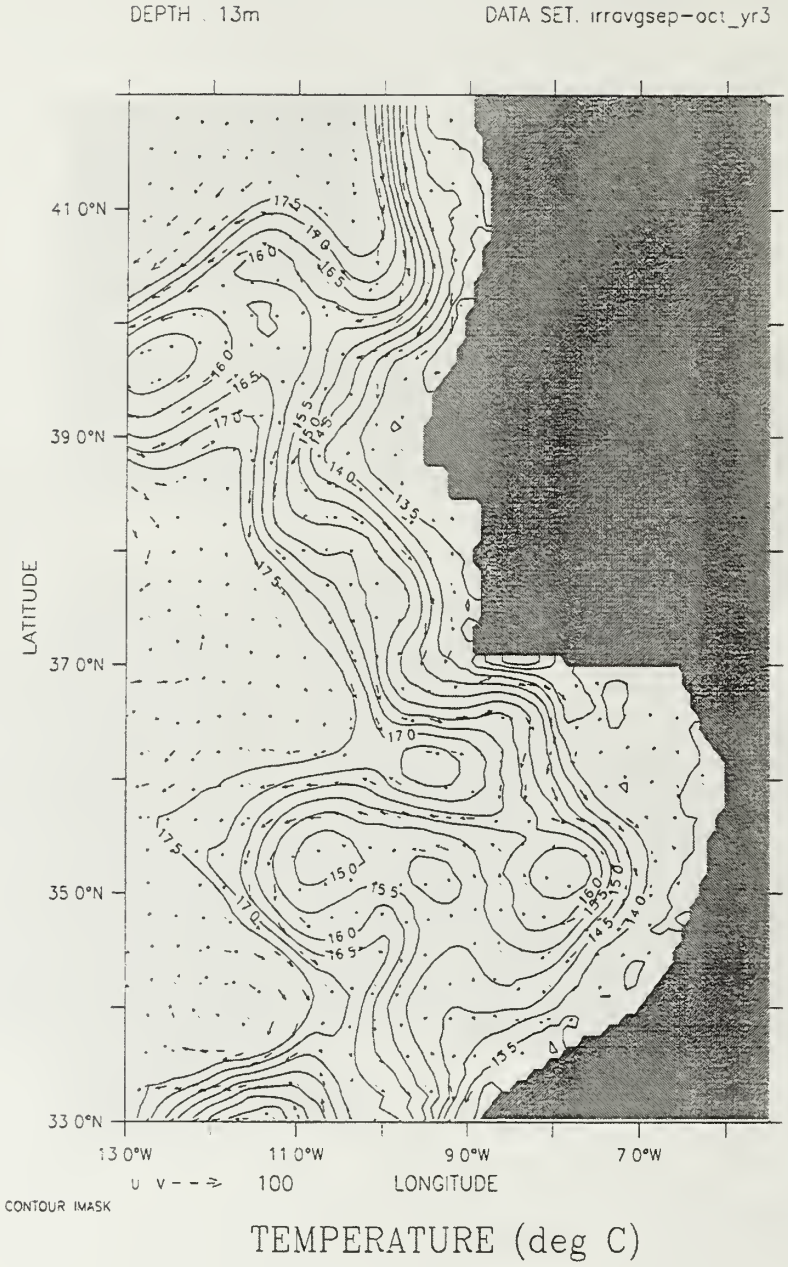

Figure 29. Experiment 2: Temperature contours and velocity vectors at 13 m depth in the third year of the model simulation time-averaged over the months of September and October shows the filament originating from the cold upwelled water southwest of Cabo de Sao Vincent and extending to the south of Cabo de Santa Maria. The contour interval is 0.5° C. Maximum current velocity is 100 cm/s.

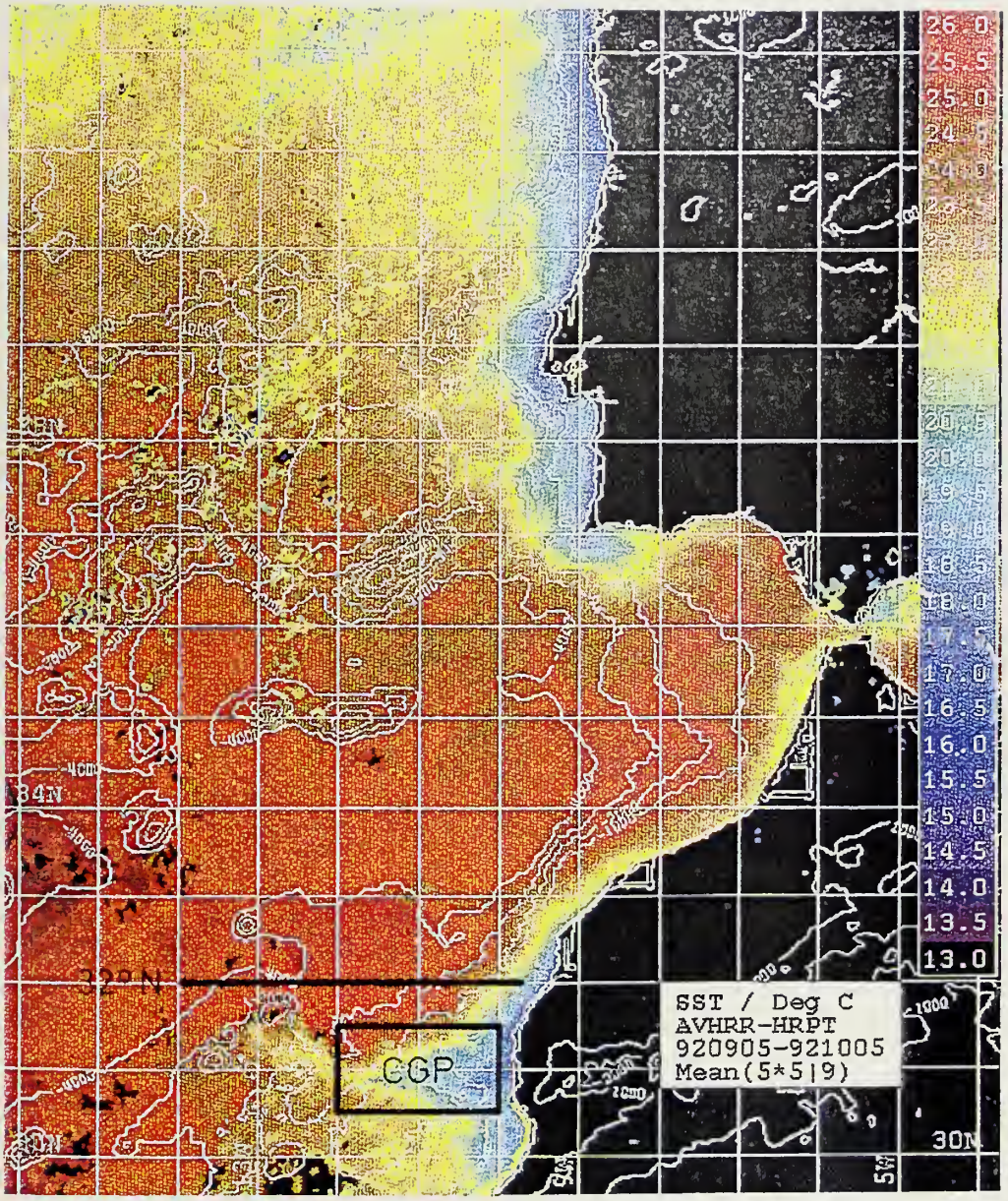

Figure 30. Rough contour of the bottom topography and orography in the northeast Atlantic Ocean; the monthly averaged SST-map (5 September - 5 October, 1992) is superimposed; a mean signal of coastal upwelling occurs off Portugal and Morocco; Hydrographic measurements are carried out along the zonal section at 32° N (15-18 September, 1992) and within the box (29 September 3 October 1992) covering the extended cold-water filament above the Cape Ghir Plateau (CGP) at about 31° N; note that the plateau is a submarine extension of the Atlas Chain onland. "From Hagen *et al.*, 1996."

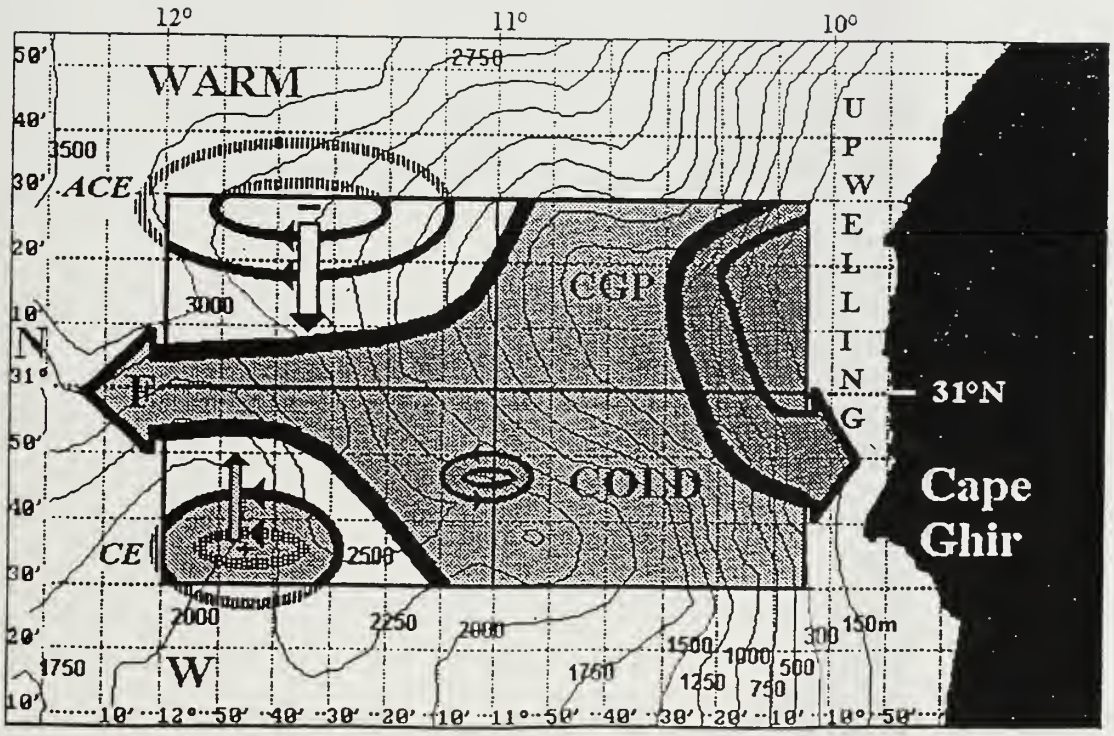

Figure 31. Area of investigation (box) with the sketch for detected (full line) and fictive (broken line) patterns of geostrophic motions within the superficial layers; arrows indicate the cyclonic course of the southward coastal jet and the westerward filament current (F) over the rough bottom topography of the CGP; isobaths in metres; shaded areas indicate cold water zones with an active upwelling cetre in the northeast corner; two oppositely rotating eddies propel upwelled water out to the open Atlantic along the filament axis at about 31° N; in addition the cyclonic eddy (CE) generates upward-directed vertical velocities (+) while the anticyclonic eddy (ACE) produces downward vertical velocities (-); data are based on CTD measurements between 29 September and 3 October. "From Hagen *et al.*, 1996."

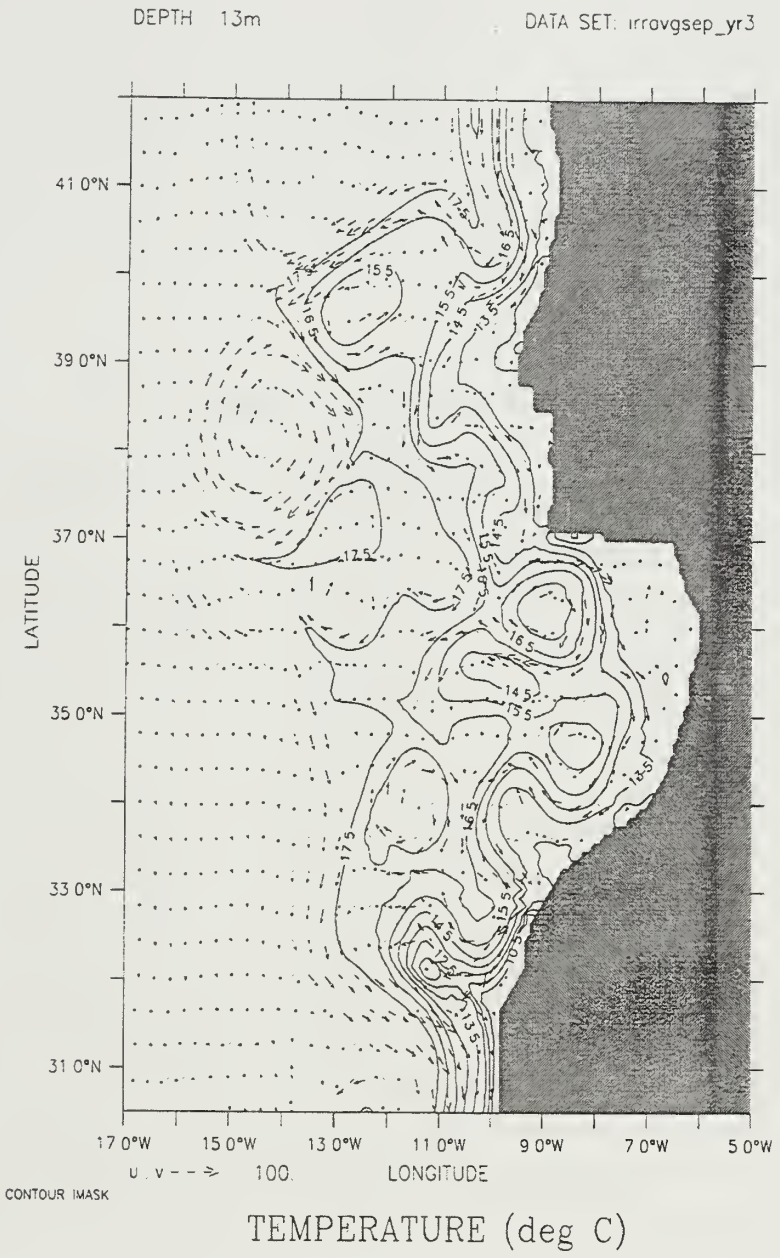

Figure 32. Experiment 2: Temperature contours and velocity vectors at 13 m depth in the coastal region in the third year of the model simulation time-averaged over the month of September shows the filament and associated eddies off Cape Ghir. The contour interval is 1° C. Maximum current velocity is 100 cm/s.

Table 1. Values of Constants Used in the Model

Constant	Value	Definition
T_0	278.2°K	Constant Reference Temperature
S_0	34.7	Constant Reference Salinity
ρ_0	1.0276 gm cm^3	Density of Sea Water At T_0 and S_0
α	2.4×10^{-4} $(°K)^{-1}$	Thermal Expansion Coefficient
β	7.5×10^{-4}	Saline Expansion Coefficient
K	10	Number of Levels In Vertical
Δx	9.0×10^5 cm	Cross-Shore Grid Spacing
Δy	1.1×10^6 cm	Alongshore Grid Spacing
H	4.5×10^5 cm	Total Ocean Depth
Δt	800 s	Time Step
f_0	0.86×10^4 s^{-1}	Mean Coriolis Parameter
g	980 cm s^2	Acceleration of Gravity
A_M	2×10^{17} cm^4 s^{-1}	Biharmonic Momentum Diffusion Coefficient
A_H	2×10^{17} cm^4 s^{-1}	Biharmonic Heat Diffusion Coefficient
K_M	0.5 cm^2 s^{-1}	Vertical Eddy Viscosity
K_H	0.5 cm^2 s^{-1}	Vertical Eddy Conductivity

LIST OF REFERENCES

Ambar, I., Mediterranean influence off Portugal, in *Present problems of oceanography in Portugal, Junta Nacional de Investigacao Cientifica e Tecnologica, Lisboa,* 73-87, 1982.

Arakawa, A., and V. R. Lamb, Computational design of the basic dynamical processes of the UCLA general circulation model, *Methods Comput. Phys.,* 17, 173-265, 1977.

Barton, E. D., A filament programme in the Iberian upwelling region, *Coastal Transition Zone Newsletter,* 1, 2-5, 1986.

Batteen, M. L., Wind-forced modeling studies of currents, meanders, and eddies in the California Current System, *J. Geophys. Res.*, 102, 985-1009, 1997.

Batteen, M. L., and Y. -J. Han, On the computational noise of finite difference schemes used in ocean models, *Tellus,* 33, 387-396, 1981.

Batteen, M. L., C .N. Lopes da Costa, and C. S. Nelson, A numerical study of wind stress curl effects on eddies and filaments off the Northwest coast of the Iberian Peninsula, *J. Mar. Systems,* 3, 249-266, 1992.

Batteen, M. L., R. L. Haney, T. A. Tielking, and P. G. Renaud, A numerical study of wind forcing of eddies and jets in the California Current System, *J. Mar. Res.,* 47, 493-523, 1989.

Bryan, K., A numerical method for the study of the circulation of the world ocean, *J. Comput. Phys., 4,* 347-376, 1969.

Camerlengo, A. L., and J. J. O'Brien, Open boundary conditions in rotating fluids, *J. Comput. Phys., 89,* 12-35, 1980.

Carton, J. A., Coastal circulation caused by an isolated storm, *J. Phys Oceanogr.*, 14, 114-124, 1984.

Carton, J. A., and S. G. H. Philander, Coastal upwelling viewed as a stochastic phenomena, *J. Phys Oceanogr.*, 14, 1499-1509, 1984.

Crowe, P. R., The trade wind circulation of the world, *Institute of British Geographers, Transactions and Papers,* 15, 37-56, 1949.

Defense Mapping Agency Hydrographic/Topographic Center (DMAH/TC), *Sailing Directions (Planning Guide) for the North Atlantic*, DMA Pub. No. 140, Washington D. C., 390 pp., 1988.

Fiuza, A. F. de G., The Portuguese coastal upwelling system, in *Present problems of oceanography in Portugal, Junta Nacional de Investigacao Cientifica e Tecnologica, Lisboa,* 45-71, 1982.

Fiuza, A. F. de G., Upwelling patterns off Portugal, in E. Suess and J. Thiede (Editors), Coastal Upwelling. Its Sediment Record. Plenum Press, New York, pp. 85-97, 1983.

Fiuza, A. F. de G., Hidrologia e dinamica das Aguas costeiras de Portugal. Dissertacao apresentada a Universidade de Lisboa para obtencao do grau de Doutor em Fisica, especializacao em Ciencias Geofisicas. Univ Lisboa, 294pp., 1984.

Fiuza, A. F. de G., and F. M. Sousa, Preliminary results of a CTD survey in the Coastal Transition Zone off Portugal during 1-9 September 1988, *Coastal Transition Zone Newsletter,* 4, 2-9, 1989.

Folkard, A. M., P. A. Davis, A. F. de G. Fiuza, I. Ambar, Remotely sensed sea surface thermal patterns in the Gulf of Cadiz and the Strait of Gibraltar: Variability, correlations, and relationships with the surface wind field, *J. Geophys. Res.*,102, 5669-5683, 1997.

Frouin, R., A. F. G. Fiuza, I. Ambar, and T. J. Boyd, Observations of a poleward surface current off the coasts of Portugal and Spain during Winter, *J. Geophys. Res.*, 95, 679-691, 1990.

Hagen, E., C. Zulicke, and R. Feistel, Near-surface structures in the Cape Ghir filament off Morocco, *Oceanol. Acta*, 19, 6, 577-598, 1996.

Haidvogel, D. B., A. Beckmann, and K. S. Hedstrom, Dynamical simulation of filament formation and evolution in the coastal transition zone, *J. Geophys. Res.*,96, 15,017-15,040, 1991.

Haney, R. L., A numerical study of the response of an idealized ocean to large-scale surface heat and momentum flux. *J. Phys. Oceanogr.*, 4, 145-167, 1974.

Haynes, R. and E. D. Barton, A poleward flow along the Atlantic coast of the Iberian Peninsula, *J. Geophys. Res.*, 95, 11425-11441, 1990.

Holland, W. R., The role of mesoscale eddies in the general circulation of the ocean-Numerical experiments using a wind-driven quasi-geostrophic model, *J. Phys. Oceanogr.*, *8*, 363-392, 1978.

Holland, W. R., and M. L. Batteen, The parameterization of subgrid scale heat diffusion in eddy-resolved ocean circulation models, *J. Phys. Oceanogr., 16,* 200-206, 1986.
Ikeda, M., W. J. Emery, and L. A. Mysak, Seasonal variability in meanders of the California Current system off Vancouver Island, *J. Geophys. Res., 89,* 3487-3505, 1984a.

Ikeda, M., L. A. Mysak, and W. J. Emery, Observations and modeling of satellite-sensed meanders and eddies off Vancouver Island, *J. Phys. Oceanogr., 14,* 3-21, 1984b.

Levitus, S., Climatological atlas of the world ocean, *U. S. Dept. Commer. NOAA Prof. Pap.* 13, 173 pp, 1982.

Lopes da Costa, C., A numerical study of wind forcing in the eastern boundary current system off Portugal, M. S. Thesis, Naval Postgraduate School, 114 pp, 1989.

McClain, C. R., S. Chao, L. P. Atkinson, J. O. Blanton, and F. Castillejo, Wind-driven upwelling in the vicinity of Cape Finisterre, Spain, *J. Geophys. Res.*, 91, 8470-8486, 1986.

McCreary, J. P., Y. Fukamachi, and P. K. Kundu, A numerical investigation of jets and eddies near an eastern ocean boundary, *J. Geophys. Res.*, 92, 2515-2534, 1991.

McCreary, J. P., P. K. Kundu, and S. Y. Chao, On the dynamics of the California Current system, *J. Mar. Res.*, 45, 1-32, 1987.

Mittelstaedt, E., The ocean boundary along the northwest African coast: Circulation and oceanographic properties at the sea surface, *Prog. Oceanog.*, 26, 307-355, 1991.

Nelson, C. S., Wind stress and wind stress curl over the California Current, NOAA Tech Rep. NMFS SSFR-714, U. S. Dept. Commerce, 87 pp., 1977.

Pares-Sierra, A., W. B. White, and C. -K. Tai, Wind-driven coastal generation of annual mesoscale eddy activity in the California Current system: A numerical model, *J. Phys Oceanogr.*, 23, 1110-1121, 1993.

Pedlosky, J., Longshore currents, upwelling, and bottom topography, *J. Phys Oceanogr.*, 4, 214-226, 1974.

Philander, S. G. H., and J. H. Yoon, Eastern boundary currents and upwelling, *J. Phys Oceanogr.*, 12, 862-879, 1982.

Semtner, A. J., An oceanic general circulation model with bottom topography. Numerical simulation of weather and climate, *Technical Report, 9,* University of California, Los Angeles, 99 pp., 1974.

Tomczak, M., and J. Stuart Godfrey, *Regional Oceanography: An Introduction*, Pergamon Press, New York, 422 pp., 1994.

Trenberth, K. E., W. G. Large, J. G. Olsen, The mean annual cycle in global ocean wind stress, *J. Phys Oceanogr.*, 20, 1742-1760, 1990.

Van Camp, L., L. Nykjaer, E. Mittelstaedt, and P. Schlittenhardt, Upwelling and boundary circulation off Northwest Africa as depicted by infrared and visible satellite observations, *Prog. Oceanog.*, 26, 357-402, 1991.

Weatherly, G. L., A study of the bottom boundary layer of the Florida Current, *J. Phys Oceanogr.*, 2, 54-72, 1972.

Wooster, W. S., and J. L. Reid, Jr., Eastern Boundary Currents in *The Sea, Vol. 2,* M. N. Hill, Ed., Wiley International, New York, 253-280, 1963.

Wooster, W. S., A. Bakun, and D. R. McLain, The seasonal upwelling cycle along the eastern boundary of the North Atlantic, *J. Mar. Res.*, 34, 131-140, 1976.

INITIAL DISTRIBUTION LIST

No. Copies

1. Defense Technical Information Center.....2
   8725 John J. Kingman Rd, STE 0944
   Ft. Belvoir, VA 22060-6218

2. Dudley Knox Library..... 2
   Naval Postgraduate School
   411 Dyer Rd
   Monterey, CA 93943-5101

3. Chairman (Code OC/Bf)..... 1
   Department of Oceanography
   Naval Postgraduate School
   Monterey, CA 93943-5122

4. Chairman (Code MR/Wx)..... 1
   Department of Meteorology
   Naval Postgraduate School
   Monterey, CA 93943-5114

5. Dr. Mary L. Batteen, (Code OC/Bv)..... 3
   Department of Oceanography
   Naval Postgraduate School
   Monterey, CA 93943-5122

6. Dr. Richard Lambert..... 1
   National Science Foundation
   4201 Wilson Boulevard
   Arlington, VA 22230

7. Dr. T. Kinder.....1
   Physical Oceanography Division
   Office of Naval Research
   800 N. Quiney Street
   Arlington, VA 22217

8. LT Eric J. Buch.....4
   PSC 817 Box 13
   FPO AE 09622